High precision CA-TIMS dating of the Hiltaba Suite, Gawler Craton

Report Book
2021/00002

EA Jagodzinski, JL Crowley,
AJ Reid, CE Wade and
MJ Bockmann

energymining.sa.gov.au

SOUTH AUSTRALIA

Government of South Australia
Department for Energy and Mining

High-precision CA-TIMS dating of the Hiltaba Suite, Gawler Craton

EA Jagodzinski[1], JL Crowley[2], AJ Reid[1, 3], CE Wade[1] and MJ Bockmann[3]

1 Geological Survey of South Australia, Department for Energy and Mining

2 Department of Geosciences, Boise State University, USA

3 Department of Earth Sciences, University of Adelaide

September 2021

Report Book 2021/00002

Department for Energy and Mining
Level 4, 11 Waymouth Street, Adelaide
GPO Box 320, Adelaide SA 5001
Phone +61 8 8463 3000
Email dem.minerals@sa.gov.au
dem.petroleum@sa.gov.au
www.energymining.sa.gov.au

South Australian Resources Information Gateway (SARIG)
SARIG provides up-to-date views of mineral, petroleum and geothermal tenements and other geoscientific data. You can search, view and download information relating to minerals and mining in South Australia including tenement details, mines and mineral deposits, geological and geophysical data, publications and reports (including company reports).
map.sarig.sa.gov.au

Disclaimer
The contents of this report are for general information only and are not intended as professional advice, and the Department for Energy and Mining (and the Government of South Australia) make no representation, express or implied, as to the accuracy, reliability or completeness of the information contained in this report or as to the suitability of the information for any particular purpose. Use of or reliance upon the information contained in this report is at the sole risk of the user in all things and the Department for Energy and Mining (and the Government of South Australia) disclaim any responsibility for that use or reliance and any liability to the user.

Acknowledgement of Country
The Department for Energy and Mining acknowledges Aboriginal people as the First Nations Peoples of South Australia. We recognise and respect the cultural connections as the traditional owners and occupants of the land and waters of South Australia, and that they continue to make a unique and irreplaceable contribution to the state.

Preferred way to cite this publication
Jagodzinski EA, Crowley JL, Reid AJ, Wade CE and Bockmann MJ 2021. *High-precision CA-TIMS dating of the Hiltaba Suite, Gawler Craton.* Report Book 2021/00002. Department for Energy and Mining, South Australia, Adelaide.

CONTENTS

TABLES

FIGURES

SHORTENED FORMS

CA-TIMS	chemical abrasion isotope dilution thermal ionisation mass spectrometry
CL	cathodoluminescence
DDH	diamond drillhole
GDA	geocentric datum of Australia
GRV	Gawler Range Volcanics
GSSA	Geological Survey of South Australia
HS	Hiltaba Suite
IDTIMS	Isotope dilution thermal ionisation mass spectrometry
IOCG	iron oxide – copper–gold
Kober	Double-filament Pb evaporation Thermal ionisation mass spectrometry (Kober 1986)
LA-ICPMS	laser ablation - inductively coupled plasma mass spectroscopy
LIP	large igneous province
Ma	million years
MGA	map grid of Australia
MSWD	mean square of weighted deviation
PPL	plane polarised light
PDD	probability density diagram
SCLM	subcontinental lithospheric mantle
SHRIMP	sensitive high resolution ion microprobe
TMI	total magnetic intensity
XPL	cross polarised light

High-precision CA-TIMS dating of the Hiltaba Suite, Gawler Craton

EA Jagodzinski, JL Crowley, AJ Reid, CE Wade and MJ Bockmann

ABSTRACT

This report provides a summary of high-precision chemical abrasion-isotope dilution-thermal ionisation mass spectrometry (CA-IDTIMS) U-Pb geochronology on zircons from five samples of Hiltaba Suite granites collected across the Gawler Craton. The oldest samples are from the Burgoyne Batholith, host to the Roxby Downs Granite and Olympic Dam Breccia Complex in the Paleoproterozoic–Mesoproterozoic basement beneath the Stuart Shelf to the east of the Gawler Craton. Sample 2131359 (DDH BRD1) from the Saddle Hill prospect east of Olympic Dam is a biotite granite with an emplacement age of 1592.62 ± 0.52 Ma. West of Olympic Dam, granite from DDH Blanche 1, represented by sample 2111460, was emplaced at 1591.79 ± 0.42 Ma.

Sample 2053554, representing the Hiltaba Suite at Tarcoola in the Central Gawler Gold Province (Ferriss and Schwarz 2003) is significantly younger at 1586.49 ± 0.49 Ma, as is the Curramulka Gabbronorite on the Yorke Peninsula (1580.21 ± 0.31 Ma), although the latter lies within the same Olympic Cu-Au Province (Skirrow et al. 2007) along the eastern margin of the Gawler Craton.

The westernmost sample 2115491, from the Fowler Domain, is the youngest with an emplacement age of 1579.37 ± 0.73 Ma.

The dates demonstrate magmatism in the Gawler Craton continued up to 8 million years after eruption of the Gawler Range Volcanics, which occurred c. 1594.5–1586.5 Ma (Jagodzinski et al. in prep).

The spatial distribution of all magmatic ages for the Gawler large igneous province (LIP) suggests that magmatism originated in the Olympic Domain (basement to the Stuart Shelf), then propagated radially outward, a pattern suggestive of mantle upwelling, and a rising then flattening plume head providing the heat source for melting of the SCLM and lower crust.

INTRODUCTION

The early Mesoproterozoic was a time of significant magmatism in the Gawler Craton, with widespread bimodal volcanism and intrusion of the c. 1595–1575 Ma Gawler Range Volcanics (GRV) and Hiltaba Suite (Flint et al. 1993, Allen et al. 2008). Mesoproterozoic magmatism was associated with regionally partitioned deformation and metamorphism that is generally referred to as the Kararan Orogeny (Daly et al. 1998, Hand et al. 2007). This major orogenic event was widespread across the Gawler Craton and has been shown to include examples of ultra-high temperature metamorphism in the northern Gawler Craton (Cutts et al. 2011) and deformation during magmatic emplacement in the southern Gawler Craton (Reid et al. 2021, Brotodewo et al. 2018). The c. 1595–1575 Ma event also saw the formation of iron oxide – copper–gold (IOCG) deposits in the Olympic Cu-Au Province (Skirrow et al. 2002, Skirrow et al. 2007) and a series of gold-dominated, structurally controlled mesothermal deposits grouped together as the Central Gawler Gold Province (Budd and Fraser 2004, Budd and Skirrow 2007) (Fig. 1). External to the Gawler Craton, c. 1595–1575 Ma magmatism is recognised in the Curnamona Province (Page et al. 2005, Wade et al. 2012), Barossa Complex (Jagodzinski et al. 2020), and Mt Painter Inlier

(Fanning 1995, Elberg et al. 2001, Fraser and Neumann 2010). The GRV, Benagerie Volcanic Suite and Hiltaba Suite are recognised as a high-silica Proterozoic LIP (Allen et al. 2008, Wade et al. 2012), which Pankhurst et al. (2011) refer to as the Gawler LIP.

The geodynamic drivers for widespread c. 1595–1575 Ma magmatism, metamorphism, deformation and mineralisation across the Gawler Craton and Curnamona Province have been debated. Extensive bimodal A-type magmatism, high-temperature metamorphism, and localised compressional deformation suggest an intracontinental setting, with many models suggesting mantle underplating or mantle plume activity as a key mechanism intrusion of mafic magmas into the lower crust causing extensive crustal melting (Giles 1988, Stewart 1994, Daly et al. 1998, Wade et al. 2019). Alternate models place the Gawler Craton and Curnamona Province in a continental back arc setting connected to far-field subduction zones that drive tectonism such as back-arc extension and subduction rollback (Wade et al. 2006, Betts, et al. 2009 Skirrow et al. 2018, Tiddy and Giles 2020).

Over the past 30 years, a wealth of geochronological data has been amassed for Hiltaba Suite aged magmatism, metamorphism and mineralisation which, due to its high economic potential (Reid 2019), has been dated more than any other time slice of South Australia's geological history. A recent review by Tiddy and Giles (2020) contains a comprehensive compilation of geological activity and associated geochronology for this c. 1595–1575 Ma event. In this report we evaluate this dataset to identify any spatial patterns in the timing of magmatism, then assess the implications for geodynamics and tectonic setting.

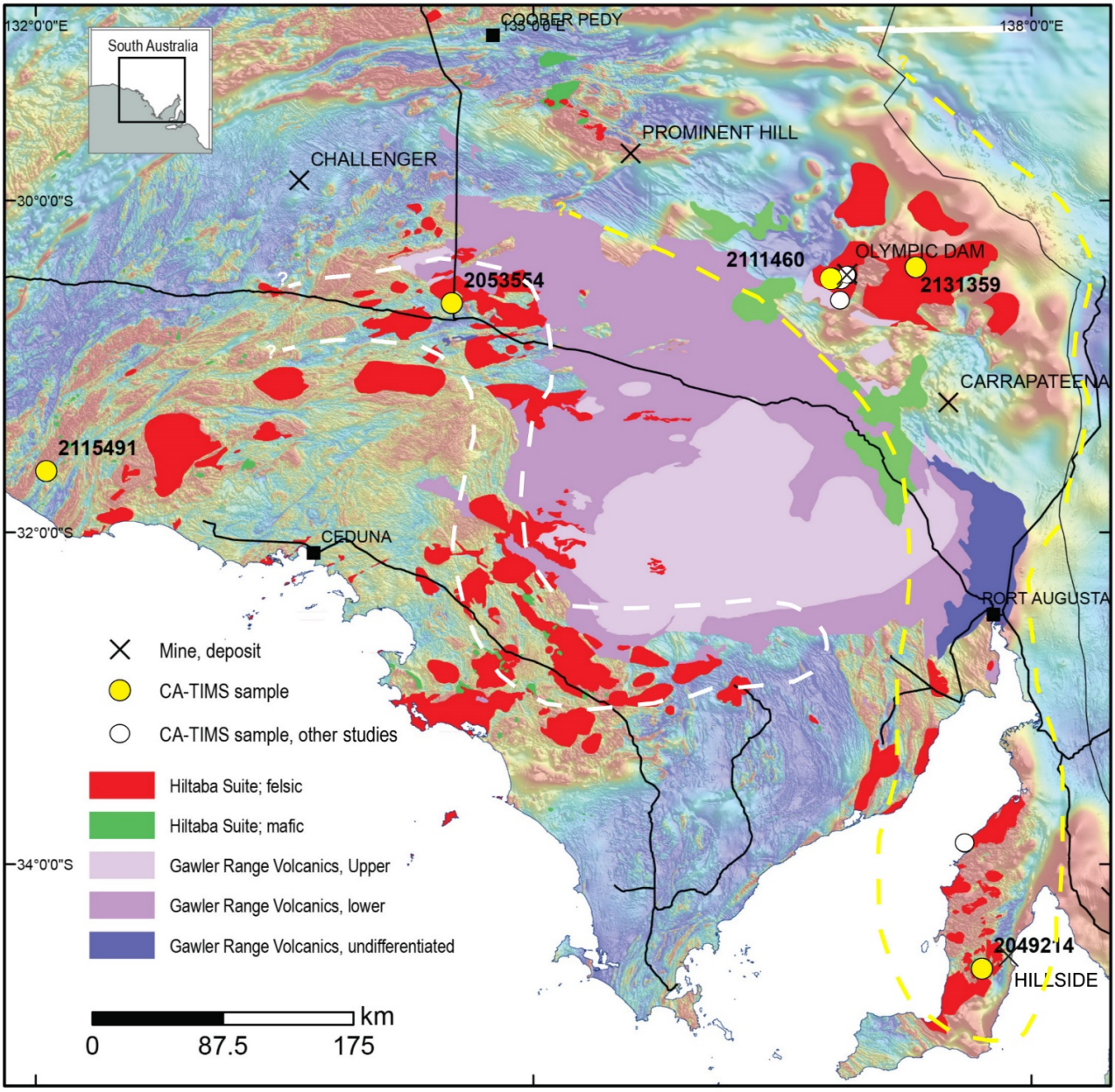

Figure 1. Simplified map of the Gawler Craton showing the distribution of the GRV and Hiltaba Suite on TMI imagery, with the location of samples dated by CA-TIMS referred to in this report book. The yellow dashed line outlines the Olympic Cu-Au Province, and the Central Gawler Gold Province is outlined in white.

CA-TIMS U-PB GEOCHRONOLOGY METHODS

U-Pb dates were obtained by the chemical abrasion-isotope dilution thermal ionisation mass spectrometry (CA-IDTIMS) method from analyses composed of single zircon grains (Appendix 2), modified after Mattinson (2005). Zircon was separated from rocks using standard techniques, placed in a muffle furnace at 900°C for 60 hours in quartz beakers, mounted in epoxy, and polished until the centres of the grains were exposed. Cathodoluminescence (CL) images were obtained with a JEOL JSM-300 scanning electron microscope and Gatan MiniCL. Zircon was removed from the epoxy mounts for dating based on CL images and laser ablation - inductively coupled plasma mass spectroscopy (LA-ICPMS) data.

Zircon was put into 3 ml Teflon PFA beakers and loaded into 300 µl Teflon PFA microcapsules. Fifteen microcapsules were placed in a large-capacity Parr vessel and the zircon partially dissolved

in 120 µl of 29 M HF for 12 hours at 180 or 190°C. Zircon was returned to 3 ml Teflon PFA beakers, HF was removed, and zircon was immersed in 3.5 M HNO_3, ultrasonically cleaned for an hour, and fluxed on a hotplate at 80°C for an hour. The HNO_3 was removed and zircon was rinsed twice in ultrapure H_2O before being reloaded into the 300 µl Teflon PFA microcapsules (rinsed and fluxed in 6 M HCl during sonication and washing of the zircon) and spiked with the Boise State University mixed ^{233}U-^{235}U-^{205}Pb tracer solution (BSU-1B). Zircon was dissolved in Parr vessels in 120 µl of 29 M HF with a trace of 3.5 M HNO_3 at 220°C for 48 hours, dried to fluorides, and re-dissolved in 6 M HCl at 180°C overnight. U and Pb were separated from the zircon matrix using an HCl-based anion-exchange chromatographic procedure (Krogh 1973), eluted together and dried with 2 µl of 0.05 N H_3PO_4.

Pb and U were loaded on a single outgassed Re filament in 5 µl of a silica-gel/phosphoric acid mixture (Gerstenberger and Haase, 1997), and U and Pb isotopic measurements made on a GV isoprobe-T multicollector thermal ionisation mass spectrometer equipped with an ion-counting Daly detector. Pb isotopes for analyses with smaller amounts of radiogenic Pb were measured by peak-jumping all isotopes on the Daly detector for 100 to 160 cycles and corrected for 0.16 ± 0.06%/a.m.u. (2σ) mass fractionation. Pb isotopes for analyses with larger amounts of radiogenic Pb were measured by a Faraday-Daly routine that cycles 150–200 times between placing mass 204 in the axial Daly collector and masses 205–208 on the H1-H4 Faraday detectors to placing mass 205 in the axial Daly and masses 206–208 in the H1-H3 Faradays, providing real-time Daly gain correction. These results were corrected for 0.10 ± 0.06%/a.m.u. (2σ) mass fractionation. Transitory isobaric interferences due to high-molecular weight organics, particularly on ^{204}Pb and ^{207}Pb, disappeared within approximately 60 cycles, while ionisation efficiency averaged 104 cps/pg of each Pb isotope. Linearity (to ≥1.4 x 106 cps) and the associated deadtime correction of the Daly detector were determined by analysis of NBS982. Uranium was analysed as UO_2^+ ions in static Faraday mode on 1012-ohm resistors for 300 cycles and corrected for isobaric interference of $^{233}U^{18}O^{16}O$ on $^{235}U^{16}O^{16}O$ with an $^{18}O/^{16}O$ of 0.00206. Ionisation efficiency averaged 20 mV/ng of each U isotope. U mass fractionation was corrected using the known $^{233}U/^{235}U$ ratio of the Boise State University tracer solution.

U-Pb dates and uncertainties were calculated using the algorithms of Schmitz and Schoene (2007), calibration of BSU-1B tracer solution of $^{235}U/^{205}Pb$ of 77.93 and $^{233}U/^{235}U$ of 1.007066 for, U decay constants recommended by Jaffey et al. (1971), and $^{238}U/^{235}U$ of 137.818 (Hiess et al. 2012). $^{206}Pb/^{238}U$ ratios and dates were corrected for initial ^{230}Th disequilibrium using DTh/U = 0.20 ± 0.05 (1σ) and the algorithms of Crowley et al. (2007), resulting in an increase in the $^{206}Pb/^{238}U$ dates of ~0.09 million years. All common Pb in analyses was attributed to laboratory blank and subtracted based on the measured laboratory Pb isotopic composition and associated uncertainty. U blanks are estimated at 0.013 pg.

Six grains were analysed from each of five samples. Isoplot 3.0 (Ludwig, 2003) is used to calculate weighted mean $^{207}Pb/^{206}Pb$ dates from equivalent dates (probability of fit > 0.05), which are used to interpret igneous crystallisation ages. The $^{207}Pb/^{206}Pb$ dates are used rather than $^{206}Pb/^{238}U$ dates due to some $^{206}Pb/^{238}U$ dates being slightly younger, presumably due to Pb loss. The dates are -0.08 to 0.69% discordant.

Errors are quoted at the 95% confidence level and are the internal errors based on analytical uncertainties only, including counting statistics, subtraction of tracer solution, and blank Pb subtraction. These errors are ± 0.42–1.57 Ma. Including the U decay constant uncertainties propagated in quadrature increases the errors to ± 2.4–2.5 Ma. Errors for single analyses are quoted at 2σ.

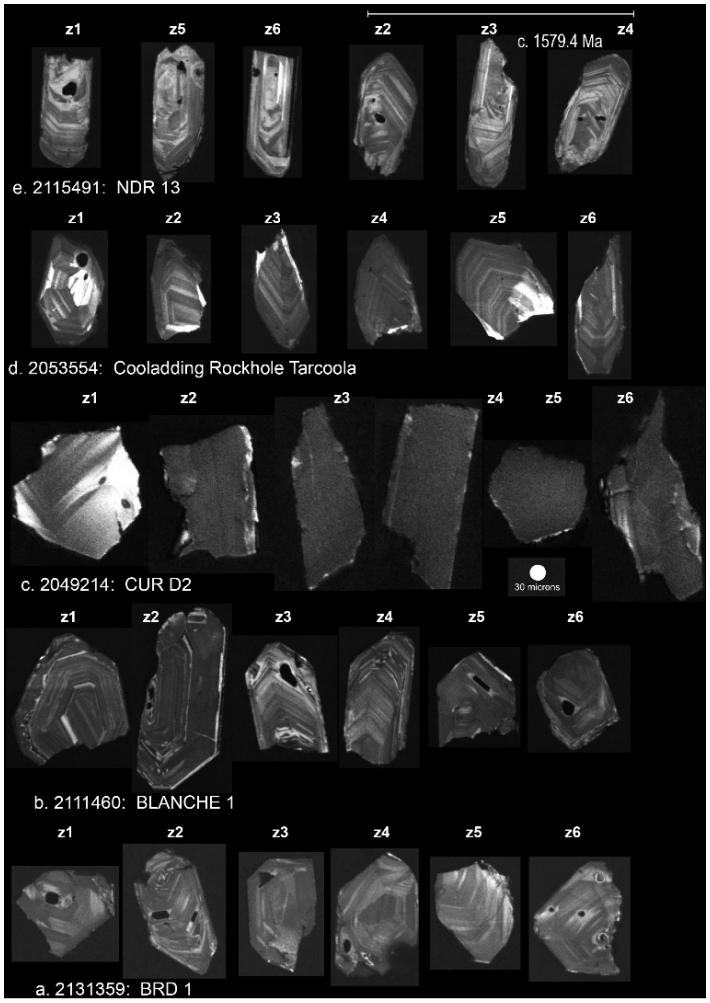

Figure 2. CL images of zircons used for CA-TIMS analysis, collected by a scanning electron microscope at Boise State University. Grain labels (e.g. z1, z2) correspond to the analysis number in the CA-TIMS dataset in Appendix 2. Brightness of CL images is comparable within, but not between samples.

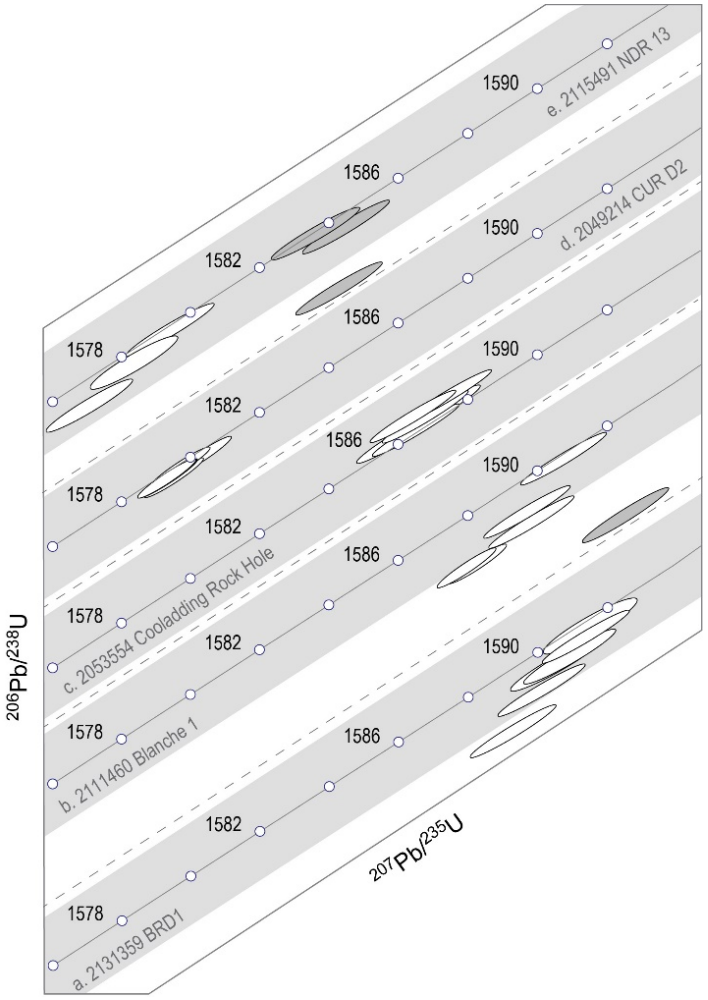

Figure 3. Wetherill concordia plots of CA-TIMS analyses for the zircons in Figure 2. The grey bands behind the line of concordia represent the decay constant uncertainty (2σ). Error ellipses are also 2σ. Grey ellipses represent analyses of inherited zircon excluded from weighted mean age calculations.

Table 1. Summary of $^{207}Pb/^{206}Pb$ CA-TIMS dates available for the Hiltaba Suite.

		UTM ZONE 53*		$^{238}U/^{235}U$ = 137.8185							
Sample	**Lithology and location**	**Easting**	**Northing**	**CA-TIMS age (Ma)**	**± c95% error (Ma)**	**[+decay constant]**	**MSWD**	**pof**	**n**	**n_t**	**Reference**
Olympic Domain (Stuart Shelf basement)											
RX8078	Granite, Acropolis prospect ACD 7 599 m	677500	6612525	1594.04	0.64		0.7	0.60	6	6	McPhie et al. 2020
LCD13	Roxby Downs Granite, RD2786A 1850 m	681920	6629625	1594.50	1.68	[2.50]	0.27	0.85	4	6	Courtney-Davies et al. 2020
LCD1	Roxby Downs Granite, RD2786A 1516 m			1595.97	0.94		1.60	0.42	6	6	Courtney-Davies et al. 2020**
LCD 11	Roxby Downs Granite, RD2786A 1810 m			1593.28	0.45	[2.41]	1.20	0.31	4	6	Courtney-Davies et al. 2020
LCD 12	Roxby Downs Granite, RD2786A 1830 m			1593.40	1.10		26	0	11	11	Courtney-Davies et al. 2020**
OD1215	Roxby Downs Granite, RD2499 529.7 m			1592.99	0.54	[2.40]	0.59	0.76	8	8	Cherry et al. 2018
OD1202	Roxby Downs Granite, RD2499 814.1 m			1593.25	0.68	[2.44]	0.84	0.54	7	7	Cherry et al. 2018
OD1201	Roxby Downs Granite, RD2488 681.9 m			1593.06	0.55	[2.43]	1.09	0.37	8	8	Cherry et al. 2018
OD1214	Roxby Downs Granite, RD2284 352.8 m			1592.68	1.26	[2.68]	2.09	0.08	5	7	Cherry et al. 2018
2000366176	Roxby Downs Granite, RD575 531 m	677814.82	6626919.06	1593.06	0.58	[2.43]	1.50	0.16	8	8	Cherry et al. 2018
2131359	biotite granite, BRD1 816–817 m	721129.63	6634853.33	1592.62	0.66	[2.40]	0.42	0.84	6	6	This study
2111460	granite, Blanche 1 1563.1-1564.6 m	672516.76	6627750.51	1591.79	0.74	[2.47]	1.57	0.18	5	6	This study
Yorke Peninsula											
2116262	Tickera Granite Mht, foliated	740615.57	6248545.53	1757.30	0.91	[2.50]	0.88	0.45	4	6	Reid et al. 2021
				1584.22	0.83 (2σ)	[2.50] (2σ)	0.80	0.37	2		
2053555	Tickera Granite Mht, weakly foliated	740606.54	6248543.54	1582.66	1.42	[2.75]	2.14	0.09	4	6	Reid et al. 2021
2116264	alkali-feldspar granite, non-foliated	740606.54	6248543.54	1579.05	0.81	[2.49]	1.38	0.23	6	6	Reid et al. 2021
2049214	gabbronorite DDH CUR D2 55–58.2 m	747770.01	6164962.55	1580.21	0.40	[2.40]	1.10	0.36	6	6	This study
Tarcoola											
2053554	K-spar rich granite, Dingo Rock Hole	452836.74	6612719.48	1586.49	0.62	[2.42]	0.71	0.61	6	6	This study
Western Gawler Craton											
2115491	foliated granite, NDR 13 94.5–94.7 m	221617.89	6497019.49	1579.37	1.57	[2.65]	0.60	0.55	3	6	This study

* All samples with an easting and northing are spatially located on Figure 1. Samples with the prefix “OD” and “LCD” are located within the Olympic Dam mine, marked by a single point on the map. Light grey eastings and northings are estimated from published maps. ** denotes upper concordia intercept ages. All other dates are weighted means.

All dates are calculated (or recalculated from the original published dates) using the $^{238}U/^{235}U$ value of 137.8185. Where n = 2 errors are 2σ. All other errors are quoted at the 95% confidence level (±c95%) = tσ for MSWD ≤ 1.0, $t\sigma\sqrt{MSWD}$ for MSWD > 1.0.

RESULTS

The five samples are described in detail in Appendix 1 and the full dataset is presented in Appendix 2. Table 1 contains a summary of the weighted mean ages and includes all other published CA-TIMS dates available for the Hiltaba Suite for comparison.

Olympic Domain (Stuart Shelf basement)

Zircon from 2131359 (BRD1) is inclusion rich and subequant to elongate with moderate oscillatory zoning (Fig. 2a). Six $^{207}Pb/^{206}Pb$ dates yield a weighted mean of 1592.62 ± 0.66 Ma (MSWD = 0.42, probability of fit = 0.84, Fig. 3a).

Zircon from 2111460 (Blanche 1) is subequant to elongate with moderate to strong oscillatory zoning and large inclusions in some grains (Fig. 2b). Five of the six $^{207}Pb/^{206}Pb$ dates yield a weighted mean of 1591.79 ± 0.74 Ma (MSWD = 1.57, probability of fit = 0.18). Another date of 1598.86 ± 1.12 Ma is interpreted as being from an inherited grain (Fig. 3b).

Yorke Peninsula

Zircons in 2049214 (Curramulka Gabbronorite CUR D2) are large, angular, subequant to elongate fragments that are homogenous or have a broad planar or oscillatory zoning. Some grains have thin fractures annealed with a bright cathodoluminescent material (Fig. 2c). Six $^{207}Pb/^{206}Pb$ dates yield a weighted mean of 1580.21 ± 0.40 Ma (MSWD = 1.10, probability of fit = 0.36, Fig. 3c).

Central Gawler Craton

Zircon from 2053554 (Cooladding Rock Hole) is elongate with sector and oscillatory zoning (Fig. 2d). Six $^{207}Pb/^{206}Pb$ dates yield a weighted mean of 1586.49 ± 0.62 Ma (MSWD = 0.71, probability of fit = 0.61, Fig. 3d).

Western Gawler Craton

Zircon from 2115491 (NDR 13, Fowler Domain) is inclusion rich and elongate with strong oscillatory zoning (Fig. 2e). Three of the six $^{207}Pb/^{206}Pb$ dates yield a weighted mean age of 1579.37 ± 1.57 Ma (MSWD = 0.60, probability of fit = 0.55), which is interpreted to be the crystallisation age of the granite. Three older analyses, one of which is 0.5% discordant (Appendix 2, Fig. 3e), are interpreted as being from inherited grains, although their chemistry (Th/U) and morphology do not notably differ from the younger grains.

DISCUSSION

Due to its economic importance, the c. 1595 – 1575 Ma Hiltaba Event has been dated more than any other time slice of South Australia's geological history. Prior to recent high-precision CA-TIMS dating, the magmatic crystallisation age of over 200 samples of granite and volcanic rocks have been determined using a variety of radiometric dating techniques, including multi-zircon/apatite/titanite IDTIMS, SHRIMP, LA-ICPMS, Ar-Ar and Kober Pb evaporation. On average, the uncertainty in these analytical methods is 0.75% at the 95% confidence level, which corresponds to ~12 million years (Appendix 3). Determining the duration of volcanism and magmatism and establishing an internal stratigraphy for the Gawler LIP has therefore been impossible. Despite the large error bars on the dates, however, some broad spatial trends can be discerned (Fig. 4):

- The Hiltaba Suite and GRV are oldest in the Olympic Dam area.
- Magmatism is youngest in the Mt Painter region.
- Most of the magmatism occurs between c. 1595–1575 Ma. About 14% of the dates are younger, between c. 1575–1545 Ma (Fig. 4). The younger granites are mainly in the Mt Painter and Mt Babbage Inliers, but also occur in the Yorke Peninsula, Peake and Denison Ranges and Fowler Domain, all located on the edges of the Gawler LIP and associated with contemporary metamorphism and deformation.
- There appears to be a westward younging in the ages.

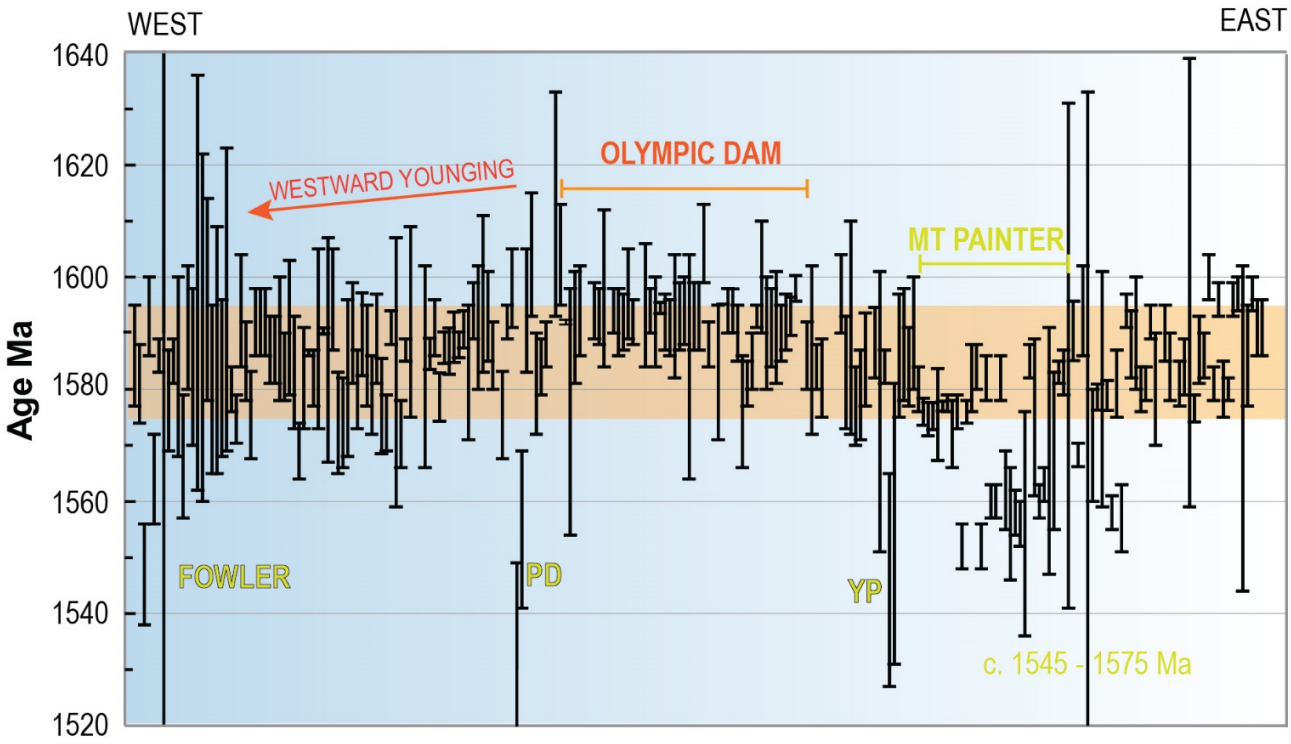

Figure 4. Magmatic ages for the Hiltaba Event, ordered from west to east. Most of the ages lie within the c. 1595–1575 Ma range, represented by the broad orange band. PD = Peake and Denisons, YP = Yorke Peninsula. All data used in this figure are presented in Appendix 3. CA-TIMS dates are excluded.

Box whisker plots, which can be used to compare the statistics of different populations, provide a better visual tool for distinguishing spatial variation in the magmatic ages across the LIP. These plots suggest that magmatism originated in the Olympic Dam region, then propagated radially outward, with younging occurring across north, southeast and west transects (Fig. 5). A contour map of the ages also illustrates this pattern (Fig. 6a).

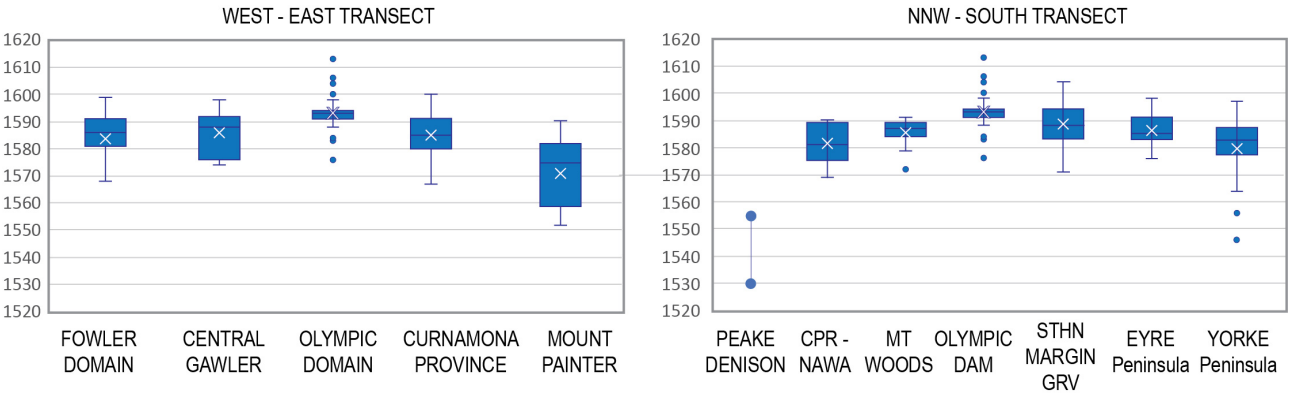

Figure 5. Box and Whisker plots comparing the range of magmatic ages across domains of the Gawler Craton, Curnamona Province and Mt Painter Inlier. The white crosses represent the mean of the populations and the blue horizontal line represents the median. CA-TIMS dates are excluded.

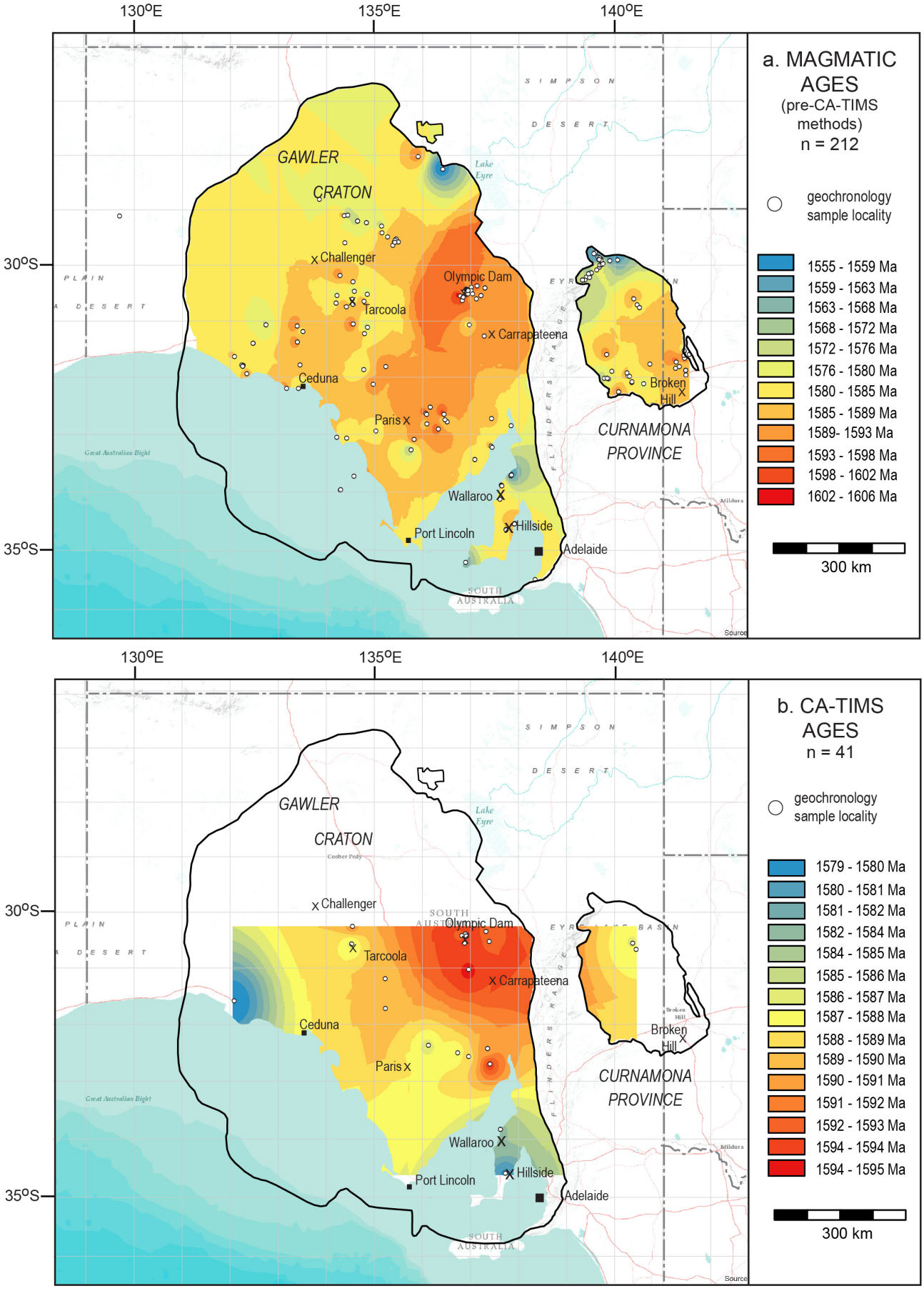

Figure 6. Contour maps of the magmatic ages show the progression of magmatism. Magmatism initiated in the Olympic Dam region, then progressed radially outward, in a temporal pattern suggestive of a rising and flattening plume head. **(a)** All data excluding CA-TIMS dates. **(b)** High-precision CA-TIMS dates.

HIGH-PRECISION CA-TIMS DATING

By careful control of laboratory conditions, particularly by reducing environmental Pb contamination, the CA-TIMS method is able to reduce analytical uncertainties to <0.05%, resolving ages to within one million years (e.g. Mattinson 2005, Metcalfe et al. 2015, Schaltegger et al. 2015). Recent studies have utilised high-precision CA-TIMS dating to successfully determine the relative timing of volcanism, magmatism and mineralisation in the Olympic Dam deposit (Cherry et al. 2018, Courtney Davies et al. 2019, 2020). These studies illustrate the important role that high-precision dating can play in developing mineral system models at the deposit scale. On a larger scale, high-precision dates for the volcanics (Jagodzinski et al. 2016, in prep) and granites (Reid et al. 2021, this study) of the Gawler LIP enable the accuracy of the less precise dates to be assessed and can either validate or negate the spatial trends observed in the larger dataset represented in Fig. 4.

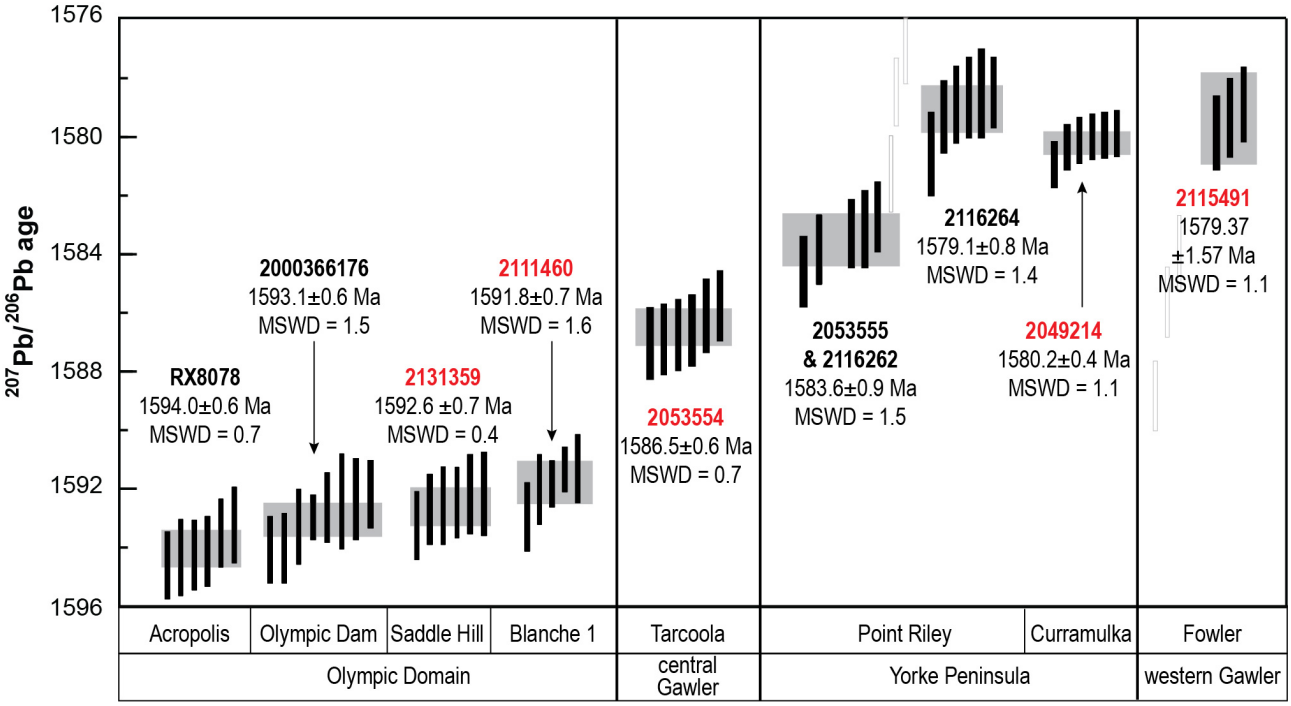

Figure 7. Plot of CA-TIMS $^{207}Pb/^{206}Pb$ dates from zircon. The five samples from this study (red) are plotted with other published CA-TIMS dates (see Table 1) to show the range and spatial variation of emplacement ages for the Hiltaba Suite. Individual error bars are 2σ. The weighted mean dates and their errors (95% confidence interval) are represented by a grey box behind the error bars. White error bars indicate analyses excluded from the mean age calculations.

Figure 7 compares high-precision ages for the Hiltaba Suite from the northern Olympic Domain, encompassing the Olympic Dam deposit and surrounding prospects, Yorke Peninsula to the south, and the central and western Gawler Craton.

Sample 2131359 (DDH BRD1) from the Saddle Hill prospect east of Olympic Dam is a biotite granite with an emplacement age of 1592.62 ± 0.66 Ma. West of Olympic Dam, granite from DDH Blanche 1, represented by sample 2111460, was emplaced at 1591.79 ± 0.74 Ma. These dates are younger than the range of published dates for the Roxby Downs Granite (1595.97 ± 0.94 Ma – 1592.68 ± 1.26 Ma, Courtney-Davies et al. 2020, Cherry et al. 2018), and the Hiltaba Granite at Acropolis (1594.04 ± 0.64 Ma, McPhie et al. 2020), but not significantly.

Granites dated on the Yorke Peninsula are considerably younger. At Point Riley, two samples of strongly and weakly foliated Tickera Granite, 2166262 (1584.22 ± 0.83 Ma) and 2053555 (1582.66 ± 1.42 Ma), constrain the timing of ductile deformation to c. 1583 Ma, synchronous with granite

emplacement. A third sample from an undeformed miarolitic alkali-feldspar granite dyke that cuts the two earlier phases was intruded about 3.5 million years later at 1579.05 ± 0.81 Ma (sample 2166264). The mafic component of the Hiltaba Suite in the Yorke Peninsula, represented by the Curramulka Gabbronorite, has an age of 1580.21 ± 0.4 Ma. The gabbronorite is significantly younger than the Tickera Granite and closer in age to the undeformed late-stage alkali-feldspar granite at Point Riley. As the gabbronorite also displays a tectonic foliation, this indicates that deformation, coupled with metamorphism, continued as late as, or later than, c. 1580 Ma in the central Yorke Peninsula. These high-precision dates indicate that magmatism and deformation in the Yorke Peninsula occurred approximately 10 to 12 million years after emplacement of the Roxby Downs granite at Olympic Dam, although both areas lie within the same Olympic Cu-Au Province (Skirrow et al. 2002, Skirrow et al. 2007) along the eastern margin of the Gawler Craton (Fig. 1).

In the central-western Gawler Craton, sample 2053554, representing the Hiltaba Suite at Tarcoola in the Central Gawler Gold Province (Ferriss and Schwarz 2003) is also significantly younger than granites of the Olympic Domain at 1586.49 ± 0.62 Ma. The easternmost sample 2115491, from the Fowler Domain, is the youngest with an emplacement age of 1579.37 ± 1.57 Ma.

Contouring the high-precision CA-TIMS ages for the Gawler LIP (Fig. 6b, Appendix 3) produces the same radially-younging pattern with the Olympic Dam region as the locus, validating the spatial trends observed in the larger dataset of less precise ages (Fig. 6a).

The high-precision CA-TIMS dates also confirm that while both volcanism and magmatism were initiated at c. 1595 Ma, magmatic intrusion was more prolonged (Fig. 8). Following cessation of volcanism at c.1586.5 Ma (Jagodzinski et al. in prep), the CA-TIMS dates indicate that intrusion of the Hiltaba Suite granites continued at least another 8 million years, with the youngest granite dated in the Fowler Domain at 1579.37 ± 1.57 Ma confirming the entire thermal event lasted at least 16 million years. This validates prior knowledge, as Hiltaba-aged magmatism is generally referred to as a c.1595–1575 Ma event.

However, according to the larger dataset of lower-precision dates (Fig. 8b), about 15% of the granite ages are c. 1575–1545 Ma, forming a younger tail on the age distribution (Fig. 8b). This suggests that granite emplacement continued another 40 million years after volcanism, making the Gawler LIP a much longer-lived event of about 50 million years. These younger granites are mainly in the Mt Painter, Mt Babbage Inliers, but also occur in the Curnamona Province, Yorke Peninsula, Peake and Denison Inlier and Fowler Domain, all located on the margins of the Gawler LIP and associated with contemporary metamorphism and deformation.

Some consideration needs to be made as to whether these younger granites are part of the Hiltaba Suite or belong to a younger tectonic event with different geodynamic drivers (Reid et al. 2021b).

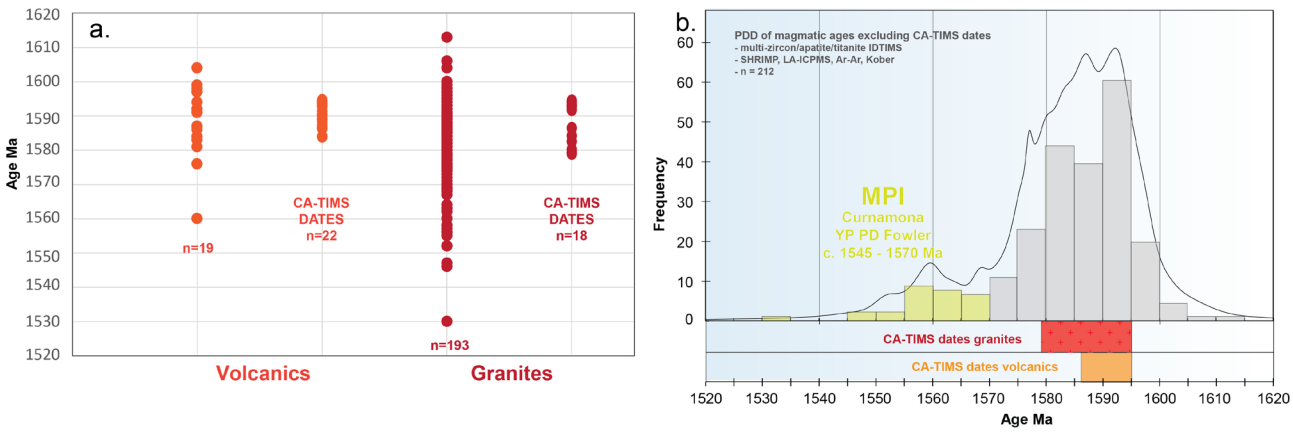

Figure 8. **(a)** Plot comparing all CA-TIMS zircon dates for the Gawler LIP with the lower precision dates from other methods listed in Fig. 8b. **(b)** The range of CA-TIMS dates for volcanics and granites of the Gawler LIP, plotted with a probability density diagram (PDD) of dates determined by the lower precision methods for comparison.

ACKNOWLEDGEMENTS

Thanks to our GSSA colleague Tom Wise for assisting with the preparation of this manuscript, drafting some of the location maps in Appendix 1. Thanks to Dr Simon Bodorkos of Geoscience Australia for advice on the propagation of errors in the data set.

REFERENCES

Allen SR, McPhie J, Ferris G and Simpson C. 2008. Evolution and architecture of a large felsic Igneous Province in western Laurentia: The 1.6 Ga Gawler Range Volcanics, South Australia. *Journal of Volcanological and Geothermal Research* 172, 132–147.

Betts PG, Giles D, Foden J, Schaefer BF, Mark G, Pankhurst MJ, Forbes CJ, Williams HA, Chalmers NC and Hills QG. 2009. Mesoproterozoic plume-modified orogenesis in eastern Precambrian Australia. *Tectonics* 28, p. TC3006.

Blisset AH, Creaser RA, Daly SL, Flint RB and Parker AJ. 1993. Gawler Range Volcanics. In JF Drexel, WV Preiss and AJ Parker eds, *The geology of South Australia, Volume 1, The Precambrian,* Bulletin 54. Geological Survey of South Australia, Adelaide, pp. 107–124.

Bockmann MJ, Wilson TC, Pawley MJ, Payne JL and Dutch RA. 2019. *LA–ICP–MS geochronology from the Tarcoola Goldfield region 2018–2019*. Report Book 2019/00015. Department for Energy and Mining, South Australia, Adelaide.

Brotodewo A, Tiddy CJ, Reid A, Wade C and Conor C. 2018. Relationships between magmatism and deformation in northern Yorke Peninsula and southeastern Proterozoic Australia. *Australian Journal of Earth Sciences* 65, 619–641.

Budd AR 2006. *The Tarcoola Goldfield of the Central Gawler Gold Province, and the Hiltaba Association Granites, Gawler Craton, South Australia.* PhD thesis unpublished, Australian National University, Canberra.

Budd AR and Fraser G 2004. Geological relationships and $^{40}Ar/^{39}Ar$ age constraints on gold mineralisation at Tarcoola, central Gawler gold province, South Australia. *Australian Journal of Earth Sciences* 51(5), 685–699.

Budd AR and Skirrow RG. 2007. The nature and origin of gold deposits of the Tarcoola goldfield and implications for the Central Gawler Gold Province, South Australia. *Economic Geology* 102, 1541–1563.

Cherry AR, Ehrig K, Kamenetsky VS, McPhie J, Crowley JL and Kamenetskya MB. 2018. Precise geochronological constraints on the origin, setting and incorporation of ca. 1.59 Ga surficial facies into the Olympic Dam Breccia Complex, South Australia. *Precambrian Research* 315, 162–178.

Conor CHH, Raymond OL, Baker T, Teale G, Say P and Lowe G. 2010. Alteration and mineralisation in the Moonta-Wallaroo copper-gold mining field region, Olympic Domain, South Australia. In TM Porter ed, *Hydrothermal iron oxide copper-gold and related deposits: A global perspective. Advances in the understanding of IOCG deposits.* PGC Publishing, Adelaide, pp. 147–170.

Conor CHH. 1995. Moonta-Wallaroo region, An interpretation of the geology of the Maitland and Wallaroo 1:100 000 sheet areas. Open File Envelope 08886. Department for Primary Industries and Resources South Australia, Adelaide.

Constable S, Fairclough MC and Gum J 2005. Nickel mineralisation models in the Fowler Domain and Musgrave Province - applying the Thompson Nickel Belt as an analogue. *MESA Journal* 39:14–21.

Cook NDJ, Fanning CM and Ashley PM 1994. New geochronological results from the Willyama Supergroup, Olary Block, South Australia. In Australian Research on Ore Genesis Symposium, Adelaide, South Australia, December 12-14. Australian Mineral Foundation Inc., Glenside, South Australia.

Courtney-Davies L, Tapster SR, Ciobanu CL, Cook NJ, Verdugo-Ihl MR, Ehrig K, Kennedy AK, Gilbert SE, Condon DJ and Wade BP. 2019. A multi-technique evaluation of hydrothermal hematite U-Pb isotope systematics: implications for ore deposit geochronology. *Chemical Geology* 513, 54–72.

Courtney-Davies L, Ciobanu CL, Tapster SR, Cook NJ, Ehrig K, Crowley JL, Verdugo-Ihl MR, Wade BP and Condon DJ. 2020. Opening the magmatic-hydrothermal window: high-precision U-Pb Geochronology of the Mesoproterozoic Olympic Dam Cu-U-Au-Ag Deposit, South Australia. *Economic Geology* 115 (8): 1855–1870.

Cowley WM. 2006. Solid geology of South Australia: peeling away the cover. *MESA Journal* 43, 4-15.

Cowley WM, Conor CHH and Zang W. 2003. New and revised Proterozoic stratigraphic units on northern Yorke Peninsula. *MESA Journal* 29, 46-58.

Creaser RA 1989. The Geology and Petrology of Middle Proterozoic Felsic Magmatism of the Stuart Shelf, South Australia. PhD thesis, La Trobe University.

Creaser RA and Cooper JA. 1993. U-Pb Geochronology of Middle Proterozoic Felsic Magmatism surrounding the Olympic Dam Cu-U-Au-Ag and Moonta Cu-Au-Ag deposits, South Australia. *Economic Geology* 88, 186–197.

Creaser RA and Fanning CM. 1993. A U-Pb zircon study of the Mesoproterozoic Charleston Granite, Gawler Craton, South Australia. *Australian Journal of Earth Sciences* 4840, 519–526.

Crowley JL, Schoene B and Bowring SA. 2007. U-Pb dating of zircon in the Bishop Tuff at the millennial scale: *Geology* 35: 1123-1126.

Cutts K, Hand M and Kelsey DE. 2011. Evidence for early Mesoproterozoic (ca. 1590 Ma) ultrahigh-temperature metamorphism in southern Australia. *Lithos* 124, 1–16.

Daly SJ, Fanning CM and Fairclough MC. 1998. Tectonic evolution and exploration potential of the Gawler Craton, South Australia. *Australian Geological Survey Organisation Journal of Australian Geology and Geophysics* 17, 145–168.

Doublier MP, Dutch, RA, Clark D, Pawley MJ, Fraser GL, Wise TW, Kennett BLN, Reid AJ, Spaggiari CV, Calvert AJ, van der Wielen S, Dulfer H, Bendall BR, Thiel S and Holzschuh J. 2015. Interpretation of the western Gawler Craton section of seismic line 13GA-EG1. In *13GA-EG1E Seismic and Magnetotelluric Workshop 2015 Extended Abstracts*. Report Book 2015/00029, pp 28–40. South Australia Department of State Development, South Australia, Adelaide.

Dougherty-Page JS and Foden J 1996. Pb—Pb zircon evaporation date for the Charleston Granite, South Australia: Comparisons with other zircon geochronology techniques. *Australian Journal of Earth Sciences* 43:2, 133-137.

Elburg MA, Bons PD, Dougherty-Page J, Janka CE, Neumann N and Schaefer B. 2001. Age and metasomatic alteration of the Mount Neill Granites at Nooldoonooldoona Waterhole, Mount Painter Inlier, South Australia. *Australian Journal of Earth Sciences* 48, 721–730.

Fanning CM 1987. U-Pb zircon geochronology. Amdel Report G6861/87 (unpublished).

Fanning CM 1990. Single grain U-Pb zircon dating of a porphyritic volcanic from the Cultana Complex. Prise geochronology report 89-080 (unpublished).

Fanning CM 1995. Geochronological synthesis of southern Australia, Part 1: the Curnamona Province, Open file Envelope 08918. Department of Primary Industries and Resources South Australia, Adelaide.

Fanning CM 1997. Geochronological synthesis of southern Australia, Part 2: The Gawler Craton, Open File Envelope 08918. Department of Primary Industries and Resources South Australia, Adelaide.

Fanning CM, Ashley PM, Cook NDJ, Teale GS and Conor CCH. 1998. A geochronological perspective of crustal evolution in the Curnamona Province. In Gibson, G. M. Broken Hill Exploration Initiative, Australian Geological Survey Organisation 1998/25, 30-37

Fanning CM, Flint RB, Parker AJ, Ludwig KR and Blissett AH. 1988. Refined Proterozoic evolution of the Gawler Craton, South Australia, through U-Pb zircon geochronology. *Precambrian Research* 40 (41), 363–386.

Fanning CM, Reid AJ and Teale GS 2007. *A geochronological framework for the Gawler Craton, South Australia*, Geological Survey, Bulletin 55. Department of Primary Industries and Resources South Australia, Adelaide.

Ferris GM. 2001. The Geology and Geochemistry of Granitoids in the Childara Region, Western Gawler Craton, South Australia: Implications for the Proterozoic tectonic History of the Western Gawler Craton, and Development of Lode-style Gold Mineralization at Tunkillia. Masters of Exploration Geology, Australia. University of Tasmania, Hobart.

Finlay J. 1993. Structural Interpretation of the Mount Woods Inlier. Honours thesis, Monash University, Melbourne, Australia.

Flint RB 1993. Hiltaba Suite. In JF Drexel, WV Preiss and AJ Parker eds, *The geology of South Australia, Volume 1, The Precambrian,* Bulletin 54. Geological Survey of South Australia, Adelaide, pp. 127–131.

Fraser G and Lyons P. 2006. Timing of Mesoproterozoic tectonic activity in the northwestern Gawler Craton constrained by $^{40}Ar/^{39}Ar$ geochronology. *Precambrian Research* 151, 160-184

Fraser G and Neumann N 2010. *New SHRIMP U-Pb zircon ages from the Gawler Craton and Curnamona Province, South Australia 2008 - 2010*. Geoscience Australia Record 2010/16. Geoscience Australia, Canberra.

Fraser GL, Reid AJ and Stern R. 2012. Timing of deformation and exhumation across the Karari Shear Zone, north-western Gawler Craton, South Australia. *Australian Journal of Earth Sciences* 59, 547–570.

Fraser GL, Skirrow RG, Schmidt-Mumm A and Holm O. 2007. Mesoproterozoic gold in the central Gawler Craton, South Australia: geology, alteration, fluids, and timing. *Economic Geology* 102, 1511–1539.

Gerstenberger H and Haase G. 1997. A highly effective emitter substance for mass spectrometric Pb isotope ratio determinations: *Chemical Geology* 136: 309-312.

Giles CW. 1988. Petrogenesis of the Proterozoic Gawler Range Volcanics, South Australia. *Precambrian Research* 40 (41), 407–427.

Hand M, Reid A and Jagodzinski L 2007. Tectonic framework and evolution of the Gawler Craton, Southern Australia. *Economic Geology* 102(8):1377–1395.

Hiess J, Condon DJ, McLean N and Noble SR. 2012. 238U/235U systematics in terrestrial uranium-bearing minerals: *Science* 335: 1610-1614.

Holm O. 2004. *New geochronology of the Mount Woods Inlier and the Central Gawler Gold Province: Gawler Craton State of Play, Adelaide, Australia, 2004*, Report Book 2004/00018. Department of Primary Industries and Resources South Australia, Adelaide, p3.

Howard KE, Hand M, Barovich KM, Payne JL and Belousova EA. 2011. U-Pb, Lu-Hf and Sm-Nd isotopic constraints on provenance and depositional timing of metasedimentary rocks in the western Gawler Craton: implications for Proterozoic reconstruction models. *Precambrian Research* 184, 43–62.

Ismail R, Ciobanu CL, Cook NJ, Teale GS, Giles D, Mumm AS and Wade, B. 2014. Rare earths and other trace elements in minerals from skarn assemblages, Hillside iron oxide–copper–gold deposit, Yorke Peninsula, South Australia. *Lithos* 184–187, 456-477.

Jaffey AH, Flynn KF, Glendenin LE, Bentley WC and Essling AM 1971, Precision measurements of half-lives and specific activities of ^{235}U and ^{238}U. *Physical Review* C4: 1889–1906.

Jagodzinski EA. 2005. Compilation of SHRIMP U-Pb geochronological data – Olympic Domain, Gawler Craton, South Australia, 2001–2003. *AGSO Record* 2005/20, pp. 197.

Jagodzinski EA. 2014. The age of magmatic and hydrothermal zircon at Olympic Dam, Australian Earth Sciences Convention, Volume 110. Geological Society of Australia Abstracts, Newcastle, Australia, pp. 260.

Jagodzinski EA and Fricke CE 2010. *Compilation of new SHRIMP U-Pb geochronological data for the southern Curnamona Province, South Australia, 2010*, Report Book 2010/00014. Department of Primary Industries and Resources South Australia, Adelaide.

Jagodzinski EA and Reid AJ. 2010. New zircon and monazite geochronology using SHRIMP and LA-ICPMS, from recent GOMA drilling, on samples from the northern Gawler Craton. In Korsch RJ and Kositcin N eds. GOMA (Gawler-Officer Basin-Musgrave Province-Amadeus Basin Seismic and MT Workshop 2010, Geoscience Australia Record 2010/39, 108–117.

Jagodzinski EA and Reid AJ. 2015. PACE *Geochronology: Results of collaborative geochronology projects 2013–2015*, Report Book 2015/00003. Department of the Premier and Cabinet, South Australia, Adelaide.

Jagodzinski EA and Reid AJ. 2016. *U-Pb geochronological data from drill holes Nundroo 3 DDH and Nundroo 2 CCH, Fowler Domain, western Gawler Craton.* Report Book 2016/00010. Department of State Development, South Australia, Adelaide.

Jagodzinski EA, Black LP, Frew RA, Foudoulis C, Reid AJ, Payne J, Zang W and Schwarz MP. 2006. *Compilation of SHRIMP U–Pb Geochronological Data for the Gawler Craton, South Australia 2005–2006.* Report Book 2006/00020. Primary Industries and Resources South Australia, Adelaide.

Jagodzinski EA, Crowley JL, Reid AJ, Wade CE and Bockmann MJ. 2021. *High precision Ca-TIMS dating of the Hiltaba Suite, Gawler Craton.* Report Book 2021/00002. Department for Energy and Mining, South Australia, Adelaide.

Jagodzinski EA, Reid A and Gribbin G. 2019. *U-Pb geochronological data from the Fowler Domain, western Gawler Craton*, Report Book 2019/00018. Department for Energy and Mining, South Australia, Adelaide.

Jagodzinski EA, Reid AJ, Chalmers NC, Swain S, Frew RA and Foudoulis C. 2007. *Compilation of SHRIMP U–Pb Geochronological Data for the Gawler Craton, South Australia, 2007.* Report Book 2007/00021. Department of Primary Industries and Resource s, South Australia, Adelaide.

Jagodzinski EA, Reid AJ, Crowley JL, McAvaney S and Wade CE. 2016. Precise zircon U-Pb dating of a Mesoproterozoic silicic large igneous province: the Gawler Range Volcanics and Benagerie Volcanic Suite, South Australia: Australian Earth Sciences Convention, Adelaide, 26-30 June 2016.

Jagodzinski EA, Reid AJ, Crowley JL, McAvaney S and Wade CE. in prep. Precise zircon U-Pb dating of a Mesoproterozoic silicic large igneous province: the Gawler Range Volcanics and Benagerie Volcanic Suite, South Australia.

Jagodzinski EA, Szpunar M, Meaney K and Fraser G. 2020. *SHRIMP U-Pb dating of the Barossa Complex, South Australia: exploring tectonic links between the Gawler Craton and Curnamona Province.* Report Book 2020/00017. Department of the Premier and Cabinet, South Australia, Adelaide.

Janka C, Bons P, Elburg M and Dougherty-Page J 1999. Reassessment of the evolution of the Mount Painter Inlier, South Australia. *Last conference of the millennium: the Specialist Group in Tectonics and Structural Geology Field Conference, Halls Gap, Victoria, abstract*, Abstracts 53. Geological Society of Australia, Sydney, pp. 112–113.

Johnson GI. 1980. The geology of the Mount Babbage Inlier, northern Mount Painter province, South Australia -a petrological, geochemical and geochronological study. University of Adelaide, Adelaide.

Johnson JP and Cross KC. 1995. U-Pb geochronological constraints on the genesis of the Olympic Dam Cu-U-Au-Ag deposit, South Australia. *Economic Geology* 90, 1046–1063.

Johnson JP. 1993. The geochronology and radiogenic isotope systematics of the Olympic Dam copper-uranium-gold-silver deposit, South Australia. PhD Thesis, The Australian National University. Canberra, Australia.

Kober B. 1986. Whole-grain evaporation for $^{207}Pb/^{206}Pb$-age-investigations on single zircons using a double-filament thermal ion source. *Contributions to Mineralogy and Petrology* 93, 482 – 490.

Kontonikas-Charos A, Ciobanu CL and Cook NJ. 2014. Albitization and redistribution of REE and Y in IOCG systems: Insights from Moonta-Wallaroo, Yorke Peninsula, South Australia. *Lithos* 208-209, 178-201.

Krogh TE. 1973. A low contamination method for hydrothermal decomposition of zircon and extraction of U and Pb for isotopic age determination: *Geochimica et Cosmochimica Acta* 37: 485-494.

Kromkhun K. 2010. Petrogenesis of high heat producing granite: implication for Mt Painter Province, South Australia. PhD thesis, University of Adelaide.

Ludwig KR 2003. *Isoplot 3.00 - a geochronological toolkit for Microsoft Excel.* Berkeley Geochronology Center Special Publication No. 4.

Ludwig KR and Cooper JA. 1984. Geochronology of Precambrian granites and associated U-Ti-Th mineralization, northern Olary province, South Australia. *Contributions to Mineralogy and Petrology* 86, 298–308.

Mattinson JM. 2005. Zircon U-Pb chemical abrasion ("CA-TIMS") method: combined annealing and multi-step partial dissolution analysis for improved precision and accuracy of zircon ages: *Chemical Geology* 220:47-66.

McPhie J, Ehrig K, Kamenetskya MB, Crowley JL and Kamenetsky VS. 2020. Geology of the Acropolis prospect, South Australia, constrained by high-precision CA-TIMS ages. *Australian Journal of Earth Sciences* 67, 699–716.

Metcalfe I, Crowley JL, Nicoll, R and Schmitz M. 2015. High-precision U-Pb CA-TIMS calibration of Middle Permian to Lower Triassic sequences, mass extinction and extreme climate-change in eastern Australian Gondwana. *Gondwana Research* 28, 61 – 81.

Meyer G. 2006. Blanche 001 Geothermal Exploration Hole Completion Report. 08098/000. https://sarigbasis.pir.sa.gov.au/WebtopEw/ws/samref/sarig1/wci/Record?r=0&m=1&w=catno=2028485

Morris BJ, Hill PW and Ferris G 1994. *Barton Bedrock Drilling Project*. Report Book 94/00019. Primary Industries and Resources South Australia, Adelaide.

Mortimer GE, Cooper JA, Paterson HL, Cross K, Hudson GRT and Uppill RK. 1988. Zircon U-Pb Dating in the Vicinity of the Olympic Dam Cu-U-Au Deposit, Roxby Downs, South Australia. *Economic Geology* 83, 694-709.

Neumann NL and Korsch RJ 2014. *SHRIMP U–Pb zircon ages from Kutjara 1 and Mulyawara 1, northwestern South Australia*, Record 2014/05. Geoscience Australia, Canberra.

Nutman AP and Ehlers K. 1998. Evidence for multiple Palaeoproterozoic thermal events and magmatism adjacent to the Broken Hill Pb-Zn-Ag orebody, Australia. *Precambrian Research* 90, 203-238

Page RW and Sun SS. 1998. Aspects of geochronology and crustal evolution in the Eastern Fold Belt, Mt Isa Inlier. *Australian Journal of Earth Sciences* 45, 343–361.

Page RW, Stevens BPJ and Gibson GM. 2005. Geochronology of the sequence hosting the Broken Hill Pb-Zn-Ag orebody, Australia. *Economic Geology* 100, 633–661.

Page RW, Stevens BPJ, Gibson GM and Conor CHH 2000. Geochronology of Willyama Supergroup rocks between Olary and Broken Hill, and comparison to Northern Australia. *Broken Hill Exploration Initiative: abstracts of papers presented at the May 2000 conference in Broken Hill*, Record 2000/10 (GeoCat 33090). Australian Geological Survey Organisation, Canberra, pp. 72–75.

Page RW. 2006. Unpublished data. Geoscience Australia SHRIMP U-Pb Geochronology Interim Data Release July 2007: http://www.ga.gov.au/oracle/ozchron/index.jsp

Pankhurst MJ, Schaefer BF, Betts PG, Phillips, N and Hand M. 2011b. A Mesoproterozoic continental flood rhyolite province: an end member example of the large igneous province clan. *Solid Earth* 2, 25–33.

Parker AJ. 1983. *Whyalla*, South Australia, Map Sheet SI53-8, Geological Atlas 1:250 000 Series. Geological Survey of South Australia, Adelaide.

Payne JL, Ferris G, Barovich KM and Hand M. 2010. Pitfalls of classifying ancient magmatic suites with tectonic discrimination diagrams: An example from the Paleoproterozoic Tunkillia Suite, southern Australia. *Precambrian Research* 177, 227–240.

Payne JL 2008. Palaeo- to Mesoproterozoic evolution of the Gawler Craton, Australia: geochronological, geochemical and isotopic constraints. PhD thesis, University of Adelaide, Adelaide, Australia.

Purvis AC. 2005. MINERALOGICAL REPORT No. 8777. Unpublished report Pontifex & Associates Pty. Ltd (available in Meyer G. 2006).

Reid AJ. 2019. The Olympic Cu-Au Province, Gawler Craton: a review of the lithospheric architecture, geodynamic setting, alteration systems, cover successions and prospectivity. *Minerals* 9, 371.

Reid AJ and Dutch R 2012. *Reconnaissance LA-ICPMS zircon U-Pb geochronology of crystalline basement outcrops on the FOWLER 1:250000 mapsheet*, Report Book 2012/00013. Department for Manufacturing, Innovation, Trade, Resources and Energy, South Australia, Adelaide.

Reid AJ and Fabris A. 2012. *Age of host rocks at the Chianti Prospect Cu-Au, eastern Gawler Craton from zircon U-Pb geochronology*, Report Book 2012/00014. Department for Manufacturing, Innovation, Trade, Resources and Energy, South Australia, Adelaide.

Reid AJ and Jagodzinski EA (Editors). 2011. *PACE Geochronology: Results of collaborative geochronology projects [performed during] 2009-2010.* Report Book 2011/00003. Department for Manufacturing, Innovation, Trade, Resources and Energy, South Australia, Adelaide.

Reid AJ and Jagodzinski EA (Editors). 2012. *PACE Geochronology: Results of collaborative geochronology projects 2011–12.* Report Book 2012/00012. Department for Manufacturing, Innovation, Trade, Resources and Energy, South Australia, Adelaide.

Reid AJ, Halpin, JA and Dutch RA. 2019. Timing and style of high-temperature metamorphism across the Western Gawler Craton during the Paleo- to Mesoproterozoic. *Australian Journal of Earth Sciences* 66:8, 1085-1111.

Reid AJ, Hand M, Jagodzinski EA, Kelsey D and Person N.,2008. Paleoproterozoic orogenesis in the southeastern Gawler Craton, South Australia. *Australian Journal of Earth Sciences* 55, 449–471.

Reid AJ, Pawley MJ, Jagodzinski EA and Dutch RA 2016. *Magmatic processes of the St Peter Suite, Gawler Craton: New U-Pb geochronological data and field observations*, Report Book 2016/00012. Department of State Development, South Australia, Adelaide.

Reid AJ, Payne JL and Wade B. 2006 A new geochronological capability for South Australia: U-Pb dating via LA-ICPMS. MESA Journal 42, 27–31. Department of Primary Industries and Resources South Australia, Adelaide.

Reid AJ, Tiddy C, Jagodzinski EA, Crowley JL, Conor C, Brotodewo A and Wade C. 2021. *Precise zircon U-Pb geochronology of Hiltaba Suite granites, Point Riley, Yorke Peninsula.* Report Book 2021/00001. Department for Energy and Mining, South Australia, Adelaide.

Reid AJ, Wade CE and Jagodzinski EA. 2021b. Mafic dykes of the southeastern Gawler Craton: c. 1563 Ma magmatism with an enriched mantle source. *Australian Journal of Earth Sciences* in press.

Reid AJ, Zhao Y, Wang T and Zhao X. 2020. *Reconnaissance zircon U-Pb geochronology of the southeastern Olympic Cu-Au Province, South Australia,* Report Book 2020/00015. Department for Energy and Mining, South Australia, Adelaide.

Rusak T. 2011. The Geochemistry of the Early Mesoproterozoic Mafic Rocks in the Northern Gawler Craton. University of Adelaide, Adelaide.

Schaltegger U, Schmitt AK and Horstwood MSA. 2015. U–Th–Pb zircon geochronology by ID-TIMS, SIMS, and laser ablation ICP-MS: recipes, interpretations, and opportunities. *Chemical Geology* 402, 89 – 110.

Schmitz M.D. and Schoene B. 2007, Derivation of isotope ratios, errors and error correlations for U-Pb geochronology using ^{205}Pb-^{235}U-(^{233}U)-spiked isotope dilution thermal ionization mass spectrometric data: Geochemistry, Geophysics, Geosystems (G^3) 8, Q08006, doi:10.1029/2006GC001492.

Schwarz M. 2003. *LINCOLN*, South Australia, Map Sheet SI53-11, Geological Atlas 1:250 000 Series, Explanatory Notes. Geological Survey of South Australia, Adelaide.

Sheard MJ, Fanning CM and Flint RB. 1992. Geochronology and definition of Mesoproterozoic volcanics and granitoids of the Mt Babbage Inlier, northern Flinders Ranges. Geological Survey of South Australia *Quarterly Geological Notes* 123, 18–32.

Sheard MJ. 2009. *Explanatory Notes for CALLABONNA 1:250 000 Geological Map, sheet SH 54-6*. South Australia. Report Book 2009/00001. Department of Primary Industries and Resources.

Skirrow RG, Bastrakov EN, Barovich K, Fraser GL, Creaser RA, Fanning CM, Raymond OL and Davidson GJ. 2007. Timing of Iron Oxide Cu-Au-(U) hydrothermal activity and Nd isotope constraints on metal sources in the Gawler Craton, South Australia. *Economic Geology* 102, 1441–1470.

Skirrow RG, van der Weilen SE, Champion DC, Czarnota K and Thiel S. 2018. Lithospheric architecture and mantle metasomatism linked to iron oxide Cu-Au ore formation: multidisciplinary evidence from the Olympic Dam region, South Australia. *Geochemistry*, *Geophysics*, *Geosystems* 19, 2673–2705.

Stewart KP. 1994. High Temperature Felsic Volcanism and the Role of Mantle magmas in Proterozoic crustal Growth, The Gawler Range Volcanic Province. PhD thesis., University of Adelaide, Adelaide, Australia.

Stewart JR and Betts PG 2010. Implications for Proterozoic plate margin evolution from geophysical analysis and crustal-scale modeling within the western Gawler Craton, Australia. *Tectonophysics* 483:151–177.

Teale GS. 1993. Geology of the Mt Painter and Mt Babbage Inliers. In JF Drexel, WV Preiss and AJ Parker eds, *The geology of South Australia, Volume 1, The Precambrian,* Bulletin 54. Geological Survey of South Australia, Adelaide, pp. 149–155.

Teasdale J. 1997. Methods for Understanding Poorly Exposed Terranes: The Interpretive Geology and Tectonothermal Evolution of the Western Gawler Craton. PhD thesis, University of Adelaide, Adelaide, Australia.

Thomas et al. 2008, Thomas JL, Direen NG and Hand M. 2008. Blind orogen: Integrated appraisal of multiple episodes of Mesoproterozoic deformation and reworking in the Fowler Domain, western Gawler Craton, Australia. *Precambrian Research*, 166(1–4), 263–282.

Thornton GD. 1980. Geology, Geochemistry and Geochronology of the Eastern Babbage Block, Mount Painter Province, South Australia. University of Adelaide, Adelaide.

Tiddy CJ and Giles D. 2020. Suprasubduction zone model for metal endowment at 1.60–1.57 Ga in eastern Australia. *Ore Geology Reviews* 122 https://doi.org/10.1016/j.oregeorev.2020.103483

Wade CE, Reid AJ, Wingate MTD, Jagodzinski EA and Barovich, K. 2012. Geochemistry and geochronology of the c. 1585 Ma Benagerie Volcanic Suite, southern Australia: Relationship to the Gawler Range Volcanics and implications for the petrogenesis of a Mesoproterozoic silicic large igneous province. *Precambrian Research* 206–207, 17–35.

Wade CE. 2011. Definition of the Mesoproterozoic Ninnerie Supersuite, Curnamona Province, South Australia. MESA Journal 62, 35–52. Department of Primary Industries and Resources South Australia, Adelaide.

Wade BP, Barovich KM, Hand M, Scrimgeour IR and Close DF. 2006. Evidence for Early Mesoproterozoic arc magmatism in the Musgrave Block, central Australia: implications for Proterozoic crustal growth and tectonic reconstructions of Australia. *Journal of Geology* 114, 43–63.

Wade CE, Payne JL, Barovich KM and Reid AJ. 2019. Heterogeneity of the sub-continental lithospheric mantle and 'non-juvenile' mantle additions to a Proterozoic silicic large igneous province. *Lithos* 340–341, 87–107.

Webb AW, Thomson BP, Blissett AH, Daly SJ, Flint RB and Parker AJ. 1986. Geochronology of the Gawler Craton, South Australia. *Australian Journal of Earth Sciences* 33:2, 119-143.

Wurst AT. 1994. Analyses of late stage, Mesoproterozoic, syn- and post-tectonic, magmatic events in the Moonta Subdomain: implications for Cu-Au mineralisation in the 'Copper Triangle' of South Australia. University of Adelaide. Bsc (Hons) thesis.

Zang WL, Fanning CM, Purvis AC, Raymond OL and Both RA. 2007. Early Mesoproterozoic bimodal plutonism in the southeastern Gawler Craton, South Australia. *Australian Journal of Earth Sciences* 54 (5), 661–674.

Zang WL and Fanning CM. 2001. Age of the Kimban Orogeny revealed—U– Pb dates on the Corny Point Paragenesis, Yorke Peninsula, South Australia. *MESA Journal* 23, 28 – 33.

Zang WL. 2002. *Late Palaeoproterozoic Wallaroo Group and early Mesoproterozoic mineralisation in the Moonta Domain, eastern Gawler Craton, SA*. Report Book 2002/00001. Department of Primary Industries and Resources South Australia, Adelaide.

Zang WL. 2006. *Maitland Special,* South Australia, Map Sheets SI53-12 and portion SI53-16, Geological Atlas 1:250 000 Series, Explanatory Notes. Geological Survey of South Australia, Adelaide.

APPENDIX 1. SAMPLE INFORMATION

2131359: GRANITE SADDLE HILL PROSPECT

Stratigraphic unit:	Hiltaba Suite		
Location GDA94:	721129.63 E	6634853.33 N	Zone 53
Location Lat-Long:	-30.3980914	137.3016807	
250k map sheet	SH5312 ANDAMOOKA		
100k map sheet	6337 Yarrawurta		
Location:	Drillhole BRD1 (number 170020) 816–817 m		
Analyst:	JL Crowley		
Analytical technique:	CA-TIMS Boise State University Idaho		
Interpreted $^{207}Pb/^{206}Pb$ age:	1592.62 ± 0.66 Ma		
Age interpretation:	Magmatic age		

Description

Drillhole BRD 1 (Fig. 9) is in the Saddle Hill prospect, located to the east of Olympic Dam and Andamooka. The drillhole itself lies close to the edge of Lake Torrens (Fig. 10). The area is considered prospective for Olympic Dam-style mineralisation in Mesoproterozoic basement rocks, which are located at depths greater than 525 m below surface.

The Hiltaba Suite in BRD 1 is described as a biotite granite with trace carbonate-chlorite-hematite-pyrite, quartz and hematite veining and minor intrusive alkali syenite. The top 0.7 m of the granite is brecciated, with intensely sericite-chlorite altered granite clasts in chlorite-sericite-hematite matrix (Fig. 11). Below this brecciated interval the granite is fractured. Narrow tectonic breccias with sharp boundaries crosscut the main granite body (Fig. 11). Below 808 m, the granite is mostly massive and coherent, varying from medium-grained and equigranular to medium-coarse grained and porphyritic.

Figure 9. Drill tray containing sample 2131359.

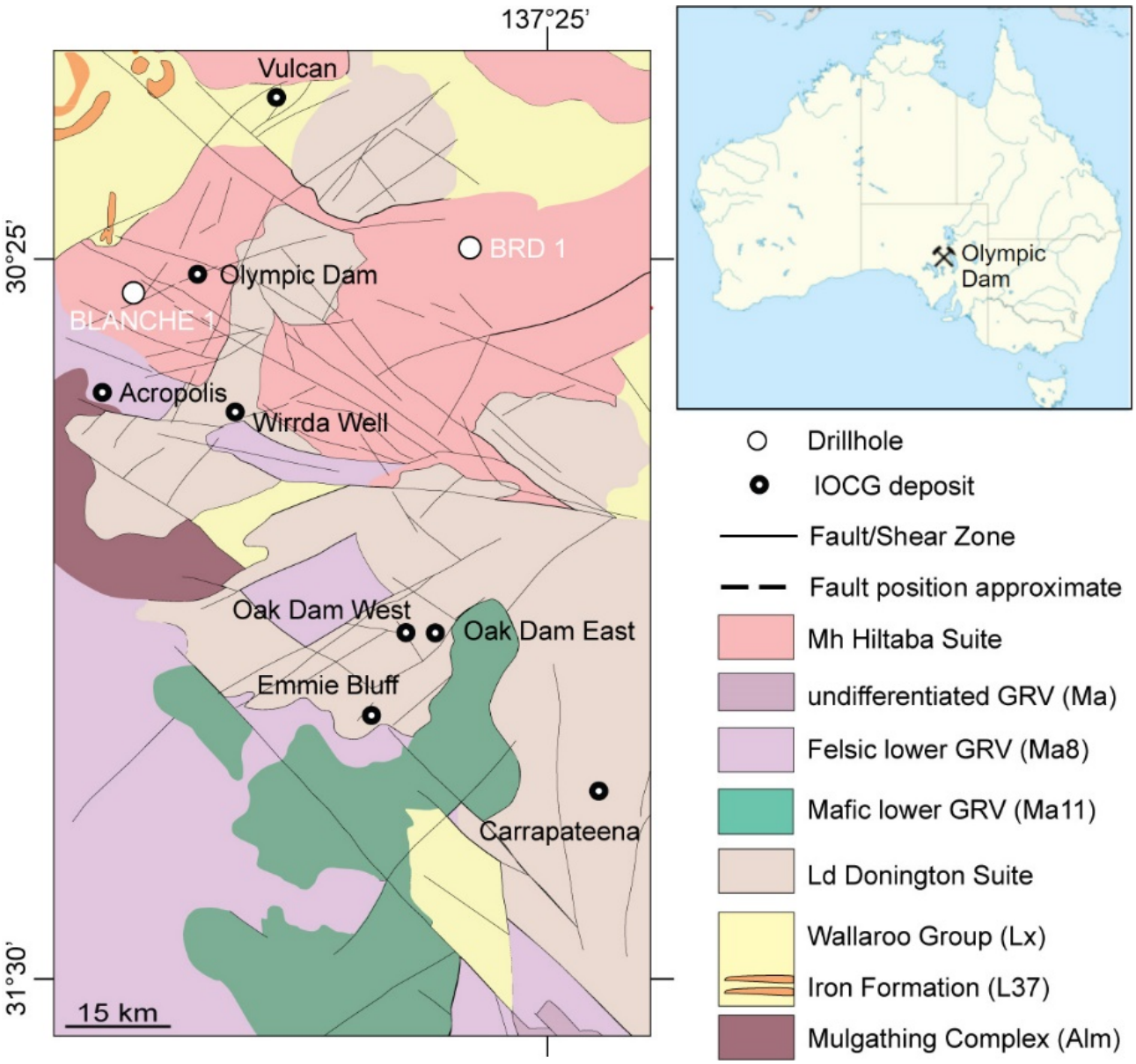

Figure 10. Simplified solid geology interpretation of pre-Neoproterozoic crystalline basement beneath the Stuart Shelf, showing the location of drillholes BRD1 and BLANCHE 1, from which samples 2131359 and 2111460 were obtained.

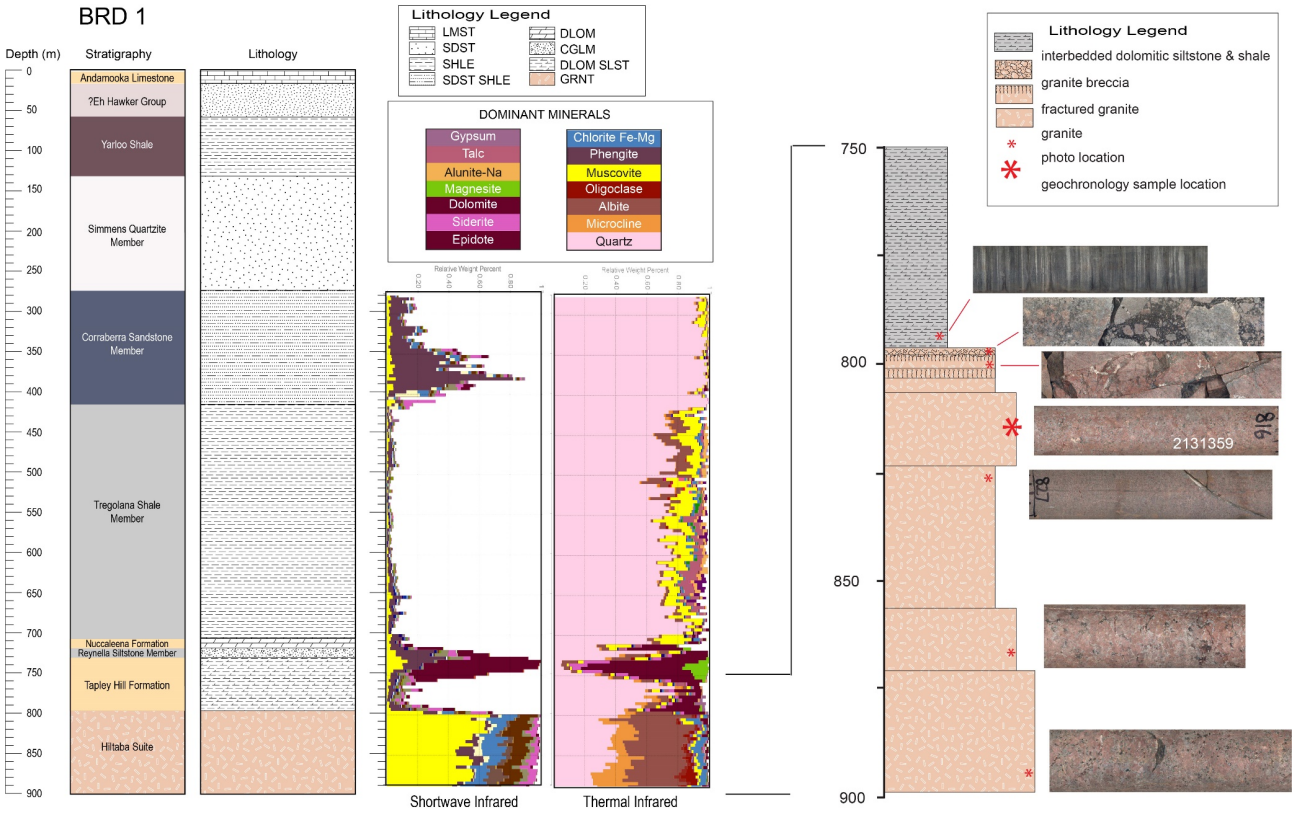

Figure 11. Summary graphic log of drillhole BRD 1. Drill core is NQ (4.7 mm in diameter). View spectral scans in more detail.

Petrography

This sample is a medium grained, equigranular granite (Fig. 12). K-feldspar is red in colour due to hematite alteration and is partly replaced by chlorite-sericite (white mica). The plagioclase is less abundant but is also sericite altered. Quartz shows weak undulose extinction. There is minor biotite in the sample, however, this is strongly altered to dark clots of chlorite and/or clays. The rock also contains elongate titanite crystals.

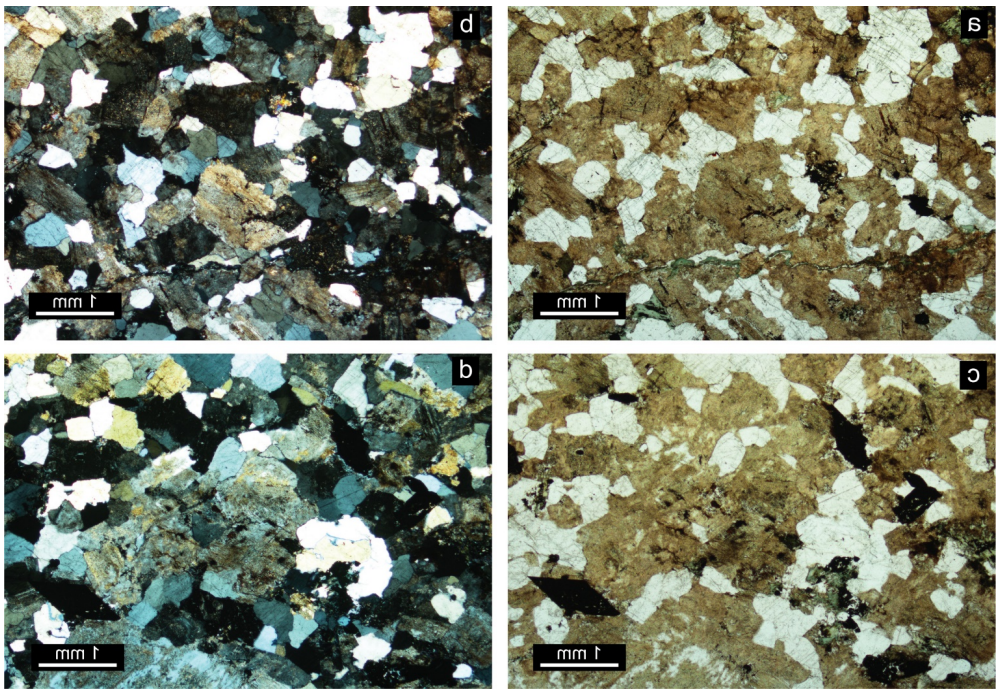

Figure 12. Photomicrographs of sample 2131359 (PPL and XPL).

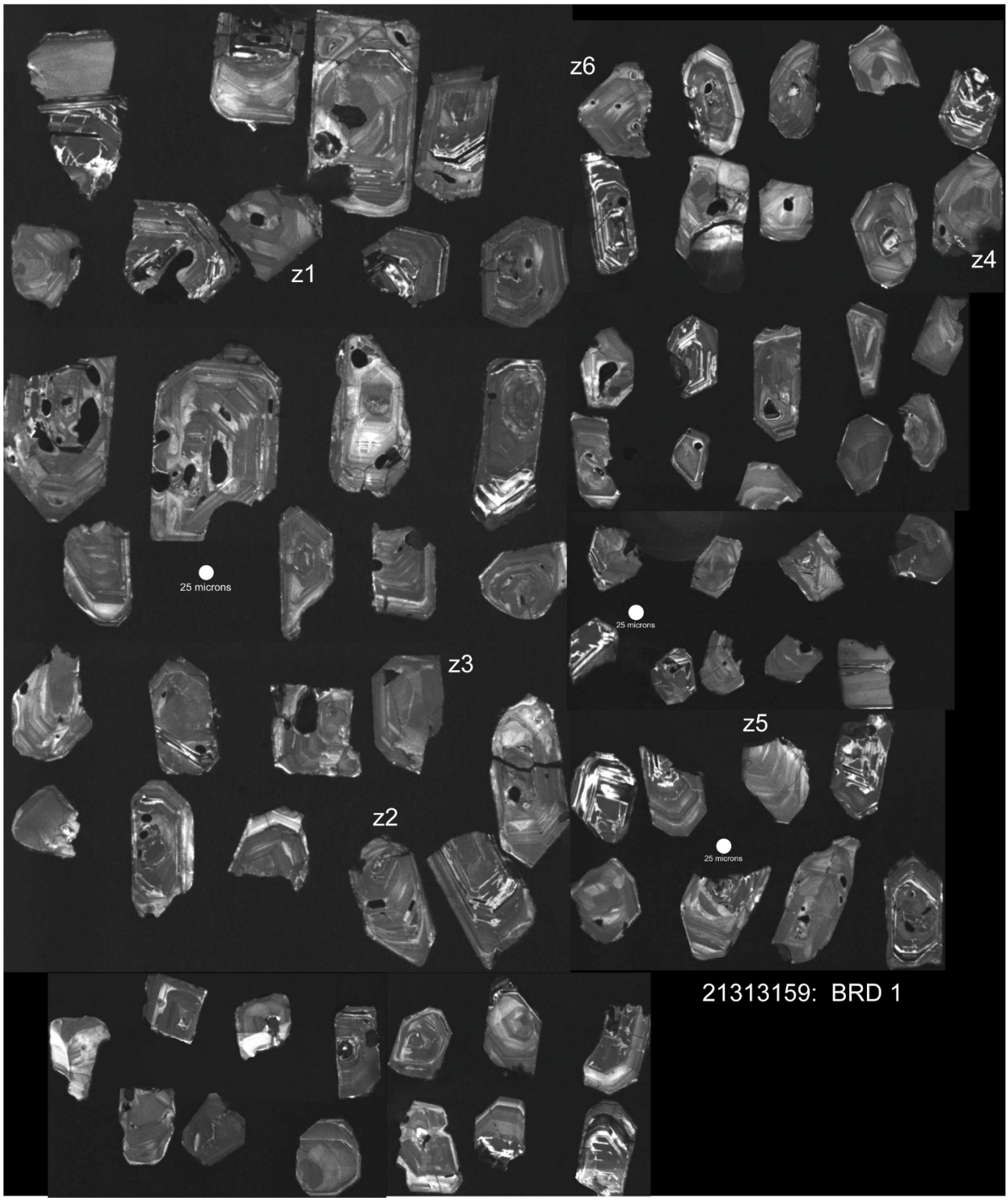

Figure 13. CL image of all zircon handpicked from sample 2131359.

2111460: GRANITE BLANCHE 1

Stratigraphic unit:	Hiltaba Suite		
Location GDA94:	672516.76 E	6627750.51 N	Zone 53
Location Lat-Long:	-30.4700925	136.797095	
250k map sheet	SH5312 ANDAMOOKA		
100k map sheet	6237 Mattaweara		
Location:	Drillhole BLANCHE 1 (number 206086) 1563.1–1564.6 m		
Analyst:	JL Crowley		
Analytical technique:	CA-TIMS Boise State University Idaho		
Interpreted $^{207}Pb/^{206}Pb$ age:	1591.79 ± 0.73 Ma		
Age interpretation:	Magmatic age		

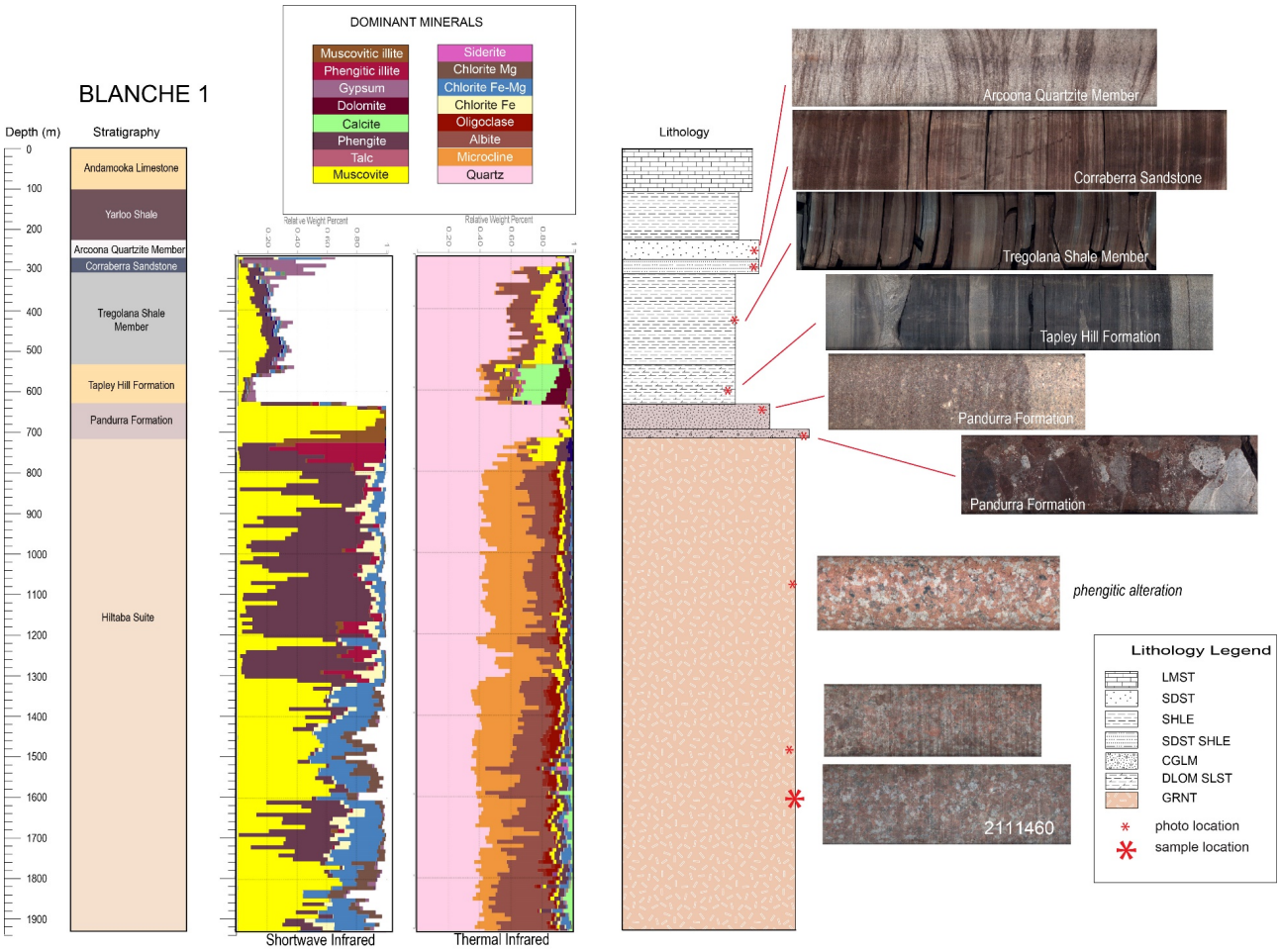

Figure 14. Summary graphic log of drillhole Blanche 1. Drill core is NQ (4.7 mm in diameter). View spectral scans in more detail.

Description

The following description is taken from the Blanche 1 well completion report (Meyer 2006). The drill site is located about 8 km southwest of Olympic Dam near the western edge of the Roxby Downs Granite, which also hosts the Olympic Dam Cu-U-Au deposit and forms part of the Burgoyne Batholith (Fig. 10). The batholith contains a suite of moderately magnetic, radiogenic granitoids that form part of a geological domain referred to as the Olympic Domain of the Gawler Craton. Blanche 1 is within the more potassic, western part of the Burgoyne Batholith referred to as the Wirrda Suite. The Burgoyne Batholith is overlain by platform sedimentary rocks of the Stuart Shelf to 718 m depth. These contain thick sequences of shale in the Yarloo Shale, Tregolana Shale and Tapley Hill Formation (Fig. 14). Blanche 1 was drilled to a depth of 1935 m to test the geothermal prospectivity of the area, the combination of thick thermally insulating cover rocks and a large, homogeneous, massive granite body at least 5000 m deep being considered favourable for a hot dry rock geothermal electrical power generation project

The granite comprises syenogranite and monzogranite, generally massive but with several zones of low- and high-angle fractures (Fig. 15).

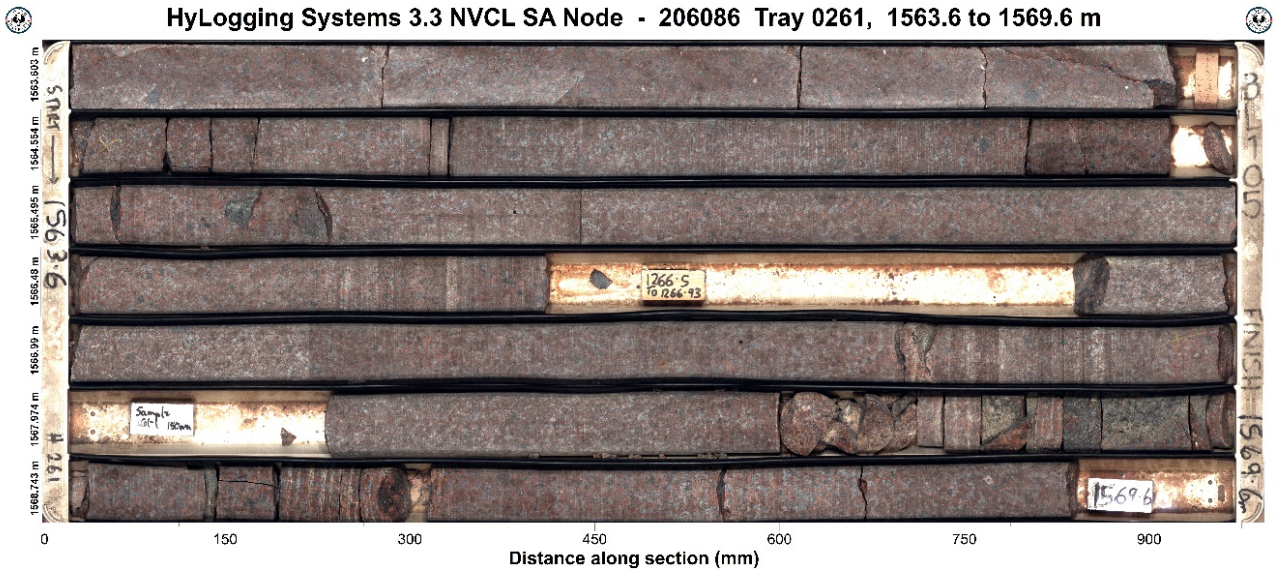

Figure 15. Drill tray containing sample 2111460.

Petrography

The following description of relatively fresh, unaltered granite from Blanche 1 is taken from Purvis (2005) in Meyer (2006).

Sample: P320929: 1184.2 m

Rock name: Relatively fresh monzogranite with some sericite-chlorite-clay-anatase alteration, partly fresh accessories (hornblende, biotite, magnetite, titanite, apatite and zircon) and open parallel fractures.

Hand specimen: Pale red granitoid with open parallel fractures normal to the core axis (Fig. 16).

Figure 16. Photograph of sample 2111460 in hand specimen.

Mineral	Vol %	Origin
Quartz	32	Igneous, partly altered
Plagioclase	32	Igneous, partly altered
Orthoclase	24.5	Igneous, partly altered
Titanite	3	Igneous, partly altered
Oxides	2	Igneous, partly altered
Biotite + chlorite	4	Igneous, partly altered
Hornblende + chlorite	2.5	Igneous, partly altered
Apatite	Trace	Igneous
Zircon	Trace	Igneous

This sample contains largely fresh hornblende and partly fresh biotite. Orthoclase up to 10 mm in grain size has pale hematite staining and plagioclase up to 8 mm has areas with sparse sericite. The quartz is partly granular but also has some subvolcanic characteristics, mostly with rounded, slightly bipyramidal grains with abundant plagioclase along resorption channels, partly as extensions of larger grains and partly fine-grained. Biotite is mostly altered to chlorite ± vermiculite and anatase, with weak chlorite alteration. Green hornblende also has weak chlorite alteration, although this is mostly fresh, and has inclusions of oxide, apatite and zircon. Separate titanite grains and titanite-magnetite aggregates are mostly fresh, with some leucoxene in titanite, and aggregates also contain apatite and zircon. Very rare sulfide occurs in opaque oxide.

The fractures in this sample are open and do not contain low-temperature hydrothermal minerals as seen in fractures where the granite is more altered.

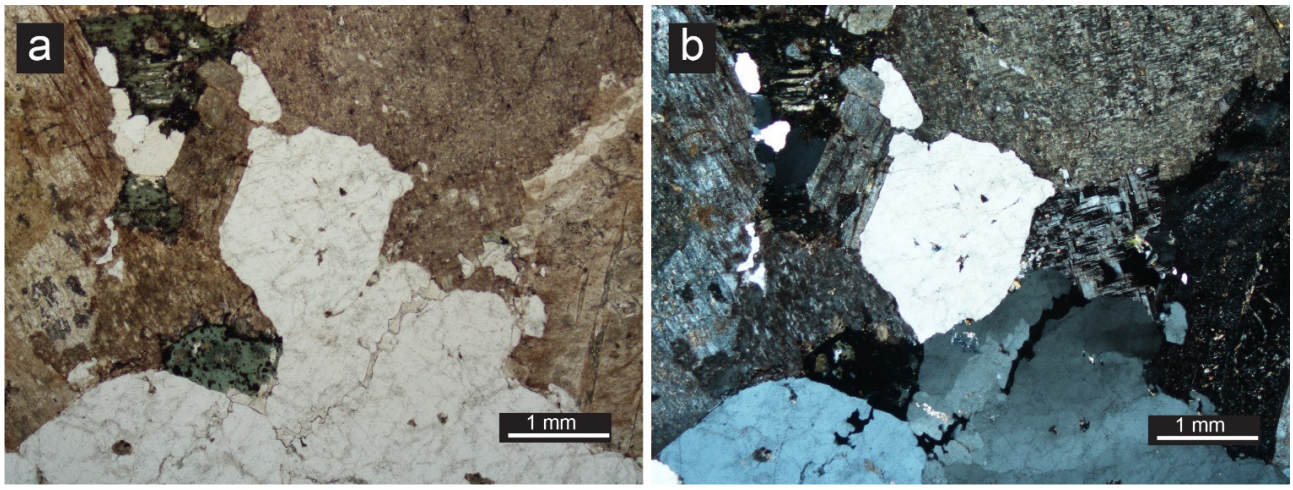

Figure 17. Photomicrographs of sample 2111460 (PPL and XPL).

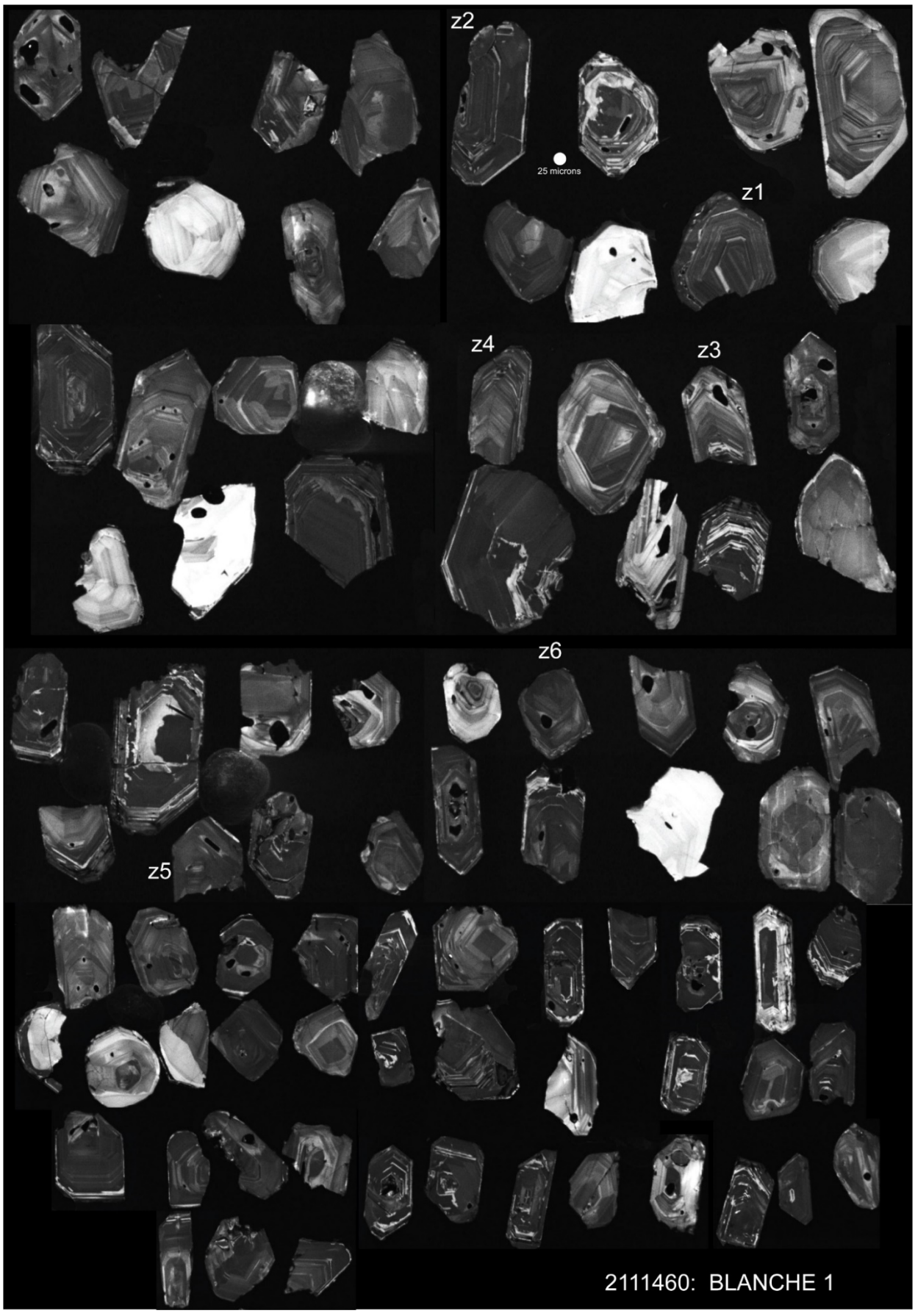

Figure 18. CL image of all zircon handpicked from sample 2111460.

2053554: UNDEFORMED GRANITE, CENTRAL GAWLER CRATON

Stratigraphic unit:	Cooladding Granite, Hiltaba Suite		
Location GDA94:	452836.74 E	6612719.48 N	Zone 53
Location Lat-Long:	-30.6171823	134.507926	
250k map sheet	SH5310 TARCOOLA		
100k map sheet	Tarcoola		
Location:	Cooladding Rock Hole		
Analyst:	JL Crowley		
Analytical technique:	CA-TIMS Boise State University Idaho		
Interpreted $^{207}Pb/^{206}Pb$ age:	1586.49 ± 0.62 Ma		
Age interpretation:	Magmatic age		

Geological context

The Tarcoola Goldfields form the northern portion of the Central Gawler Gold Province in the central Gawler Craton (Fig. 19). Tarcoola Ridge and adjacent areas have hosted more than 50 mines, workings and deposits since the first discovery of alluvial gold in 1893.

The Tarcoola region is composed of Mulgathing Complex basement, which is overlain by metasedimentary packages including the Tarcoola, Eba and Labyrinth formations (Daly et al. 1998, Howard et al. 2011). There are numerous granitic suites in the region including the syn- to post-Kimban Paxton Granite (c. 1722–1715 Ma) and c. 1680 Ma Tunkillia Suite (Budd 2006, Budd and Skirrow 2007, Payne et al. 2010), and the c. 1590–1575 Ma Hiltaba Suite (Hand et al. 2007). The region is cut by a series of shear zones and faults (Fig. 19). Shear zones are typically curviplanar and east-northeast- to northeast-trending, and commonly located along major lithological boundaries. Faults are commonly northwest-trending and form prominent aeromagnetic lineaments that are well developed in the granite plutons.

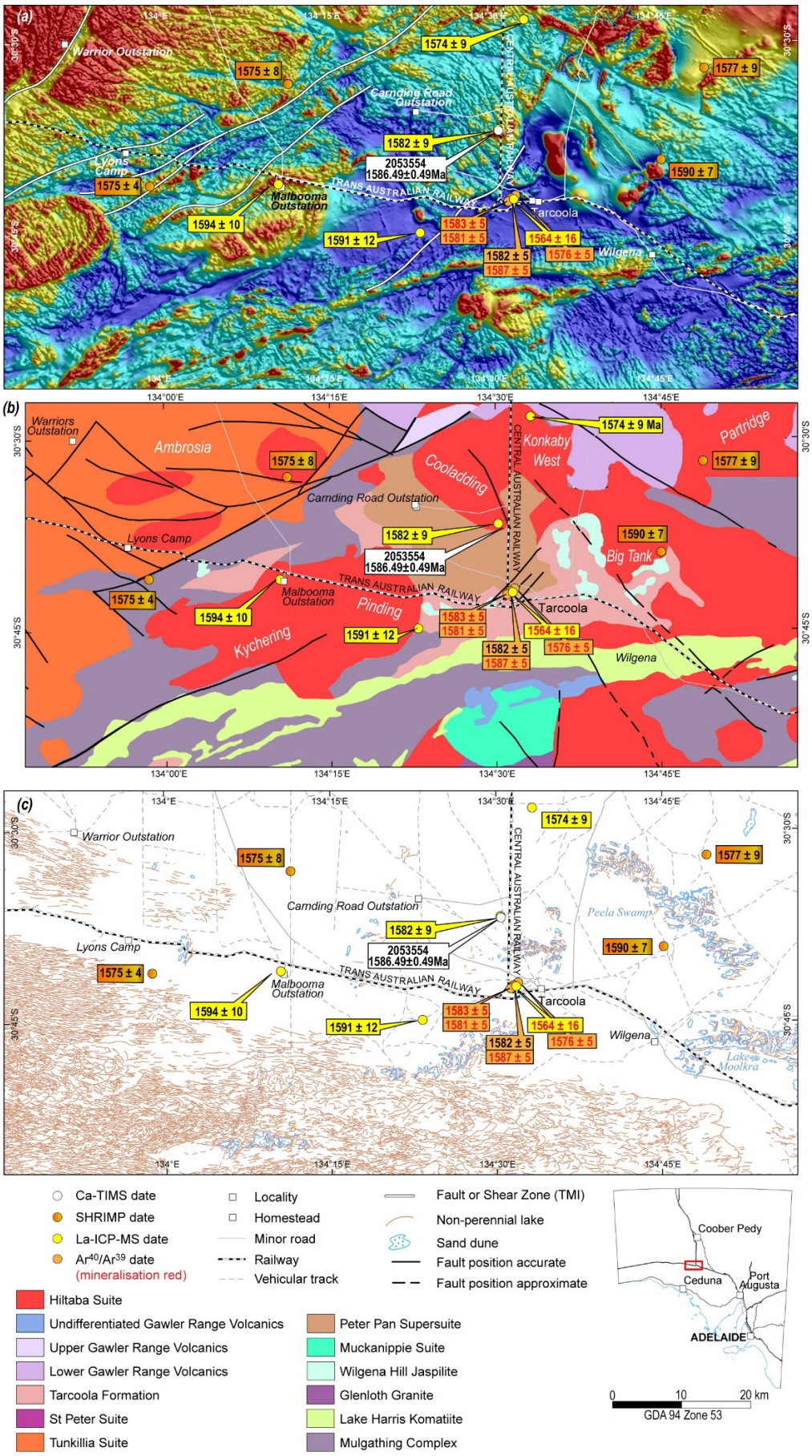

Figure 19. Locations of geochronology samples from the Tarcoola area. (a) Reduction to pole TM.I **(b)** 100k interpreted solid geology map. **(c)** Topography. Modified from plans 205232-001 and 205232-002 in Bockmann et a. (2019). Granite plutons are labelled in white.

Hiltaba Suite magmatism is extensive in the Tarcoola region with 15 granite plutons, which Budd (2006) grouped into two I-type supersuites based on geochemical characteristics: the Malbooma Supersuite defined by strongly fractionated and highly evolved compositions and the Jenners Supersuite, which is mildly fractionated and more juvenile. Budd (2006) posited two intrusive events at c. 1590 Ma and 1575 Ma but could not determine a relationship between the age and composition of the plutons. With more data, Bockmann et al. (2019) refined this model, suggesting that with a few exceptions (Ambrosia Granite, Kychering Granite) the granite plutons become younger and more fractionated toward the east, and represent a single continuously evolving magmatic system from c. 1590–1575 Ma, of which the Malbooma and Jenners supersuites are the two endmembers (Fig. 20).

To investigate this in more detail, more precise geochronology is required from more of the Hiltaba granite plutons in the Tarcoola region. The current dataset is too small and requires greater precision to be able to identify meaningful trends between granite fractionation, evolution and age, and resolve the anomalies of the Ambrosia and Kychering granites.

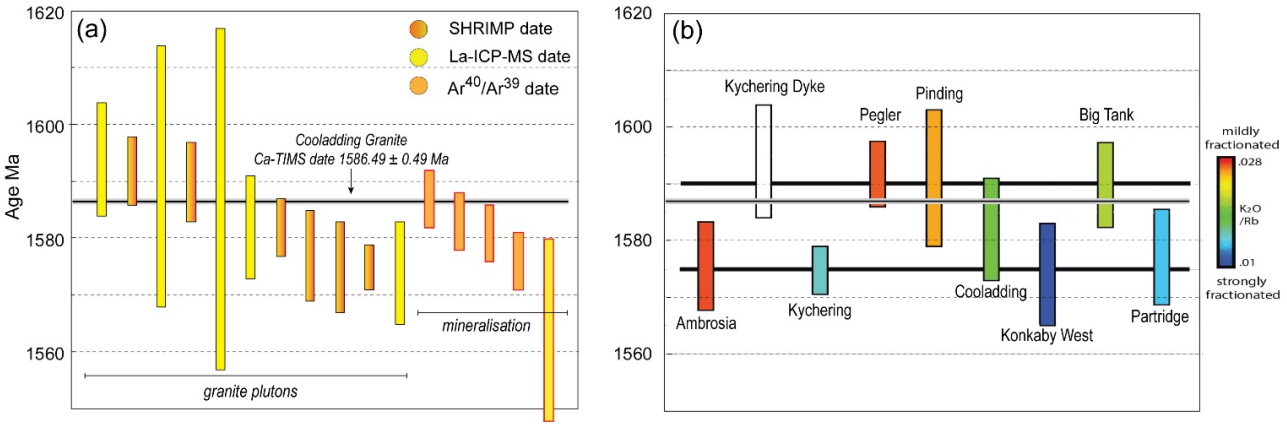

Figure 20. Dates for Hiltaba granite plutons in the Tarcoola region. The CA-TIMS date for 2053554 is plotted as a grey horizontal bar for comparison, with 2σ error represented by the surrounding grey envelope. **(a)** Ordered by age and coloured by dating method with mineralisation ages plotted for comparison. **(b)** Coloured by mean K_2O/Rb value as a proxy for fractionation, reproduced from Bockmann et al. (2019). Ages are ordered in the approximate east–west distribution of granite plutons.

Table 2. Published dates for the Hiltaba Suite in the Tarcoola region.

Sample	Location		Lithology	Age (Ma)	Mineral	Interpretation	Method	Reference
Magmatism								
2695960	421017	6605194	Felsic dyke, Kychering	1594 ± 10	Zircon	? Inheritance	LA-ICP-MS	Bockmann et al. 2019
2001363093	428366	6659598	Pegler Granite	1592 ± 6	Zircon	Emplacement	SHRIMP	Budd 2006
2695962	441569	6598137	Pinding Granite	1591 ± 12	Zircon	Emplacement	LA-ICP-MS	Bockmann et al. 2019
2001363031	476402	6608480	Big Tank Granite	1590 ± 7	Zircon	Emplacement	SHRIMP	Budd 2006
51677	465553	6604051	granite	1587 ± 20	Zircon	Emplacement	SHRIMP	Fanning et al. 2007
2695958	452772	6613119	Cooladding Granite	1582 ± 9	Zircon	Emplacement	LA-ICP-MS	Bockmann et al. 2019
2002363008A	454701.1	6602759	Lady Jane Diorite	1582 ± 5	Hornblende	Emplacement	Ar^{40}/Ar^{39}	Budd and Fraser 2004
2001363044	482997	6622783	Partridge Granite	1577 ± 9	Zircon	Emplacement	SHRIMP	Budd 2006
2001363078	422354	6619954	Ambrosia Granite	1575 ± 8	Zircon	Emplacement	SHRIMP	Budd 2006
2001363067	402982	6605010	Kychering Granite	1575 ± 4	Zircon	Emplacement	SHRIMP	Budd 2006
2695959	457300	6628799	Konkaby West Granite	1574 ± 9	Zircon	Emplacement	LA-ICP-MS	Bockmann et al. 2019
Mineralisation								
2000363017A	454972	6603053	DDH TD005	1587 ± 5	Sericite	Mineralisation	Ar^{40}/Ar^{39}	Budd and Fraser 2004
2000363014	454663	6602578	DDH GP005D	1583 ± 5	Sericite	Mineralisation	Ar^{40}/Ar^{39}	Budd and Fraser 2004
2000363011	454708.6	6602752	DDH GP005D	1581 ± 5	Sericite	Mineralisation	Ar^{40}/Ar^{39}	Budd and Fraser 2004
2000363007A	454677	6602701	altered Paxton Granite	1576 ± 5	Sericite	Mineralisation	Ar^{40}/Ar^{39}	Budd and Fraser 2004
2695967	455116	6603222	mineralised metagranite	1564 ± 16	Monazite	Mineralisation	LA-ICP-MS	Bockmann et al. 2019

NB: The plutons of the Hiltaba Suite have undergone a recent reclassification (https://energymining.sa.gov.au/__data/assets/pdf_file/0008/388547/GSSA_Hiltaba_Workshop_Presentation_Megan_Williams.pdf).
The Kychering Granite has been renamed the Tolmer Granite, The Big Tank Granite has been renamed the Salt Springs Granite and the Konkaby West Granite is not an extension of the Cooladding Granite The new nomenclature is used in Appendix 3.

Figure 21. Photograph of sample 2053554 in hand specimen.

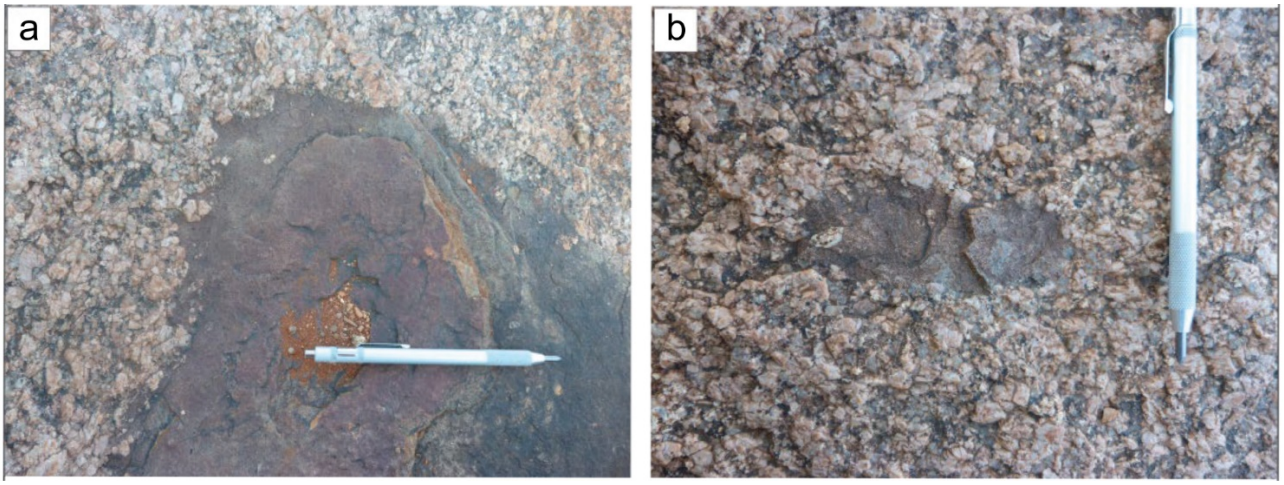

Figure 22. Outcrop of the Cooladding Granite approximately 250 m north of Cooladding Rock Hole showing mafic enclaves in the granite.

The following description (including petrography) is taken from Bockmann et al. (2019). It describes sample 2695958, which was collected ~ 200 m to the north-northwest of the TIMS sample. Sample 2053554 represents the Cooladding Granite, from an extensive area of large platforms and boulder outcrop of granite about 9.5 km north of the Tarcoola Goldfields and 1 km to the west of the railway line (Fig 19). The granite lies within a large, irregular pluton of Hiltaba Suite Granite (30 x 24 km), poorly exposed but spatially delineated using aeromagnetic imagery. The southern and southwestern margins of the pluton are lobate and intrude the Paxton Granite (Budd 2006). The northern margins are truncated by the northeast-trending Bulgunnia Shear Zone and the northwest-trending Lake Labyrinth Fault, with the granite juxtaposed against rocks of the lower GRV. In the northeastern corner, near Pompeter Bore, the granite appears to intrude the metasedimentary rocks of the Tarcoola Formation. The eastern margin is defined by the north-northeast-trending Tarcoola Fault (Bockmann et al. 2019), which juxtaposes the granite against rocks of the lower GRV and a magnetically low granite of the Hiltaba Suite. Cooladding Rock Hole is in the southern part of this pluton.

The granite is cream to pale grey on weathered surfaces, and red-pink where fresh, reflecting the colour of the feldspars. The granite is massive, inequigranular and homogenous, with euhedral/subhedral equant to tabular, <1 cm K-feldspars in a medium-grained groundmass of feldspar, quartz and minor biotite (Fig. 21). The quartz forms medium-grained rounded phenocrysts and angular interstitial grains. The biotite forms mm-scale equant aggregates. There are scattered rounded, equant medium-grained mafic enclaves up to 25 cm in diameter, but generally smaller

(Fig 22). The enclaves often contain feldspars near the margin, suggesting they were comagmatic and comingling, with the transfer of crystals between the two phases.

La-ICP-MS sample 2695958, which lies about 200 m north of TIMS sample 2053554, and 2695959 representing the 'Konkaby West' Granite from the north of the pluton have dates of 1582 ± 9 Ma and 1573 ± 9 Ma, respectively (Fig 20, Table 2, Bockmann et al. 2019).

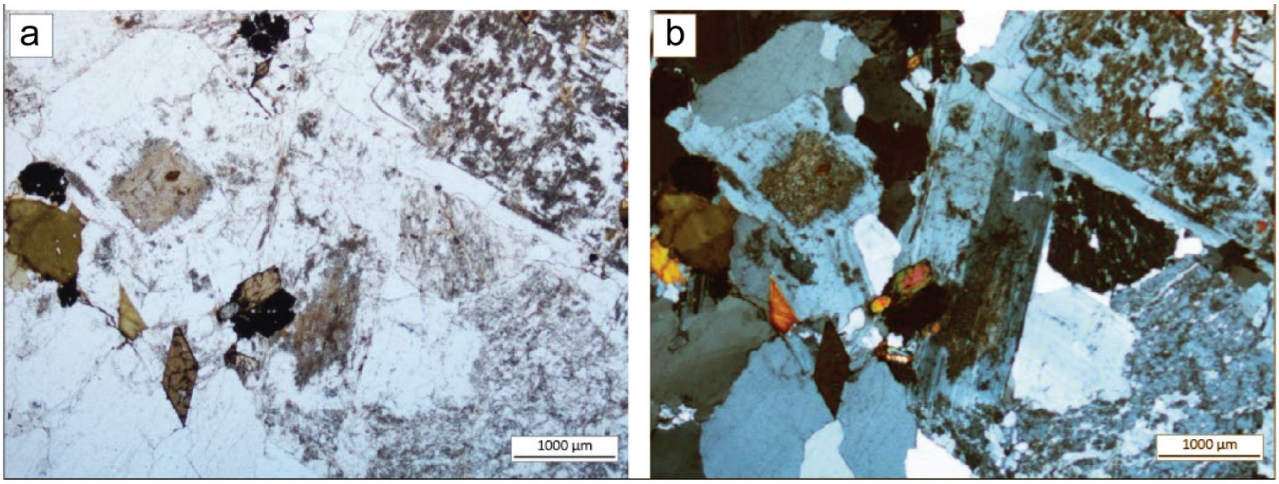

Figure 23. Photomicrograph of a biotite + titanite + ilmenite + zircon aggregate in the Cooladding Granite (PPL and XPL).

Petrography

In thin section, the coarse-grained, massive granite comprises (<1 cm) euhedral phenocrysts of K-feldspar, commonly with tartan twinning, euhedral to subhedral plagioclase and quartz (both up to 3.5 mm). Quartz and sometimes plagioclase occur as angular interstitial grains between phenocrysts (Fig. 23).

Titanite, biotite, ilmenite, rare hornblende and zircon are often observed forming together in aggregates. Titanite is typically euhedral and forms grains between 50 µm to 1 mm in length, often intergrown with other titanite grains or forming on the edge of ilmenite. Rare hornblende is observed as inclusions in plagioclase and titanite and is seen intergrown with biotite. Biotite occurs as two distinctly different styles. Firstly, it forms subhedral grains with prominent uniaxial cleavage and strong pleochroism from pale to dark brown. Secondly, biotite forms anhedral grains that have no observable cleavage and only minor pleochroism, which are often in contact with the subhedral biotite grains. The anhedral biotite varies in birefringence between different grains from low 2nd order to 6th order, potentially indicating partial conversion of hornblende into biotite. Both forms of biotite exhibit clear signs of partial break down at grain boundaries.

Mineral	Vol %	Origin
K-Feldspar	30–70	Igneous
Quartz	5–29	Igneous
Plagioclase	5–29	Igneous
Biotite	1–4	Igneous
Titanite	Trace	Igneous
Ilmenite	Trace	Igneous
Hornblende	Trace	Igneous
Zircon	Trace	Igneous

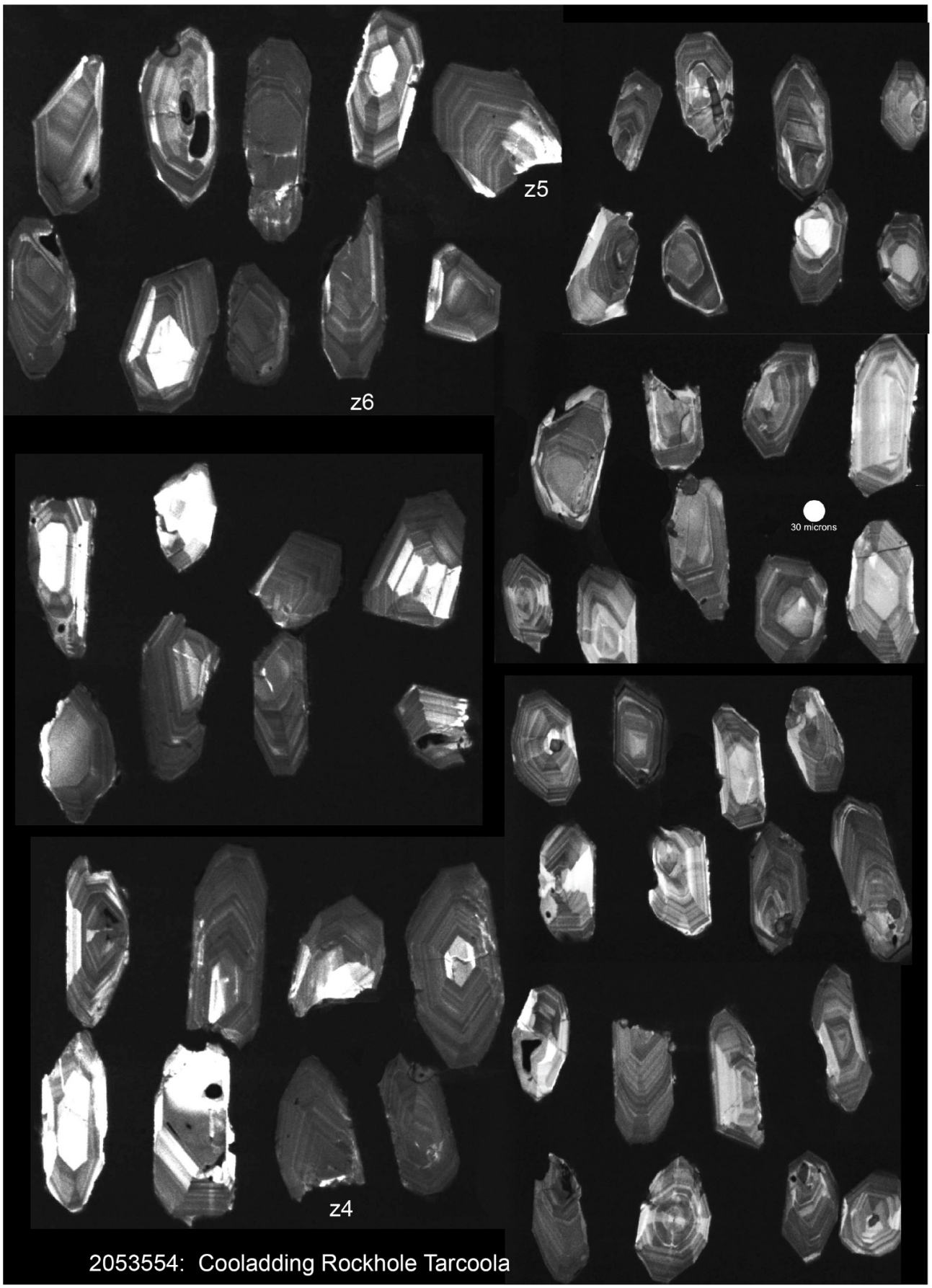
z5
z6
30 microns
z4
2053554: Cooladding Rockhole Tarcoola

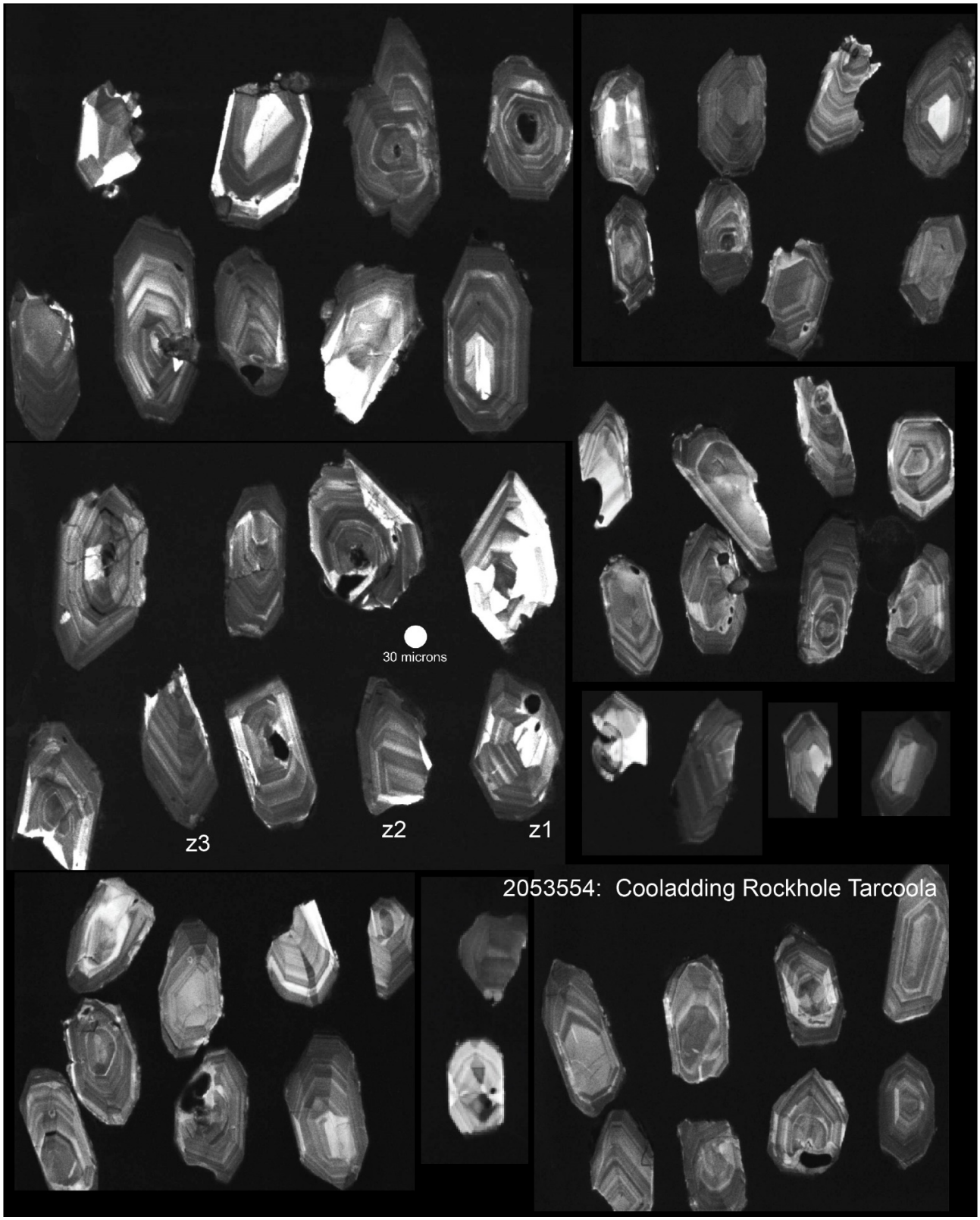

Figure 24. CL image of all zircon handpicked from sample 2053554.

2049214: CURRAMULKA GABBRONORITE YORKE PENINSULA

Stratigraphic unit:	Hiltaba Suite		
Location GDA94:	6164962.55 E	747770.01 N	Zone 53
Location Lat-Long:	-34.6273184	137.7026824	
250k map sheet	5312 MAITLAND		
100k map sheet	6428 Stansbury		
Location:	Drillhole CUR D2 (number 143970) 55–58.2m		
Analyst:	JL Crowley		
Analytical technique:	CA-TIMS Boise State University Idaho		
Interpreted $^{207}Pb/^{206}Pb$ age:	1580.21 ± 0.40 Ma		
Age interpretation:	Magmatic age		

Geological context

Yorke Peninsula is located on the southeastern margin of the Gawler Craton, and is part of the Olympic Cu–Au province (Skirrow et al. 2002), which extends along the eastern margin of the Gawler Craton, from Yorke Peninsula in the south to the Olympic Dam region and the Mt Woods Inlier in the north. The basement geology is characterised by late Paleoproterozoic siliciclastic metasediments and bimodal metavolcanics of the Wallaroo Group interpreted to have been deposited in a continental rift margin at c. 1750 Ma (Parker 1993, Conor 1995, Zang 2002, Cowley et al. 2003). The Wallaroo Group overlies older Paleoproterozoic units which include migmatitic paragneisses of the c. 1850 Ma Corny Point Paragneiss (Zang and Fanning 2001) and gneissic granitoids of the c. 1850 Ma Donington Suite (Schwarz 2003, Zang 2006, Jagodzinski et al. 2006). These rocks were subjected to high-grade metamorphism and deformation during the c.1850 Ma Cornian Orogeny (Reid et al. 2008).

The early Mesoproterozoic was a time of magmatic and orogenic activity in the Yorke Peninsula region, with intrusion of mafic and felsic rocks of the Hiltaba Suite broadly coeval with widespread deformation, metamorphism, metasomatism and mineralisation across the region (Conor 1995, Conor et al. 2010, Ismail et al. 2014). Intense metasomatism in some areas has modified some rock packages to such an extent that they form as a distinct unit, the Oorlano Metasomatite (Cowley et al. 2003, Kontonikas-Charos et al. 2014). The Hiltaba Suite granitoids comprise two felsic intrusions referred to as the Tickera and Arthurton granites, and a mafic component represented by the Curramulka Gabbronorite (Creaser and Cooper 1993, Parker 1983; Zang et al. 2007). The Tickera Granite is a composite body that includes granite, leucomonzonite and leucotonalite (Wurst 1994), and is generally deformed, with local extreme strain partitioning constrained to narrow structural corridors in which foliated, lineated, gneissic and mylonitic fabrics are developed (Conor 1995). The Curramulka Gabbronorite displays a major foliation defined by biotite and hornblende alignment. The Arthurton Granite is an A-type pluton, ranging in composition from granite through adamellite to quartz monzonite (Wurst 1994), and is generally not foliated.

Prior to this study and Reid et al. (2021), the existing geochronology for the Yorke Peninsula was relatively imprecise, with significant overlap in uncertainties. The Tickera Granite at the Pt Riley locality has SHRIMP U-Pb ages that range between 1597 ± 7 Ma and 1577 ± 7 Ma, while weakly deformed granite at this locality had been dated at 1591 ± 9 Ma (Fanning et al. 2007). The Arthurton Granite has a date of 1582 ± 7 Ma (Creaser and Cooper 1993) and the Curramulka Gabbronorite is dated at 1589 ± 5 Ma (Zang et al. 2007). These larger errors on the dates meant that the timing of magmatic and deformation processes on the Yorke Peninsula were poorly constrained.

The Proterozoic basement rocks are overlain by undeformed Neoproterozoic, Cambrian, Permian and Cenozoic sedimentary rocks.

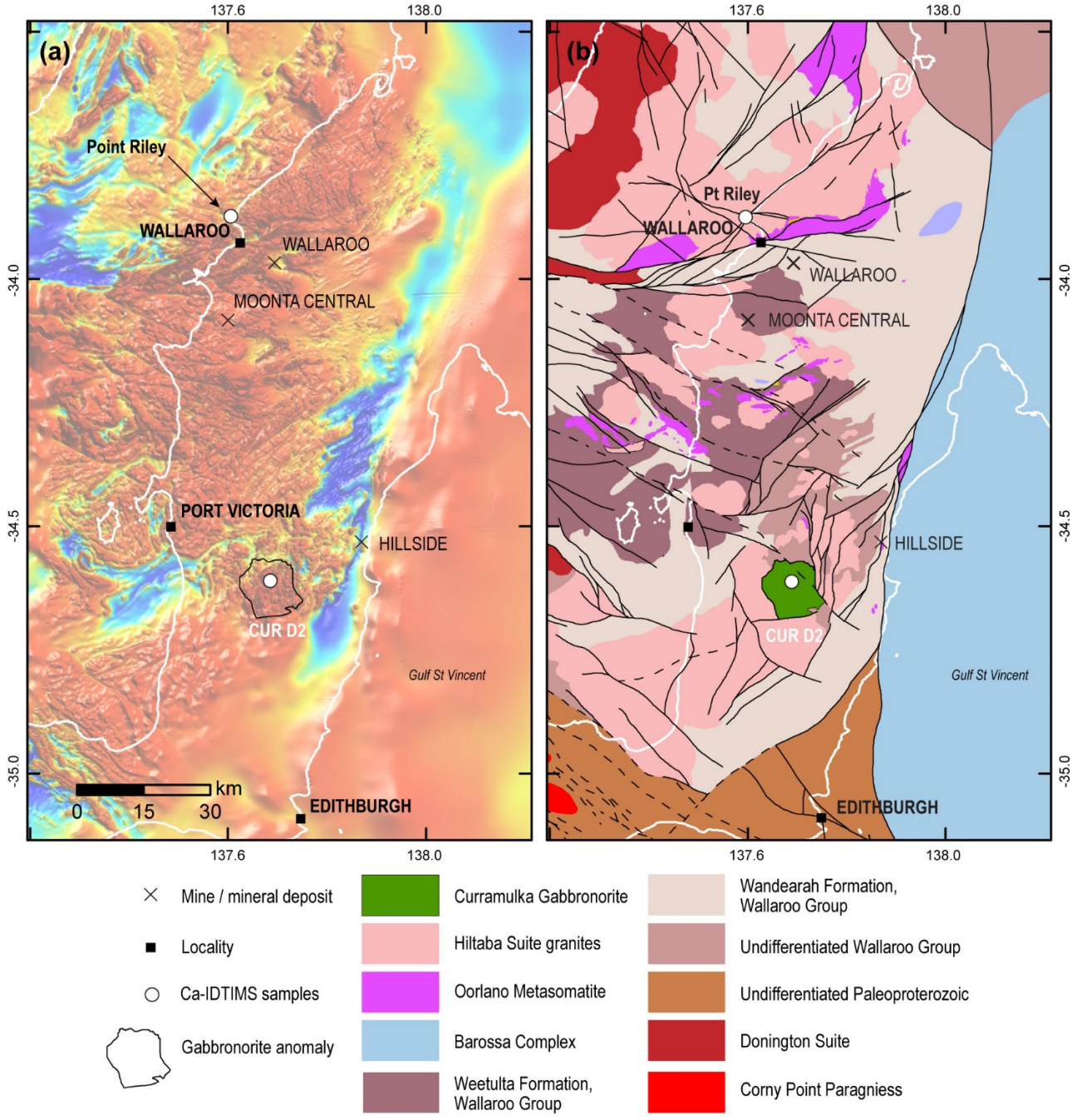

Figure 25. The Yorke Peninsula, showing the location of the Curramulka Gabbronorite, and drillhole CUR D2. The Pt Riley locality, where three samples of the Tickera Granite have been dated by CA-TIMS (Reid et al. 2021), is also plotted. **(a)** Total magnetic intensity image. **(b)** Interpreted basement geology, after Cowley (2006).

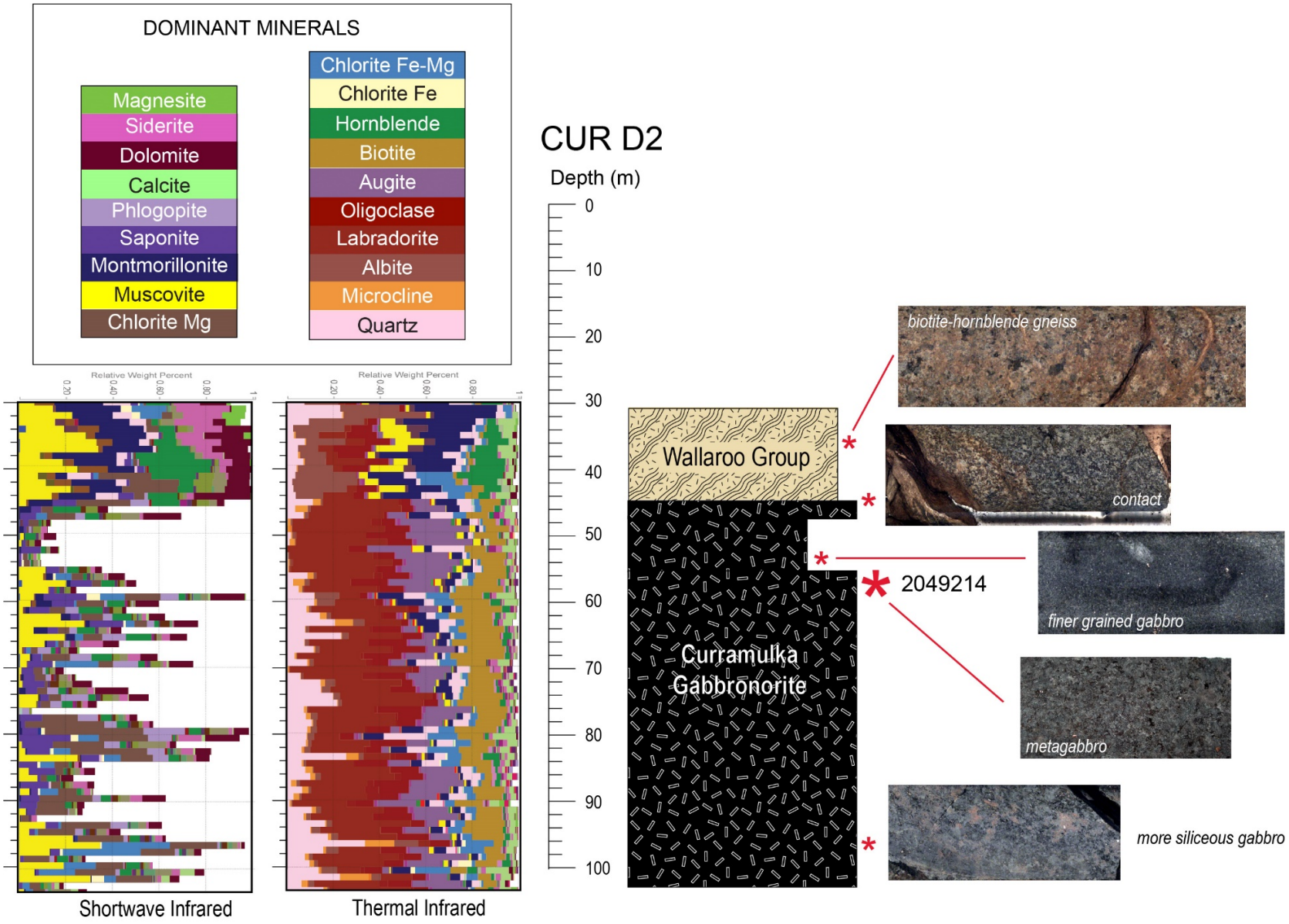

Figure 26. Summary graphic log of drillhole CUR D2. Drill core is BQ (3.6 mm in diameter). View spectral scans in more detail.

Figure 27. Drill tray containing sample 2049214.

Description

The following description is taken from Zang et al. (2007). The Curramulka Gabbronorite is a subsurface plutonic body in the Curramulka region, on the Yorke Peninsula, southeastern Gawler Craton. Interpretation of TMI data suggests it is about 15 x 30 km in size (Fig. 25). The Curramulka Gabbronorite has a continental tholeiitic composition and igneous layering that is partly of cumulus origin, probably an orthocumulate, with well-layered pyroxenes and plagioclase, but also contains magmatic segregations formed by fractionation, some of which have provided zircons for dating (Purvis 1997).

There are two phases of deformational fabrics in the Curramulka Gabbronorite. Initial deformation produced a major foliation defined by alignment of biotite and hornblende blades and is considered to have formed either coeval with, or shortly after, emplacement of the gabbronorite. Later retrogression, mainly restricted to late-stage shear zones, resulted in the formation of chlorite, albite, sericite and epidote assemblages (Huffadine 1993).

In drill core, the gabbronorite can be seen to have intruded scapolite-bearing metasandstone and conglomerate of the Wandearah Formation, and in turn intruded by granite and pegmatite dykes. The metasandstone has a foliation defined by the alignment of biotite and quartz–feldspar elongation and is folded. There is some evidence that an earlier fabric had been developed in the metasandstone prior to the major foliation. The foliations in the gabbronorite and metasandstone layering are concordant with the main regional foliation, suggesting syntectonic intrusion.

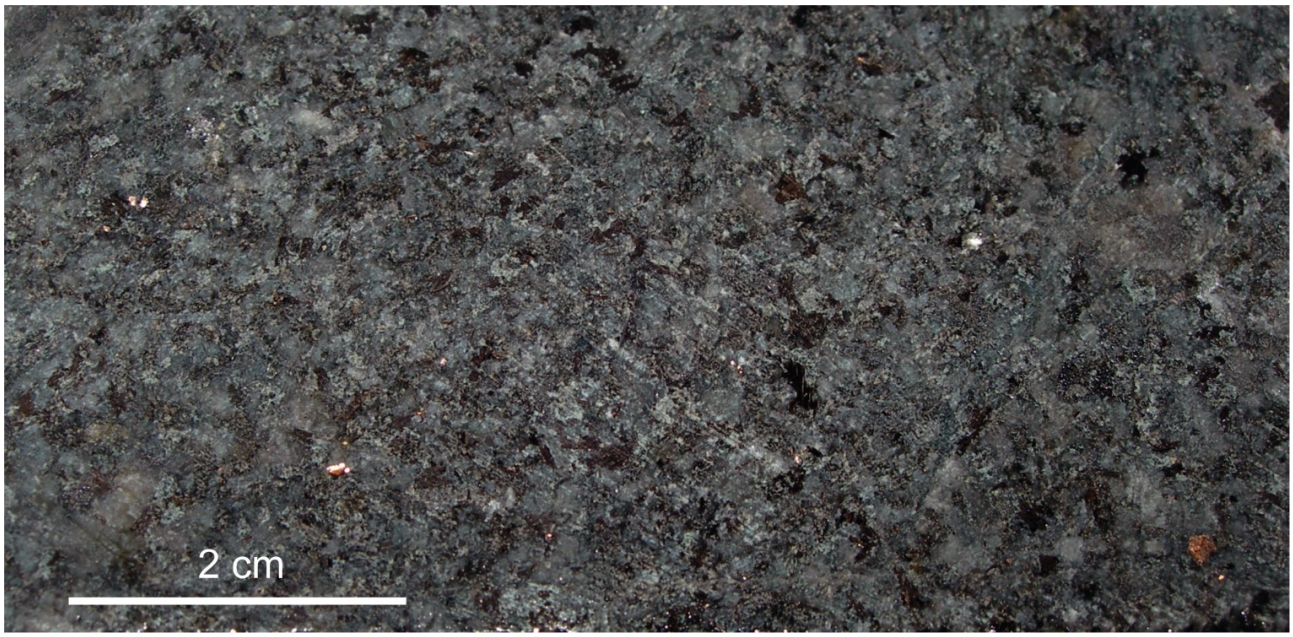

Figure 28. Photograph of sample 2049214 in hand specimen.

Petrography

Zang et al. (2007) provides a general description of the Curramulka Gabbronorite as mainly composed of plagioclase, clinopyroxene and orthopyroxene + quartz + orthoclase, apatite and opaque oxides, with hornblende and/or biotite in some samples. The mineralogy is variable, reflecting phase layering and variations in water activity, forming hornblende and biotite in some samples, rather than pyroxenes and orthoclase, but with relatively constant plagioclase contents. A sample from drillhole MCD1 is described as having a layered cumulate texture and two tectonic fabrics, with locally bent plagioclase laths defining an igneous layering, partly layer-parallel and partly imbricated, and biotite and green hornblende defining a foliation about 15° to the primary layering, and chlorite–albite–sericite–epidote assemblages in shear zones, at ~45° to the primary layering. Zircon grains concentrate in small pods or layers and are clear, with no inherited cores, indicating a magmatic origin. The zircon is considered to have crystallised from trapped fractionated magma in interstitial voids between pyroxene and plagioclase grains.

The igneous layering and foliations are not obvious in drillhole CUR 2, in which large biotite crystals are randomly oriented (Fig. 29 a–b). Plagioclase and pyroxenes are also randomly oriented and not organised into cumulate layers (Fig 29 c–f). The gabbronorite contains both pyroxene and amphibole (Fig. 29 e–f). Myrmekite is present between K-feldspar and plagioclase crystals (Fig. 29 g–h).

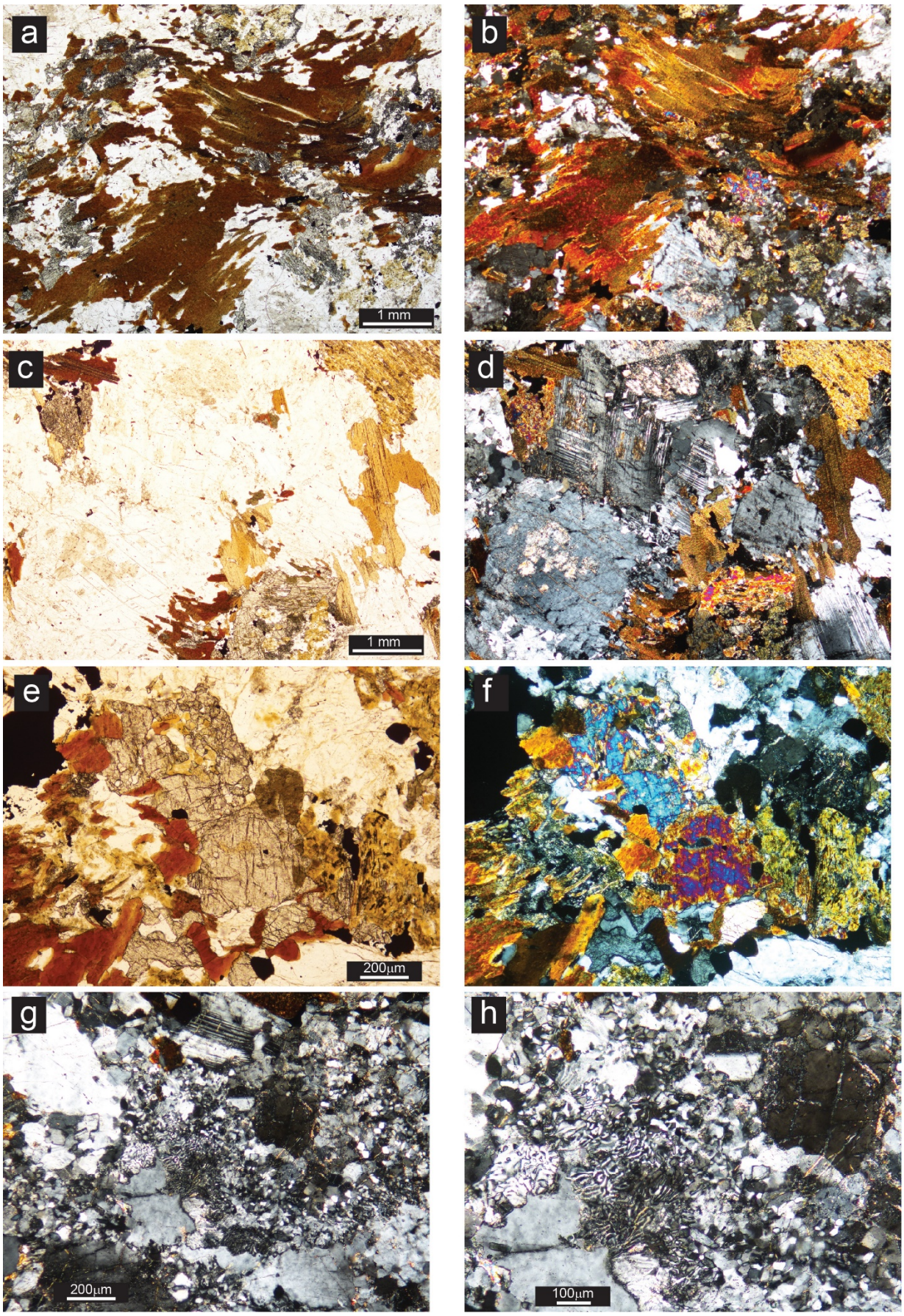

Figure 29. Photomicrographs of Curramulka Gabbronorite from a sample collected at 61 m.

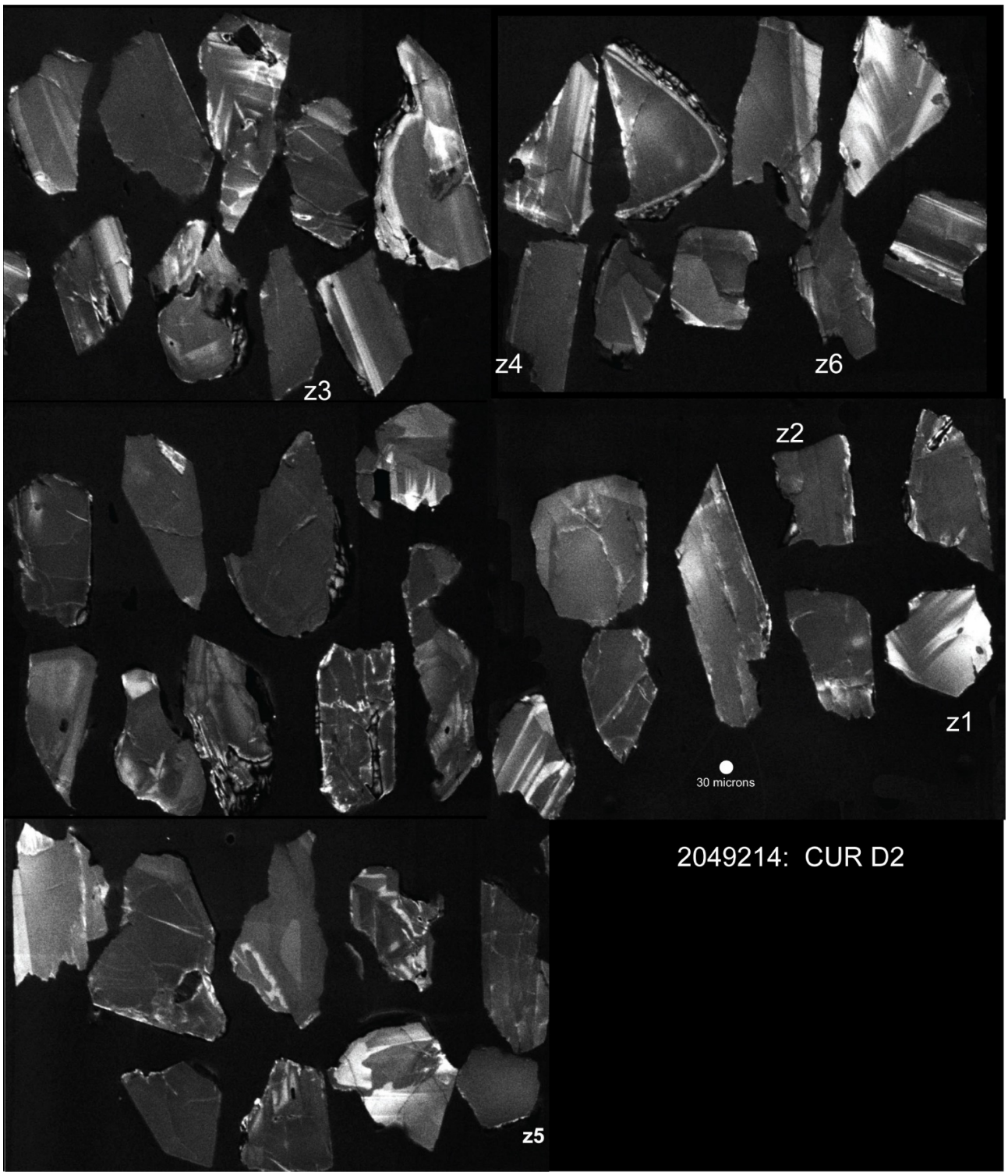

Figure 30. CL image of all zircon handpicked from sample 2049214.

2115491: FOLIATED GRANITE FOWLER DOMAIN

Stratigraphic unit:	Hiltaba Suite		
Location GDA94:	221617.89 E	6497019.49 N	Zone 53
Location Lat-Long:	-31.6283253	132.0651264	
250k map sheet	SH5313 FOWLER		
100k map sheet	5334 Coorabie		
Location:	NDR 13 (number 898) 94.5–94.7m		
Analyst:	JL Crowley		
Analytical technique:	CA-TIMS Boise State University Idaho		
Interpreted $^{207}Pb/^{206}Pb$ age:	1579.37 ± 1.57 Ma		
Age interpretation:	Magmatic age		

Geological context

The Fowler Domain is a northeast-trending belt of deformed rocks in the western Gawler Craton. Lithologies are typically gneissic in character and range from aluminous felsic gneiss interpreted to be sedimentary in origin, to felsic and intermediate meta-igneous lithologies such as tonalite and granodiorite, through to mafic and ultramafic lithologies such as primitive gabbros and chromite-bearing olivine-rich ultramafic rocks (Morris et al. 1994, Daly et al. 1998). Mineral exploration in the region has focused on shear zone hosted gold and nickel sulfides related to these mafic intrusions (Constable et al. 2005).

The Fowler Domain is deformed by a series of anastomosing shear zones that trend towards the northeast and separate subdomains of differing metamorphic grade and lithological character (Teasdale 1997, Thomas et al. 2008, Stewart and Betts 2010). Historically, Teasdale (1997) divided the Fowler Domain into four blocks bounded by major shear zones (the Nundroo, Central, Barton and Colona blocks, Fig. 31). Geophysically, these domains are broadly similar, with the intense magnetic signature being ascribed to a combination of mafic, ultramafic, intermediate-felsic igneous and metasedimentary lithologies. However, the geological character of these blocks differs considerably, containing different metamorphic and geochronological records.

Based on lithostratigraphic variation, Reid (2019) divided the Fowler Domain into the west and east region separated by the Chimpering Shear Zone (Doublier et al. 2015, Fig. 32). The western Fowler Domain comprises reworked Tunkillia Suite and Archean basement (Mulgathing Suite) that was deformed and metamorphosed during the Kimban Orogeny. In contrast, the eastern Fowler Domain has equivalent lithostratigraphy to the Nuyts Domain, dominated by reworked St Peter Suite and Hiltaba Suite, with local evidence for high-temperature metamorphism occurring during the early Mesoproterozoic Kararan Orogeny (Fig. 32).

SHRIMP dates for the Hiltaba Suite and associated metamorphism range between c. 1568–1586 Ma (Table 3). A later c. 1470–1530 Ma period of magmatism and metamorphism is also recognised in the east Fowler Domain (Fraser and Lyons 2006, Fraser et al. 2012, Jagodzinski et al. 2019)

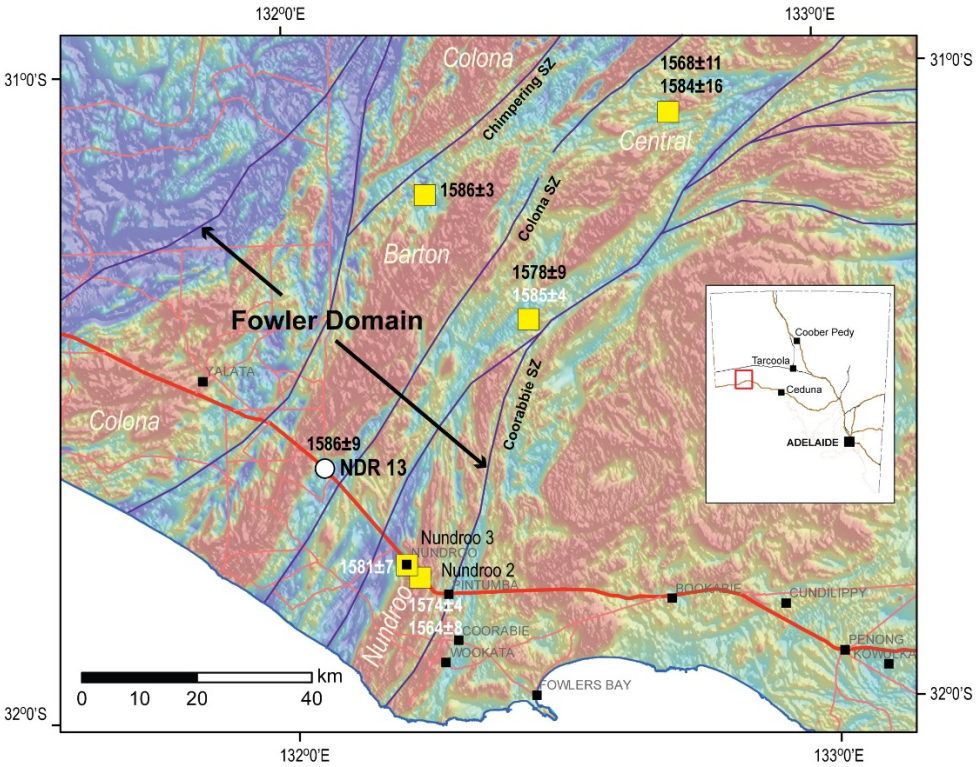

Figure 31. Location of drillhole NDR 13. Backdrop is TMI image for the southwestern Gawler Craton. SHRIMP zircon dates for Hiltaba Suite magmatism (black text) and contemporary metamorphism (white text) are also plotted (Table 3).

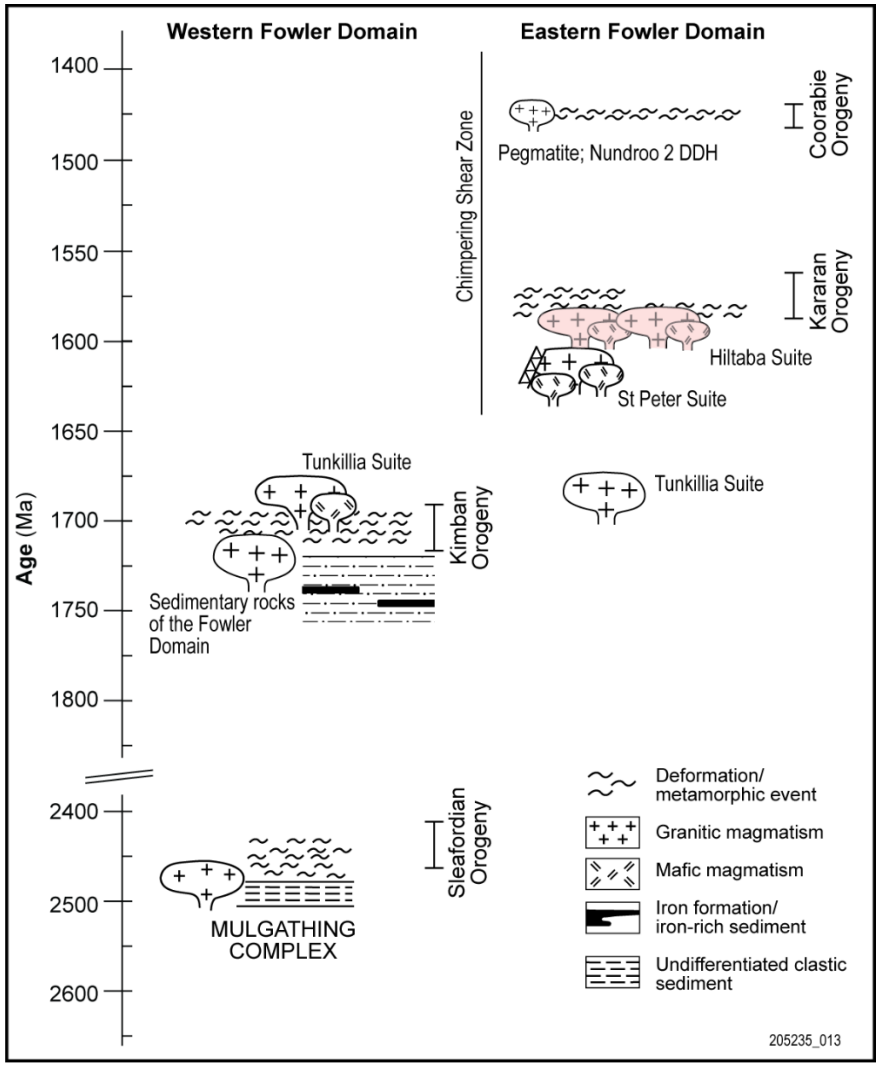

Figure 32. Schematic time–space plot showing the major lithostratigraphic units of the Fowler Domain. Reproduced from Reid (2019).

Table 3. U-Pb dates for the Hiltaba Suite and related metamorphism in the eastern Fowler Domain.

		MGA Zone 53		Depth					
Sample Number	**DH name**	**East**	**North**	**From**	**To**	**Lithology**	**Magmatic age/Dmax**	**Meta-morphic age**	**Reference**
R2145321	WGAC0045	239580	6480094	88.00	108.00	gt-sill qf gneiss	1586 ± 3	c. 1530–1500	Jagodzinski et al. 2019
R215780	Outcrop	282572	6560119			granite gneiss	1568 ± 11		Fanning et al. 2007
R2322233	FBD1	257720	6523313	209.47	210.36	plag-qtz-hbl granitoid	1578 ± 9		Jagodzinski et al. 2019
R2322236	FBD2	257749	6523272	234.82	236.70	qf gneiss	1612 ± 5	1585 ± 4	Jagodzinski et al. 2019
R215773	NDR13	221618	6497019	94.00	94.70	foliated granite	1586 ± 9		Fanning et al. 2007
2115492	Nundroo 3	236403	6480094	72.15	72.4	gt-bt qf gneiss		1581 ± 7	Reid et al. 2019
R5115514	Nundroo 2	238453	6477761	321.80	323.00	gt qf gneiss	1616 ± 5	1574 ± 4	Jagodzinski and Reid 2016
R2115501	Nundroo 2	238453	6477761	124.00	126.00	metagabbro		1564 ± 8	Jagodzinski and Reid 2016

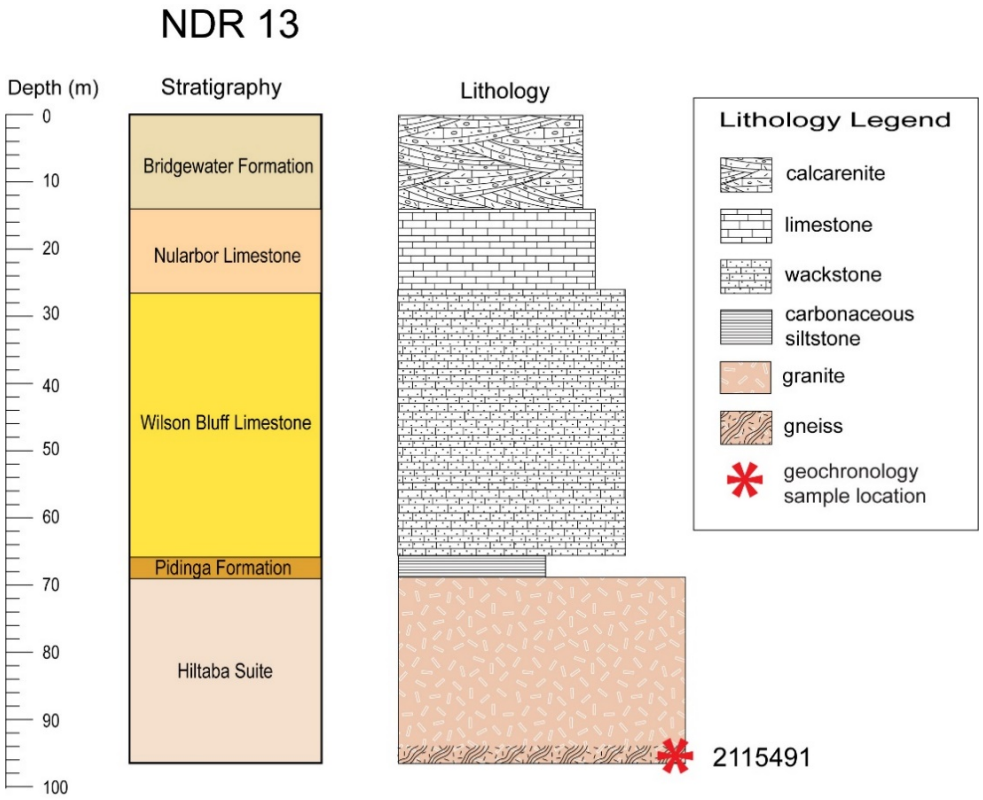

Figure 33. Summary graphic log of drillhole. View spectral scans.

Petrography

Sample 2115491 is a foliated granite. The sample has medium- to coarse-grained biotite intergrown with quartz and feldspar (Fig. 34). While much of the rock shows a typical granitic granoblastic texture, there are numerous zones that have narrow bands of dynamically recrystallised quartz and feldspar. These deformation zones appear to truncate the biotite-defined mineral alignment within the rock and some crystals of K-feldspar appear to also be partly recrystallised, with the microcline twining showing kinking (Fig. 35).

Figure 34. Photograph of sample 2115491 in hand specimen.

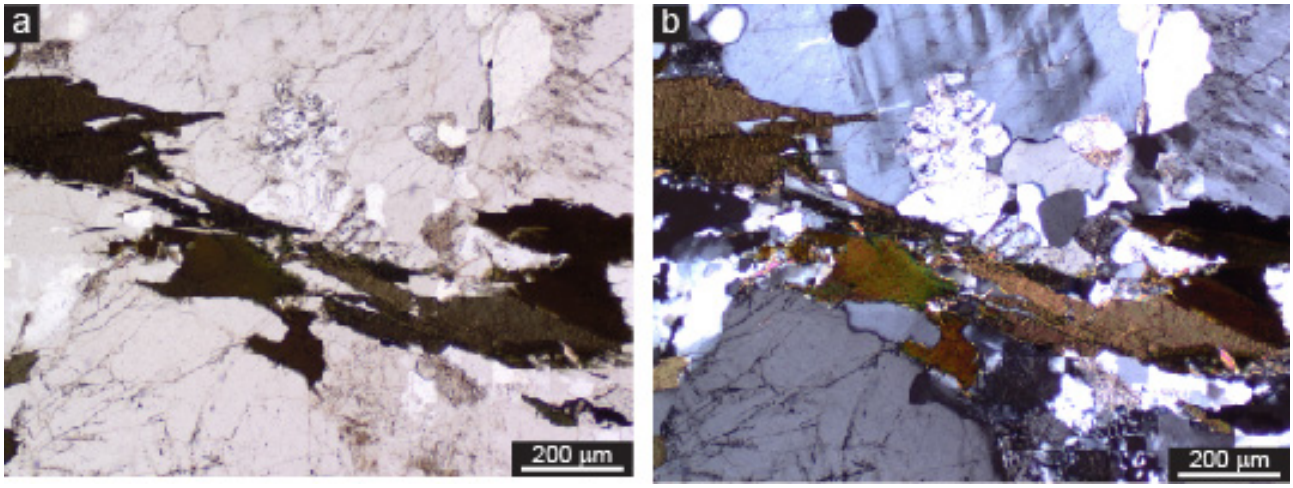

Figure 35. Photomicrographs of sample 60084, collected immediately below geochronology sample 2115491 (94.26–94.3 m) (PPL and XPL).

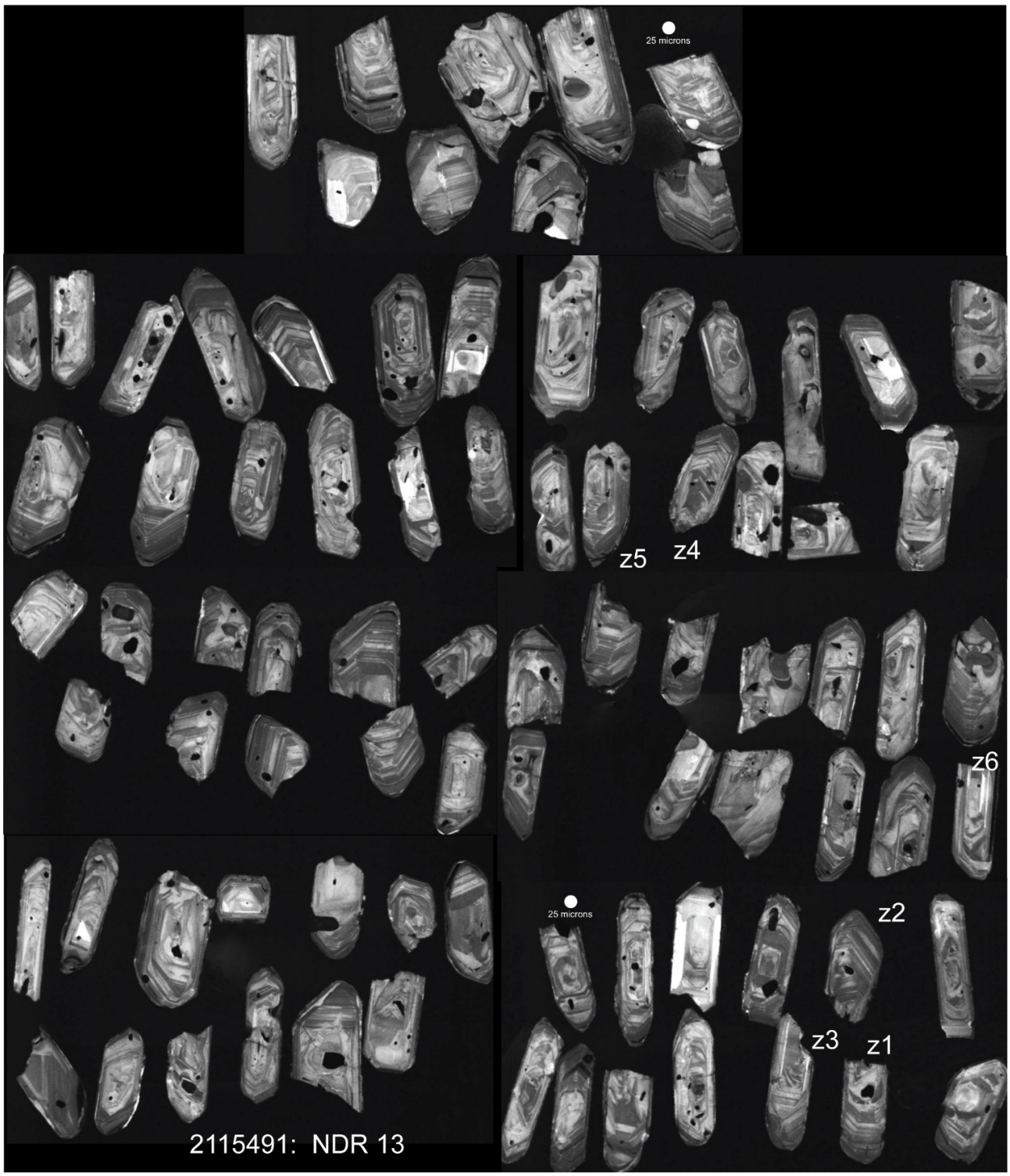

Figure 36. CL image of all zircon handpicked from sample 2115491.

APPENDIX 2. CA-TIMS ZIRCON U-PB ISOTOPIC DATA

Sample	Collector for Pb	Th/U	$^{206}Pb^*$ x10^{-13} mol	mol % 206Pb*	Pb* (pg)	Pb*/Pb$_c$	Pb$_c$ (pg)	$^{206}Pb/^{204}Pb$	$^{208}Pb/^{206}Pb$	$^{207}Pb/^{206}Pb$	% err	$^{207}Pb/^{235}U$	% err	$^{206}Pb/^{238}U$	% err	corr. coef.	$^{207}Pb/^{206}Pb$	±	$^{207}Pb/^{235}U$	±	$^{206}Pb/^{238}U$	±	% disc.	include in weighted mean?	*Weighted Mean Calculations*			
(a)		(b)	(c)		(c)		(c)	(d)	(e)	(e)	(f)	(e)	(f)	(e)	(f)		(g)	(f)	(g)	(f)	(g)	(f)	(h)					
2131359																												
z1	Daly	0.721	9.6602	99.97%	261	0.21	1225	67799	0.213	0.098404	0.062	3.783877	0.127	0.279008	0.070	0.969	1593.26	1.16	1589.33	1.02	1586.36	0.98	0.43	x	$^{207}Pb/^{206}Pb$ date ± random (+tracer) [+decay constant]			
z2	Daly	0.644	6.3443	99.96%	169	0.19	900	50709	0.190	0.098375	0.064	3.787764	0.128	0.279377	0.069	0.968	1592.71	1.19	1590.15	1.03	1588.22	0.97	0.28	x	**1592.62**	**± 0.52**	[2.41]	2σ
z3	Daly	0.687	2.7312	99.89%	73	0.26	285	15913	0.202	0.098369	0.071	3.791550	0.135	0.279675	0.071	0.955	1592.59	1.32	1590.96	1.09	1589.73	1.00	0.18	x		**± 0.66**	[2.40]	c95%
z4	Daly	0.803	4.9473	99.94%	136	0.25	548	29798	0.237	0.098364	0.064	3.793787	0.129	0.279854	0.069	0.971	1592.49	1.20	1591.43	1.04	1590.63	0.98	0.12	x	MSWD =	0.42		
z6	Daly	0.702	2.8521	99.87%	77	0.31	249	13880	0.207	0.098348	0.072	3.789859	0.136	0.279608	0.071	0.948	1592.20	1.35	1590.60	1.09	1589.39	1.00	0.18	x	pof =	0.84		
z5	Daly	0.709	2.5512	99.92%	69	0.18	388	21546	0.209	0.098347	0.076	3.794420	0.138	0.279947	0.073	0.924	1592.18	1.42	1591.56	1.11	1591.10	1.03	0.07	x	n =	6		
2111460																												
z1	Daly	0.989	21.2694	99.99%	610	0.21	2959	154412	0.291	0.098700	0.060	3.799243	0.127	0.279303	0.072	0.967	1598.86	1.12	1592.59	1.02	1587.85	1.01	0.69		$^{207}Pb/^{206}Pb$ date ± random (+tracer) [+decay constant]			
z6	Daly	0.830	9.8015	99.97%	272	0.24	1144	61804	0.245	0.098389	0.062	3.786433	0.126	0.279240	0.068	0.969	1592.97	1.17	1589.87	1.01	1587.54	0.96	0.34	x	**1591.79**	**± 0.42**	[2.40]	2σ
z3	Daly	0.900	6.2742	99.95%	177	0.24	741	39458	0.265	0.098340	0.063	3.785791	0.127	0.279333	0.068	0.970	1592.03	1.18	1589.74	1.02	1588.00	0.96	0.25	x		**± 0.74**	[2.47]	c95%
z4	Faraday-Daly	0.897	15.1138	99.97%	425	0.34	1237	65857	0.265	0.098330	0.042	3.779098	0.087	0.278868	0.051	0.950	1591.85	0.78	1588.31	0.70	1585.66	0.72	0.39	x	MSWD =	1.57		
z2	Faraday-Daly	0.824	18.2497	99.98%	505	0.29	1723	93206	0.243	0.098303	0.041	3.777605	0.087	0.278832	0.052	0.955	1591.34	0.76	1588.00	0.70	1585.48	0.73	0.37	x	pof =	0.18		
z5	Daly	0.705	7.4706	99.97%	201	0.20	1001	55643	0.208	0.098303	0.062	3.790804	0.127	0.279808	0.069	0.972	1591.33	1.16	1590.80	1.02	1590.39	0.97	0.06	x	n =	5		
2053554																												
z2	Daly	1.194	6.6257	99.96%	198	0.23	850	42544	0.352	0.098075	0.064	3.773476	0.129	0.279174	0.071	0.964	1587.01	1.19	1587.12	1.04	1587.20	1.00	-0.01	x	$^{207}Pb/^{206}Pb$ date ± random (+tracer) [+decay constant]			
z4	Daly	1.044	14.1376	99.93%	410	0.86	476	23901	0.308	0.098068	0.063	3.775152	0.127	0.279319	0.068	0.972	1586.87	1.17	1587.48	1.02	1587.93	0.96	-0.07	x	**1586.49**	**± 0.49**	[2.41]	2σ
z3	Daly	1.083	6.2514	99.94%	183	0.29	629	32185	0.319	0.098061	0.064	3.770709	0.128	0.279012	0.069	0.973	1586.73	1.19	1586.53	1.03	1586.38	0.97	0.02	x		**± 0.62**	[2.42]	c95%
z5	Daly	1.206	8.0930	99.96%	243	0.30	822	41007	0.355	0.098052	0.063	3.771980	0.128	0.279131	0.069	0.970	1586.56	1.19	1586.80	1.03	1586.98	0.97	-0.03	x	MSWD =	0.71		
z1	Daly	1.253	5.5442	99.95%	168	0.25	685	33881	0.369	0.098026	0.065	3.768571	0.130	0.278952	0.069	0.966	1586.07	1.22	1586.08	1.04	1586.08	0.97	0.00	x	pof =	0.61		
z6	Daly	1.233	9.7862	99.97%	295	0.25	1177	58430	0.363	0.098008	0.063	3.770329	0.127	0.279134	0.068	0.971	1585.72	1.17	1586.45	1.02	1587.00	0.96	-0.08	x	n =	6		
2049214																												
z1	Faraday-Daly	1.103	40.4235	99.99%	1188	0.27	4386	223527	0.325	0.097758	0.040	3.741599	0.087	0.277716	0.052	0.956	1580.94	0.75	1580.32	0.70	1579.85	0.73	0.07	x	$^{207}Pb/^{206}Pb$ date ± random (+tracer) [+decay constant]			
z3	Faraday-Daly	1.227	52.6657	99.99%	1588	0.24	6655	330574	0.362	0.097727	0.040	3.737811	0.087	0.277522	0.052	0.955	1580.35	0.75	1579.50	0.70	1578.87	0.73	0.09	x	**1580.21**	**± 0.31**	[2.38]	2σ
z6	Faraday-Daly	1.134	45.0855	99.99%	1333	0.28	4803	243193	0.334	0.097715	0.041	3.738756	0.086	0.277626	0.051	0.956	1580.13	0.76	1579.71	0.69	1579.39	0.71	0.05	x		**± 0.40**	[2.40]	c95%
z4	Faraday-Daly	1.204	28.8452	99.99%	866	0.26	3289	164149	0.355	0.097708	0.040	3.737048	0.086	0.277519	0.051	0.959	1579.99	0.75	1579.34	0.69	1578.85	0.71	0.07	x	MSWD =	1.10		
z2	Faraday-Daly	1.077	38.4241	99.99%	1123	0.27	4186	214487	0.318	0.097706	0.040	3.736964	0.086	0.277519	0.051	0.957	1579.95	0.75	1579.32	0.69	1578.85	0.71	0.07	x	pof =	0.36		
z5	Faraday-Daly	1.243	29.3109	99.99%	886	0.30	2942	145693	0.367	0.097702	0.041	3.736802	0.087	0.277516	0.052	0.953	1579.89	0.76	1579.29	0.70	1578.84	0.73	0.07	x	n =	6		
2115491																												
z5	Daly	0.549	5.2402	99.97%	136	0.14	942	54272	0.162	0.098172	0.064	3.760274	0.129	0.277924	0.070	0.966	1588.85	1.19	1584.31	1.03	1580.90	0.98	0.50		$^{207}Pb/^{206}Pb$ date ± random (+tracer) [+decay constant]			
z1	Daly	0.570	3.8412	99.96%	100	0.13	778	44604	0.168	0.098003	0.064	3.761214	0.130	0.278472	0.071	0.967	1585.64	1.20	1584.51	1.04	1583.66	0.99	0.12		**1579.37**	**± 0.73**	[2.47]	2σ
z6	Daly	0.596	3.6065	99.93%	95	0.22	438	24958	0.176	0.097915	0.068	3.757012	0.131	0.278411	0.069	0.961	1583.96	1.27	1583.61	1.05	1583.35	0.97	0.04			**± 1.57**	[2.65]	c95%
z4	Daly	0.605	3.1062	99.93%	82	0.18	447	25443	0.178	0.097701	0.066	3.737241	0.131	0.277553	0.070	0.964	1579.86	1.24	1579.38	1.05	1579.03	0.98	0.05	x	MSWD =	0.60		
z2	Daly	0.490	6.5290	99.97%	167	0.16	1053	61576	0.145	0.097675	0.070	3.732351	0.131	0.277265	0.070	0.933	1579.35	1.32	1578.33	1.05	1577.57	0.98	0.11	x	pof =	0.55		
z3	Daly	0.487	4.4781	99.95%	115	0.18	642	37549	0.144	0.097651	0.066	3.726275	0.131	0.276881	0.070	0.958	1578.90	1.24	1577.03	1.05	1575.63	0.98	0.21	x	n =	3		

(a) z1, z2 etc. are labels for analyses composed of single zircon grains that were annealed and chemically abraded (Mattinson 2005).
(b) Model Th/U ratio calculated from radiogenic $^{208}Pb/^{206}Pb$ ratio and $^{207}Pb/^{235}U$ date.
(c) Pb* and Pbc are radiogenic and common Pb, respectively. mol % $^{206}Pb^*$ is with respect to radiogenic and blank Pb.
(d) Measured ratio corrected for spike and fractionation only. Pb fractionation correction for analyses done with tracer solution BSU1B is 0.16 ± 0.03 (1 sigma) %/amu (atomic mass unit) for single-collector Daly analyses, based on analysis of EARTHTIME ^{202}Pb-^{205}Pb ET2535 tracer solution. Pb fractionation correction for analyses done with tracer solution ET2535 is based on measurement of $^{202}Pb/^{205}Pb$ in the tracer solution.
(e) Corrected for fractionation and spike. Common Pb is assigned to procedural blank with composition of $^{206}Pb/^{204}Pb$ = 18.04 ± 0.61%; $^{207}Pb/^{204}Pb$ = 15.54 ± 0.52%; $^{208}Pb/^{204}Pb$ = 37.69 ± 0.63% (1 sigma). $^{206}Pb/^{238}U$ and $^{207}Pb/^{206}Pb$ ratios corrected for initial disequilibrium in $^{230}Th/^{238}U$ using a Th/U[magma] of 3.0 ± 0.5 (1 sigma).
(f) Errors are 2 sigma, propagated using algorithms of Schmitz and Schoene (2007) and Crowley et al. (2007).
(g) Calculations based on the decay constants of Jaffey et al. (1971). $^{206}Pb/^{238}U$ and $^{207}Pb/^{206}Pb$ dates corrected for initial disequilibrium in $^{230}Th/^{238}U$ using a Th/U[magma] of 3.0 ± 0.5 (1 sigma).
(h) % discordance = (1 - ($^{206}Pb/^{238}U$ date / $^{207}Pb/^{206}Pb$ date)) * 100.

APPENDIX 3. COMPILATION OF MAGMATIC AGES FOR THE HILTABA EVENT

Sample_Number	Stratigraphic_unit	Latitude	Longitude	Age	Error	Method	Mineral	Reference
PEAKE AND DENISON INLIER								
1472969	undifferentiated Hiltaba Suite	-28.0384	135.8763	1591	11	SHRIMP	zircon	Fanning et al. 2007
1472971	undifferentiated Hiltaba Suite	-28.2694	136.3879	1530	19	SHRIMP	zircon	Fanning et al. 2007
1472970	undifferentiated Hiltaba Suite	-28.2694	136.3879	1555	14	SHRIMP	zircon	Fanning et al. 2007
COOBER PEDY RIDGE AND NAWA DOMAIN								
1699629	Leonard Rise Norite	-29.2131	134.6204	1590	9	La-ICPMS	zircon	Rusak 2010
1700878	undifferentiated Hiltaba Suite	-29.2377	134.8028	1589	8	La-ICPMS	zircon	Rusak 2010
1472871	undifferentiated Hiltaba Suite	-29.1161	134.3435	1589	11	SHRIMP	zircon	Fanning et al. 2007
1699628	Leonard Rise Norite	-29.2131	134.6204	1582	14	La-ICPMS	zircon	Rusak 2010
2007371005c	undifferentiated Hiltaba Suite	-28.8200	133.8273	1580	4	SHRIMP	monazite	Fraser et al. 2012
1700866	undifferentiated Hiltaba Suite	-29.2377	134.8028	1579	7	La-ICPMS	zircon	Rusak 2010
1699621	Leonard Rise Norite	-29.2131	134.6204	1574	8	La-ICPMS	zircon	Rusak 2010
1707896	undifferentiated Hiltaba Suite	-29.1019	134.4146	1569	5	SHRIMP	zircon	Jagodzinski and Reid 2010
MOUNT WOODS INLIER								
	Balta Granite	-29.5870	135.3816	1591	5	SHRIMP	zircon	Holm 2004
	Balta Granite?	-29.5894	135.4667	1590.7	3.3	SHRIMP	zircon	Holm 2004
	Balta Granite?	-29.5333	135.4209	1589.3	4.5	SHRIMP	zircon	Holm 2004
	undifferentiated Hiltaba Suite	-29.5894	135.4667	1587.9	2.3	SHRIMP	zircon	Holm 2004
	Balta Granite?	-29.5977	135.3917	1587.4	2.8	SHRIMP	zircon	Holm 2004
	Balta Granite?	-29.4237	135.1286	1587	2	SHRIMP	zircon	Holm 2004
200236 8028b	undifferentiated Hiltaba Suite	-29.5561	135.3949	1586.8	4.1	SHRIMP	zircon	Jagodzinski 2005
200136 8015f	Balta Granite?	-29.6507	135.3498	1586.3	2.8	SHRIMP	zircon	Jagodzinski 2005
Balta Granite	Balta Granite	-29.4981	135.24	1584	18	SHRIMP	zircon	Finlay 1993
	Balta Granite?	-29.5977	135.3917	1578.6	4.3	SHRIMP	zircon	Holm 2004
2013958	Balta Granite?	-29.3035	135.1177	1572	6	SHRIMP	zircon	Jagodzinski and Reid 2015
MULGATHING COMPLEX								
2016110	undifferentiated Hiltaba Suite	-29.5999	134.3589	1584	6	SHRIMP	zircon	Jagodzinski and Reid 2015

Sample_Number	Stratigraphic_unit	Latitude	Longitude	Age	Error	Method	Mineral	Reference
OLYMPIC DOMAIN								
RD87	Burgoyne Granite	-30.5553	136.7529	1613	20	ID-TIMS	multi zircon	Mortimer et al. 1988
RD80	Burgoyne Granite	-30.5196	136.9098	1606	7	ID-TIMS	multi zircon	Mortimer et al. 1988
mixed source	Burgoyne Granite	-30.6419	136.795	1604	9	ID-TIMS	multi apatite	Mortimer et al. 1988
200036 6006	Burgoyne Granite	-30.3761	137.0989	1600	0	SHRIMP	zircon	Jagodzinski 2005
9373	Burgoyne Granite	-30.4125	137.2631	1598	2.3	ID-TIMS	titanite	Creaser and Cooper 1993
RX3212	Roxby Downs Syenogranite	-30.4371	136.8749	1598	14	SHRIMP	zircon	Johnson 1993
RX2820 and X4544	ash-fall tuff clast in ODBC	-30.4404	136.8857	1597	8	SHRIMP	zircon	Johnson and Cross 1995
LCD1	Roxby Downs Syenogranite	-30.4518	136.8947	1595.97	0.94	CA-TIMS	zircon	Courtney-Davies et al. 2020
RX3698	Roxby Downs Syenogranite	-30.4450	136.8905	1595	11	SHRIMP	zircon	Johnson 1993
LCD30A	lower GRV	-30.4759	136.8877	1594.63	0.86	CA-TIMS	zircon	Courtney-Davies et al. 2020
2131354	lower GRV	-31.0732	136.9379	1594.53	0.88	CA-TIMS	zircon	this study
LCD13	Roxby Downs Syenogranite	-30.4518	136.8947	1594.5	1.68	CA-TIMS	zircon	Courtney-Davies et al. 2020
RX8078	Burgoyne Granite	-30.6067	136.8516	1594.04	0.64	CA-TIMS	zircon	McPhie et al. 2020
OD055	lower GRV	-30.4759	136.8877	1594.03	0.80	CA-TIMS	zircon	Cherry et al. 2018
2000366168	Olympic Dam Breccia Complex	-30.4488	136.9013	1594	6	SHRIMP	zircon	Jagodzinski 2014
2000366166	Olympic Dam Breccia Complex	-30.4394	136.8766	1594	4	SHRIMP	zircon	Jagodzinski 2014
2000366165	Olympic Dam Breccia Complex	-30.4535	136.8918	1594	4	SHRIMP	zircon	Jagodzinski 2014
2000366174	Roxby Downs Syenogranite	-30.4643	136.8488	1594	8	SHRIMP	zircon	Jagodzinski 2014
2000366005	Burgoyne Granite	-30.4023	136.9785	1594	3.9	SHRIMP	zircon	Jagodzinski 2005
2000366176	Roxby Downs Syenogranite	-30.4768	136.8524	1594	5	SHRIMP	zircon	Jagodzinski 2014
2000366000	Roxby Downs Syenogranite	-30.4624	136.9763	1594	4	SHRIMP	zircon	Jagodzinski 2014
OD1207	lower GRV	-30.4759	136.8877	1593.94	0.69	CA-TIMS	zircon	Cherry et al. 2018
OD487	lower GRV	-30.4759	136.8877	1593.68	0.68	CA-TIMS	zircon	Cherry et al. 2018
LCD 12	Roxby Downs Syenogranite	-30.4518	136.8947	1593.4	1.1	CA-TIMS	zircon	Courtney-Davies et al. 2020
LCD 11	Roxby Downs Syenogranite	-30.4518	136.8947	1593.28	0.45	CA-TIMS	zircon	Courtney-Davies et al. 2020
OD1202	Roxby Downs Syenogranite	-30.4759	136.8877	1593.25	0.68	CA-TIMS	zircon	Cherry et al. 2018
OD20	lower GRV	-30.4759	136.8877	1593.19	0.87	CA-TIMS	zircon	McPhie et al. 2020
OD1201	Roxby Downs Syenogranite	-30.4759	136.8877	1593.06	0.55	CA-TIMS	zircon	Cherry et al. 2018
2000366176	Roxby Downs Syenogranite	-30.4768	136.8524	1593.06	0.58	CA-TIMS	zircon	Cherry et al. 2018

Sample_Number	Stratigraphic_unit	Latitude	Longitude	Age	Error	Method	Mineral	Reference
OD1178	lower GRV	-30.4759	136.8877	1593.04	1.3	CA-TIMS	zircon	McPhie et al. 2020
2000366173	Olympic Dam Breccia Complex	-30.4497	136.9015	1593	6	SHRIMP	zircon	Jagodzinski 2014
2000366167	Olympic Dam Breccia Complex	-30.4476	136.9031	1593	6	SHRIMP	zircon	Jagodzinski 2014
SS-180	Wirrda Granite	-30.6064	137.0855	1593	2	ID-TIMS	multi titanite	Creaser 1989
9383	Wirrda Granite	-30.4125	137.2631	1593	3.4	ID-TIMS	multi titanite	Creaser and Cooper 1993
2000366178	Olympic Dam Breccia Complex	-30.4326	136.8699	1593	5	SHRIMP	zircon	Jagodzinski 2014
2000366169	Olympic Dam Breccia Complex	-30.4489	136.9013	1593	11	SHRIMP	zircon	Jagodzinski 2014
2000366170	Olympic Dam Breccia Complex	-30.4489	136.9013	1593	6	SHRIMP	zircon	Jagodzinski 2014
OD1215	Roxby Downs Syenogranite	-30.4759	136.8877	1592.99	0.54	CA-TIMS	zircon	Cherry et al. 2018
2131365	lower GRV	-30.5755	137.3676	1592.79	0.71	CA-TIMS	zircon	this study
OD1214	Roxby Downs Syenogranite	-30.4759	136.8877	1592.68	1.26	CA-TIMS	zircon	Cherry et al. 2018
2131359	Burgoyne Granite	-30.3981	137.3017	1592.62	0.66	CA-TIMS	zircon	Jagodzinski et al. 2021
2000366166	lower GRV	-30.4394	136.8766	1592.21	0.66	CA-TIMS	zircon	this study
2000366179	Olympic Dam Breccia Complex	-30.4388	136.8851	1592	6	SHRIMP	zircon	Jagodzinski 2014
2000366164	Olympic Dam Breccia Complex	-30.4532	136.8871	1592	4	SHRIMP	zircon	Jagodzinski 2014
9288	Wirrda Granite	-30.4125	137.2631	1592	5	ID-TIMS	multi zircon	Creaser and Cooper 1993
RX3222	Roxby Downs Syenogranite	-30.4508	136.8922	1592	8	SHRIMP	zircon	Johnson and Cross 1995
2000366172	Olympic Dam Breccia Complex	-30.4438	136.895	1592	5	SHRIMP	zircon	Jagodzinski 2014
2000366175	Roxby Downs Syenogranite	-30.4742	136.8857	1592	5	SHRIMP	zircon	Jagodzinski 2014
2111460	Burgoyne Granite	-30.4701	136.7971	1591.79	0.74	CA-TIMS	zircon	Jagodzinski et al. 2021
SS-103	Wirrda Granite	-30.5507	137.1802	1591	7	ID-TIMS	multi titanite	Creaser 1989
ACD-5	GRV	-30.5798	136.8118	1591	10	ID-TIMS	multi zircon	Creaser and Cooper 1993
1901138	undifferentiated Hiltaba Suite	-31.2676	137.2516	1591	10	SHRIMP	zircon	Reid and Fabris 2012
2000366171	Olympic Dam Breccia Complex	-30.4489	136.9013	1591	5	SHRIMP	zircon	Jagodzinski 2014
OD239	lower GRV	-30.4759	136.8877	1590.35	1.13	CA-TIMS	zircon	Cherry et al. 2018
9287	Burgoyne Granite	-30.4125	137.2631	1590	5	ID-TIMS	multi zircon	Creaser and Cooper 1993
9347	Burgoyne Granite	-30.5507	137.1802	1590	10	ID-TIMS	multi zircon	Creaser and Cooper 1993
PD3	Burgoyne Granite	-30.5216	137.008	1590	5	SHRIMP	zircon	Mortimer et al. 1988
OD41	lower GRV	-30.4759	136.8877	1589.86	1.19	CA-TIMS	zircon	Cherry et al. 2018
9330	Roxby Downs Syenogranite	-30.4617	136.9123	1588	4	ID-TIMS	multi zircon	Creaser and Cooper 1993

Sample_Number	Stratigraphic_unit	Latitude	Longitude	Age	Error	Method	Mineral	Reference
RX3223	Roxby Downs Syenogranite	-30.4497	136.9015	1584	20	SHRIMP	zircon	Johnson and Cross 1995
R17251 & R17252	GRV	-31.0732	136.9379	1583	12	SHRIMP	zircon	Fanning et al. 2007
ACD5	GRV	-30.5798	136.8118	1576	22	ID-TIMS	multi zircon	Mortimer et al. 1988
CENTRAL GAWLER CRATON								
698670	Yardea Dacite	-32.5191	136.1257	1598	10	LA-ICPMS	zircon	Reid et al. 2006
387444	undifferentiated Hiltaba Suite	-31.0582	134.5313	1596	9	SHRIMP	zircon	Fanning et al. 2007
2695960	felsic dyke, Tolmer Granite	-30.6834	134.1754	1594	10	LA-ICPMS	zircon	Bockmann et al. 2019
6132 RS56	Yardea Dacite, UGRV	-32.5191	136.1257	1592	3	ID-TIMS	multi zircon	Fanning et al. 1988
2001363093	Pegler Granite	-30.1930	134.2558	1592	6	SHRIMP	zircon	Budd 2006
5934 RS185	Childera Dacite, LGRV	-31.8070	135.2054	1592	17	ID-TIMS	multi zircon	Blisset et al. 1993
5833 RS33	Waganny Dacite, LGRV	-32.1200	134.9455	1591	3	ID-TIMS	multi zircon	Fanning et al. 1988
2695962	Pinding Granite	-30.7483	134.3895	1591	12	LA-ICPMS	zircon	Bockmann et al. 2019
2016125	lower GRV	-30.3033	134.5271	1590.35	0.64	CA-TIMS	zircon	this study
2001363031	Salt Springs Granite	-30.6546	134.755	1589.8	7.4	SHRIMP	zircon	Budd 2006
2746487	lower GRV	-31.2361	135.2062	1589.19	0.32	CA-TIMS	zircon	this study
2721839	lower GRV	-31.7648	135.2091	1589.19	0.48	CA-TIMS	zircon	this study
5737 RS25	Ealbara Rhyolite, LGRV	-30.3033	134.5271	1589	16	ID-TIMS	multi zircon	Blisset et al. 1993
2018616	Bittali Rhyolite, lower GRV	-32.6085	136.9372	1588.47	0.66	CA-TIMS	zircon	this study
51677	undifferentiated Hiltaba Suite	-30.7094	134.5278	1587	20	SHRIMP	zircon	Fanning et al. 2007
1998158	Eucarro Rhyolite, UGRV	-32.5476	136.7093	1586.65	0.64	CA-TIMS	zircon	this study
2053554	Cooladding Granite	-30.6172	134.5079	1586.49	0.62	CA-TIMS	zircon	Jagodzinski et al. 2021
1998160	Moonaree Dacite Member, UGRV	-32.4151	136.1033	1586.39	0.66	CA-TIMS	zircon	this study
961807	GRV	-31.2277	134.7636	1586	9	SHRIMP	zircon	Jagodzinski et al. 2006
2695958	Cooladding Granite	-30.6136	134.5073	1582	9	LA-ICPMS	zircon	Bockmann et al. 2019
2002363008A	Lady Jane Diorite	-30.7071	134.5269	1582	5	SHRIMP	zircon	Budd and Fraser 2004
469740	Kondoolka Batholith	-31.8639	134.7486	1580	7	SHRIMP	zircon	Ferris 2001
2001363044	Partridge Granite	-30.5272	134.8228	1577	8.5	SHRIMP	zircon	Budd 2006
2001363078	Ambrosia Granite	-30.5488	134.1918	1575.4	7.8	SHRIMP	zircon	Budd 2006
2001363067	Tolmer Granite	-30.6851	134.175	1574.7	4.3	SHRIMP	zircon	Budd 2006
2695959	Cooladding Granite	-30.4723	134.5552	1574	9	LA-ICPMS	zircon	Bockmann et al. 2019

Sample_Number	Stratigraphic_unit	Latitude	Longitude	Age	Error	Method	Mineral	Reference
1124963	Kokatha Granite	-31.1153	134.8259	1574	5	SHRIMP	zircon	Fanning et al. 2007
SOUTHERN MARGIN GRV								
1124962	GRV	-32.6463	136.4145	1604	11	SHRIMP	zircon	Fanning et al. 2007
1951826	GRV	-32.6293	136.0378	1597	14	SHRIMP	zircon	Reid and Jagodzinski 2012
1124961	GRV	-32.6463	136.4145	1594	11	SHRIMP	zircon	Fanning et al. 2007
2017742	lower GRV	-32.7424	137.3834	1593.61	0.19	CA-TIMS	zircon	this study
698129	Kooma-Vue Monzogabbro	-33.0827	135.7921	1593	5	SHRIMP	zircon	Jagodzinski et al. 2007
1893809	GRV	-32.6502	136.0556	1591	8	SHRIMP	zircon	Reid and Jagodzinski 2012
2116682	lower GRV	-32.4671	137.3294	1590.35	0.65	CA-TIMS	zircon	this study
2116683	lower GRV	-32.4671	137.3294	1590.18	0.94	CA-TIMS	zircon	this study
2003362501	Weednana Granite	-32.7758	136.4799	1588	4	SHRIMP	zircon	Fraser et al. 2007
RX4574	GRV	-32.7234	137.4	1587	15	SHRIMP	zircon	Johnson 1993
1835184	undifferentiated Hiltaba Suite	-32.7770	136.4781	1585	5	SHRIMP	zircon	Reid et al. 2012
5832 RS15	Inkster Norite	-32.9363	135.0009	1583	24	K-Ar	biotite	Webb et al. 1986
1832111	undifferentiated Hiltaba Suite	-32.7378	136.4345	1581	9	ID-TIMS	Sm-Nd	Reid and Jagodzinski 2012
662450	Waroona Norite	-33.2635	135.7306	1571	38	SHRIMP	zircon	Jagodzinski et al. 2006
EYRE PENINSULA								
2009371027	Cunyarie Granite	-32.9040	136.29376	1598	7	SHRIMP	zircon	Fraser and Neumann 2010
1039359	Calca Granite?	-33.7173	134.5449	1595	6	SHRIMP	zircon	Jagodzinski et al. 2006
1039265	Pearson Isles Granite	-33.9600	134.262	1592	6	SHRIMP	zircon	Jagodzinski et al. 2007
06-MNJ-05	Munjeela Suite	-32.1923	133.1483	1591	11	LA-ICPMS	zircon	Payne 2008
1948994	Samphire Granite	-33.2018	137.3897	1586	6	SHRIMP	zircon	Jagodzinski and Reid 2015
2009371024	Buckleboo Granite	-32.8104	136.05821	1586	6	SHRIMP	zircon	Fraser and Neumann 2010
1039269	Pearson Isles Granite	-33.9520	134.2719	1585	7	SHRIMP	zircon	Jagodzinski et al. 2007
LTU9445	Midgee Granite	-33.4322	137.0551	1585	5	SHRIMP	zircon	Creaser and Fanning 1993
2134835	Calca Granite	-33.0450	134.1857	1585	7	SHRIMP	zircon	Reid et al. 2016
20883	Cultana Granite	-32.8443	137.8069	1584	3	ID-TIMS	multi zircon	Blisset et al. 1993
1948990	Samphire Granite	-33.2200	137.412	1584	4	SHRIMP	zircon	Jagodzinski and Reid 2015
1124964	Calca Granite	-33.0600	134.3953	1583	10	SHRIMP	zircon	Fanning et al. 2007
Charleston Granite	Midgee Granite	-33.4322	137.0551	1581	4	Kober	zircon	Dougherty-Page and Foden 1996

Sample_Number	Stratigraphic_unit	Latitude	Longitude	Age	Error	Method	Mineral	Reference
06-MNJ-32	Munjeela Suite	-32.1940	133.3948	1580	15	LA-ICPMS	zircon	Payne 2008
6331 RS176	Midgee Granite	-33.4322	137.0551	1576		SHRIMP	zircon	Fanning et al. 1988
YORKE PENINSULA								
142526	Point Riley Tonalite	-33.8758	137.602	1597	7	SHRIMP	zircon	Fanning et al. 2007
142524	Tickera Granite	-33.8836	137.6071	1591	19	SHRIMP	zircon	Fanning et al. 2007
1831634	Tickera Granite	-34.5304	137.8769	1590	10	SHRIMP	zircon	Reid and Jagodzinski 2011
364685	Curramulka Gabbronorite	-34.6273	137.7027	1588.3	6.3	SHRIMP	zircon	Zang et al. 2007
1831629	Tickera Granite	-34.5378	137.8719	1588	10	SHRIMP	zircon	Reid and Jagodzinski 2011
1831630	Oorlano metasomatite?	-34.5378	137.8719	1586	11	SHRIMP	titanite	Reid and Jagodzinski 2011
364682	Curramulka Gabbronorite	-34.6408	137.7016	1585.3	8.3	SHRIMP	zircon	Zang et al. 2007
2116262	Tickera Granite	-33.8760	137.6014	1584.22	0.83	CA-TIMS	zircon	Reid et al. 2021
1831633	Oorlano metasomatite?	-34.5377	137.8725	1584	7	SHRIMP	allanite	Reid and Jagodzinski 2011
142525	Tickera Granite	-33.8830	137.606	1583	10	SHRIMP	zircon	Fanning et al. 2007
2053555	Point Riley Tonalite	-33.8760	137.6013	1582.66	1.42	CA-TIMS	zircon	Reid et al. 2021
9392	Tickera Granite	-34.1158	137.572	1582	7	ID-TIMS	multi zircon	Creaser and Cooper 1993
2049214	Curramulka Gabbronorite	-34.6273	137.7027	1580.21	0.4	CA-TIMS	zircon	Jagodzinski et al. 2021
2116264	Myponie Syenogranite	-33.8760	137.6013	1579.05	0.81	CA-TIMS	zircon	Reid et al. 2021
786133	Curramulka Gabbronorite	-34.6408	137.7016	1579	8	LA-ICPMS	zircon	Reid et al. 2006
142523	Tickera Granite	-33.8894	137.6155	1577	7	SHRIMP	zircon	Fanning et al. 2007
2665675	Tickera Granite	-33.7121	137.8001	1576	25	LA-ICPMS	zircon	Reid et al. 2020
2665668	Tickera Granite	-33.6916	137.8173	1556	25	LA-ICPMS	zircon	Reid et al. 2020
698213	Daly Head Metadolerite	-35.1923	136.8616	1564	4	SHRIMP	zircon	Reid et al. 2021b
2665666	Tickera Granite	-33.6986	137.8168	1546	19	LA-ICPMS	zircon	Reid et al. 2020
FOWLER DOMAIN								
1834114	Jellabinna Granite	-31.0924	133.3676	1599	37	LA-ICPMS	zircon	Reid and Dutch 2012
1834093	Poondinga Granite	-31.3781	133.37	1596	18	LA-ICPMS	zircon	Reid and Dutch 2012
1834091	Jellabinna Granite	-31.1909	133.4871	1596	27	LA-ICPMS	zircon	Reid and Dutch 2012
2115512	undifferentiated Hiltaba Suite	-31.8058	132.2373	1593	7	LA-ICPMS	zircon	Reid et al. 2019
1964851	undifferentiated Hiltaba Suite	-29.1178	129.6809	1591	11	SHRIMP	zircon	Neumann and Korsch 2014
1834092	Poondinga Granite	-31.3781	133.37	1591	31	LA-ICPMS	zircon	Reid and Dutch 2012

Sample_Number	Stratigraphic_unit	Latitude	Longitude	Age	Error	Method	Mineral	Reference
1834110	undifferentiated Hiltaba Suite	-31.9330	132.3228	1590	88	LA-ICPMS	zircon	Reid and Dutch 2012
1834106	Inila Granite	-31.7776	133.4266	1587	22	LA-ICPMS	zircon	Reid and Dutch 2012
215773	undifferentiated Hiltaba Suite	-31.6283	132.0651	1586	9	SHRIMP	zircon	Fanning et al. 2007
2145321	undifferentiated Hiltaba Suite	-31.7851	132.2498	1586	3	SHRIMP	zircon	Jagodzinski et al.2019
2322236	undifferentiated Hiltaba Suite	-31.3999	132.4521	1585	4	SHRIMP	zircon	Jagodzinski et al. 2019
1834115	Jellabinna Granite	-31.0932	133.367	1584	14	LA-ICPMS	zircon	Reid and Dutch 2012
WGC193	Remote pluton	-31.0740	132.7196	1584	16	Kober	zircon	Teasdale 1997
1834090	Jellabinna Granite	-31.1909	133.4871	1582	14	LA-ICPMS	zircon	Reid and Dutch 2012
2115492	undifferentiated Hiltaba Suite	-31.7828	132.2177	1581	7	SHRIMP	monazite	Reid et al. 2019
2115491	undifferentiated Hiltaba Suite	-31.6283	132.0651	1579.37	1.57	CA-TIMS	zircon	Jagodzinski et al. 2021
2322233	undifferentiated Hiltaba Suite	-31.3995	132.4518	1578	9	SHRIMP	zircon	Jagodzinski et al. 2019
215780	Remote pluton	-31.0726	132.721	1568	11	SHRIMP	zircon	Fanning et al. 2007
2115501	undifferentiated Hiltaba Suite	-31.8043	132.2387	1564	8	SHRIMP	zircon	Jagodzinski and Reid 2016
48117	undifferentiated Hiltaba Suite	-31.8058	132.2373	1547	9	SHRIMP	zircon	Fanning et al. 2007
BAROSSA COMPLEX								
695754	undifferentiated Hiltaba Suite	-35.4852	138.3027	1580	4	SHRIMP	zircon	Jagodzinski et al. 2020
CURNAMONA PROVINCE								
	Cartwrights Creek Metasediments	-31.7309	141.2332	1600	4	SHRIMP	zircon	Page 2006
	Benagerie Volcanic Suite	-30.7652	140.4712	1599	40	SHRIMP	zircon	Fanning 1995
	Lf gneiss	-31.8741	141.4294	1597	3	SHRIMP	zircon	Page et al. 2000
99185514	Bimbowrie Supersuite	-31.8739	141.4282	1597	3	SHRIMP	zircon	Page et al. 2005
	Mundi Supersite Granite	-31.6640	141.4044	1596	3	SHRIMP	zircon	Page et al. 2000
99185513	Bimbowrie Supersuite	-31.6135	141.3937	1596	3	SHRIMP	zircon	Page et al. 2005
2002185870	Bimbowrie Supersuite	-32.2538	140.0372	1594	3	SHRIMP	zircon	Page unpublished
1707876	Ninnerie Supersuite	-31.5977	139.7897	1592	7	SHRIMP	zircon	Jagodzinski and Fricke 2010
	Mundi Nunneries Granite	-31.9553	141.4354	1591	5	SHRIMP	zircon	Page et al. 2000
99185515	Bimbowrie Supersuite	-31.5960	141.5001	1591	5	SHRIMP	zircon	Page et al. 2005
	Bimbowrie Suite	-31.9709	140.2305	1590		SHRIMP	zircon	Cook et al. 1994
2049215	Benagerie Volcanic Suite	-30.7159	140.4188	1587.31	0.51	CA-TIMS	zircon	this study
1709059	Benagerie Volcanic Suite	-31.7637	140.6866	1587	6	SHRIMP	zircon	Wade et al. 2012

Sample_Number	Stratigraphic_unit	Latitude	Longitude	Age	Error	Method	Mineral	Reference
2016105	Bimbowrie Suite	-32.0892	140.3089	1587	4	SHRIMP	zircon	Jagodzinski unpublished
2049213	Benagerie Volcanic Suite	-30.6052	140.3474	1586.44	0.78	CA-TIMS	zircon	this study
95BH10	Lf gneiss	-31.8741	141.4294	1586	9	SHRIMP	zircon	Nutman and Ehlers 1998
	Umberumberka type granite	-31.8384	141.2186	1586	4	SHRIMP	zircon	Page 2006
697455	Bimbowrie Supersuite	-31.9193	140.2114	1585	6	SHRIMP	zircon	Jagodzinski unpublished
668303	Benagerie Volcanic Suite	-30.7159	140.4188	1584	6	SHRIMP	zircon	Wade et al. 2012
668422	Benagerie Volcanic Suite	-30.7652	140.4712	1584	5	SHRIMP	zircon	Wade et al. 2012
	Benagerie Volcanic Suite	-30.7652	140.4712	1581	4	SHRIMP	zircon	Fanning et al. 1998
	Champion type granite	-31.8088	141.297	1581	3	SHRIMP	zircon	Page 2006
	Windamerta Diorite	-31.8917	139.8981	1581	6	SHRIMP	zircon	Fanning pers comm. Wade 2011
	Bimbowrie Suite	-32.0746	140.3178	1580		SHRIMP	zircon	Cook et al. 1994
A4	Bimbowrie Suite	-32.0126	139.8018	1580	21	ID-TIMS	multi zircon	Ludwig and Cooper 1984
	Mundi Windmeter Granite	-31.5355	141.3999	1580	2	SHRIMP	zircon	Page 2006
99185502	Bimbowrie Supersuite	-31.5283	141.3956	1580	5	SHRIMP	zircon	Page et al. 2005
2002185863	Bimbowrie Supersuite	-31.9828	140.2653	1580	4	SHRIMP	zircon	Page unpublished
B1	Bimbowrie Suite	-32.0241	139.8262	1578.9	2.7	ID-TIMS	multi zircon	Ludwig and Cooper 1984
A1	Bimbowrie Suite	-32.0126	139.8018	1578.6	2.3	ID-TIMS	multi zircon	Ludwig and Cooper 1984
695603	Lone Pine Dyke	-32.1102	140.5552	1577	3	SHRIMP	zircon	Jagodzinski unpublished
95BH10	Lf gneiss	-31.8741	141.4294	1573	29	SHRIMP	zircon	Nutman and Ehlers 1998
A3	Bimbowrie Suite	-32.0126	139.8018	1570	10	ID-TIMS	multi zircon	Ludwig and Cooper 1984
A9	Bimbowrie Suite	-32.0148	139.7425	1568.3	2.1	ID-TIMS	multi zircon	Ludwig and Cooper 1984
A2	Bimbowrie Suite	-32.0126	139.8018	1567	66	ID-TIMS	multi zircon	Ludwig and Cooper 1984
MOUNT PAINTER								
MN029	Mt Neill Granite	-29.9797	139.7128	1590.4	5.3	LA-ICP-MS	zircon	Kromkhun 2010
2009378038	unnamed granite	-30.6048	140.3526	1590	5	SHRIMP	zircon	Fraser and Neumann 2010
SD015	Box Bore Granite	-29.9797	139.7128	1586	45	LA-ICP-MS	zircon	Kromkhun 2010
2007379016	Mount Neill Granite	-30.0430	139.6414	1585	3	SHRIMP	zircon	Fraser and Neumann 2010
2007379001	unnamed migmatite	-30.1696	139.4423	1584	4	SHRIMP	zircon	Fraser and Neumann 2010
961972	Pepegoona Porphyry	-30.0904	139.5812	1584	5	SHRIMP	zircon	Jagodzinski unpublished
2007379015	Box Bore Granite	-29.9784	139.6948	1583	2	SHRIMP	zircon	Fraser and Neumann 2010

Sample_Number	Stratigraphic_unit	Latitude	Longitude	Age	Error	Method	Mineral	Reference
1851562	M14 of Sheard 2009	-29.9834	139.6988	1582	5	SHRIMP	zircon	Jagodzinski unpublished
2007379007	Hot Springs Gneiss	-30.1424	139.4727	1582	4	SHRIMP	zircon	Fraser and Neumann 2010
2007379004	Hot Springs Gneiss	-30.1687	139.4421	1582	6	SHRIMP	zircon	Fraser and Neumann 2010
1040064	Mt Painter Granite	-30.2185	139.3668	1579	5	SHRIMP	zircon	Jagodzinski unpublished
B60	Mount Neill Granite	-30.2706	139.2878	1577.5	1.5	Kober	zircon	Elberg et al. 2001
B59	Mount Neill Granite	-30.2706	139.2878	1577	0.9	Kober	zircon	Elberg et al. 2001
	Nooldoonooldoona Trondhjemite	-30.2722	139.2873	1576	2.4	Kober	zircon	Janka et al. 1999
	Ninnerie 3 porphyritic rhyolite	-30.2250	139.4366	1576	2	SHRIMP	zircon	Teale 1993
B61	Mount Neill Granite	-30.2706	139.2878	1575.5	8.2	Kober	zircon	Elberg et al. 2001
HS13	Mount Neill Granite	-30.2706	139.2878	1575.2	2.4	Kober	zircon	Elberg et al. 2001
	dacitic tuff	-30.0038	139.6475	1575	14	SHRIMP	zircon	Teale 1993
J32	Mount Neill Granite	-30.2706	139.2878	1574.7	3	Kober	zircon	Elberg et al. 2001
1851566	Nooldoonooldoona Trondhjemite	-30.2700	139.338	1570	7	SHRIMP	zircon	Jagodzinski unpublished
	Mount Neill Granite	-29.9919	139.6903	1569	14	SHRIMP	zircon	Fanning 1995
MN101	Terrapinna Granite	-29.9151	139.6725	1569	22	LA-ICP-MS	zircon	Kromkhun 2010
2007379014	Wattleowie Granite	-29.8942	139.6661	1563	3	SHRIMP	zircon	Fraser and Neumann 2010
SD022	Wattleowie Granite	-29.8594	139.6137	1562	7	LA-ICP-MS	zircon	Kromkhun 2010
2007379011	Terrapinna Granite	-29.9184	139.6647	1560	3	SHRIMP	zircon	Fraser and Neumann 2010
37335	Petermorra Volcanics	-29.7748	139.552	1560	3	ID-TIMS	zircon	Sheard et al. 1992
6838 RS 678	Petermorra Volcanics	-29.7965	139.5281	1560	3	ID-TIMS	zircon	Sheard et al. 1992
2009378027	UNNAMED CALC-SILICATE	-29.9257	139.8542	1558	3	SHRIMP	zircon	Fraser and Neumann 2010
2007379013	Yerila Granite	-29.9038	139.6258	1558	4	SHRIMP	zircon	Fraser and Neumann 2010
6938 RS 25	Terrapinna Granite	-29.9073	140.0144	1557	6	ID-TIMS	zircon	Sheard et al. 1992
	Yerila Granite	-29.9044	139.6253	1556	10	ID-TIMS	multi zircon	Johnson 1980 in Sheard 1992
SD060	Yerila Granite	-29.8731	139.6386	1556	20	LA-ICP-MS	zircon	Kromkhun 2010
	Terrapinna Granite	-29.9031	139.6358	1556	4	ID-TIMS	multi zircon	Thornton 1980
2007379005	Hodgkinson Granodiorite	-30.1415	139.4703	1552	4	SHRIMP	zircon	Fraser and Neumann 2010
2007379008	Hodgkinson Granodiorite	-30.1606	139.4114	1552	4	SHRIMP	zircon	Fraser and Neumann 2010

n = 252 with 41 CA-TIMS dates.

Latitudes and Longitudes in grey are estimated from maps in publications.

CA-TIMS = Chemical abrasion Thermal ionisation mass spectrometry
ID-TIMS = Isotope dilution Thermal ionisation mass spectrometry

K-Ar = Potassium-Argon

Kober = Double-filament Thermal ionisation mass spectrometry (Kober 1986)

La-ICPMS = Laser Ablation Inductively Coupled Plasma Mass Spectrometry

SHRIMP = Sensitive High Resolution Ion Microprobe

Pluton names for the Hiltaba Suite are informal, and in the process of being registered with the Australian Stratigraphic Units Database

All CA-TIMS dates were calculated using a $^{238}U/^{235}U$ value of 137.8185 (Hiess et al. 2012). Where publications have used a $^{238}U/^{235}U$ value of 137.88 (Steiger and Jäger 1977), they have been recalculated.

All CA-TIMS errors are quoted at the 95% confidence level, which is $t\sigma$ where MSWD ≤ 1 and $t\sigma\sqrt{MSWD}$ where MSWD > 1, where t = the student's t multiplier for small values of n. Where n = 2, errors are 2σ.

All SHRIMP errors are quoted at the 95% confidence level.

For all other dating techniques, the errors quoted are those published, and the confidence interval is unknown.